PERFORMANCE-BASED PROBABILISTIC ASSESSMENT OF LIQUEFACTION-INDUCED BUILDING SETTLEMENTS

A Dissertation
Presented to
The Academic Faculty

by

Qiwei Mao

In Partial Fulfillment
of the Requirements for the Degree
Master of Science in the
School of Civil and Environmental Engineering

Georgia Institute of Technology
May 2020

PERFORMANCE-BASED PROBABILISTIC ASSESSMENT OF LIQUEFACTION-INDUCED BUILDING SETTLEMENTS

Approved by:

Dr. Jorge Macedo, Advisor
School of Civil and Environmental Engineering
Georgia Institute of Technology

Dr. J. David Frost
School of Civil and Environmental Engineering
Georgia Institute of Technology

Dr. Norman Abrahamson
School of Civil and Environmental Engineering
University of California, Berkeley

Dr. Gabriel Candia
Facultad de Ingeniería Civil
Universidad del Desarrollo, Chile

Dr. Zhigang Peng
School of Earth and Atmospheric Sciences
Georgia Institute of Technology

Date Approved: Jan 10th, 2020

ACKNOWLEDGEMENTS

I would like to thank my advisor, Dr. Jorge Macedo, for sparking my curiosity in geotechnical earthquake engineering. Dr. Macedo's gift for teaching and attention to details guided my research in this area, and I will forever be grateful. I would like to thank also Dr. Norman Abrahamson for facilitating the information to develop the ground motion models in this study and for providing guidance. I would like to thank Chenying Liu, for his effortless help on the research. I would like to thank my thesis committee for reviewing the thesis document and providing feedback on my first experience as researcher.

I would like to thank the Geosystems group, they made me feel at home during my time at Georgia Tech. I will never forget the time we spent in the lab, not to mention the coffee break.

I would like to thank my parents, Xinjun and Shufang, for their love and unconditional support throughout my life.

Lastly, I would like to thank my girlfriend Zhuyuan, for her encouragement and support during my time at Georgia Tech.

TABLE OF CONTENTS

LIST OF TABLES

LIST OF FIGURES

SUMMARY

Shallow founded buildings on liquefiable soils may suffer significant settlement during earthquake loading. The damage observed during the Canterbury earthquake sequence in New Zealand and the Maule earthquake in Chile are good examples of the amount of damage that can be caused due to liquefaction in buildings with shallow foundations. Earthquake scenarios similar to the ones in the Canterbury earthquake sequence are often used for design in the United States. Hence the proper estimation of liquefaction-induced building settlements (*Ds*) is of primary importance for areas in the U.S. affected by earthquakes (e.g. the Pacific Northwest, the Cascadia subduction zone, the New Madrid seismic zone, etc.). Existing procedures to estimate *Ds* are formulated under a deterministic or pseudo-probabilistic framework where there is not a quantification of the existing hazard for *Ds,* and only the hazard associated with ground motion intensity measure parameters is considered. The quantification of the *Ds* hazard would allow more informed decisions in engineering practice, because the hazard is directly quantified and related to the amount of *Ds*. In Addition, a *Ds* hazard quantification is fully consistent with performance-based engineering concepts because the engineering design of a geotechnical system can now be directly related to the hazard in *Ds* and not only to the hazard in a ground motion parameter. This study focuses on the implementation of a performance-based, hazard-consistent framework for the estimation of *Ds*. The following components, which are currently not available in engineering practice, for a performance-based estimation of *Ds* are developed in this study: (1) new conditional ground motion models and scenario based models for the cumulative absolute velocity (*CAV*), which is a primary

intensity measure parameter to estimate *Ds*, (2) coefficients of correlation between *CAV* and spectral accelerations, which are necessary for performance-based implementations, and (3) performance-based implementation of *Ds* models that are currently used in deterministic or pseudo-probabilistic approaches.

Finally, this study offers examples of the application of the developed procedures for the performance-based estimation of *Ds* in engineering practice considering 3 different sites in the United States (California, Salt Lake, Seattle).

CHAPTER 1. INTRODUCTION

Earthquakes cause tremendous damage to civil structures and result in numerous casualties every year. Liquefaction occurs when saturated or partially saturated soil significantly loses strength in response to strong dynamic earthquake shaking, which can result in large settlement to shallow founded buildings. As is shown in Figure 1-1 by Bray et al., (2014), the Christchurch earthquake (2011) caused settlements as large as 30 cm to the CTUC building. Considering the wide-spreading damage, it is important to develop procedures for estimating liquefaction-induced building settlement (*Ds*), which is dependent on the characteristics of earthquakes, building parameters and site conditions. A performance-based framework for the estimation of *Ds* is developed in this study.

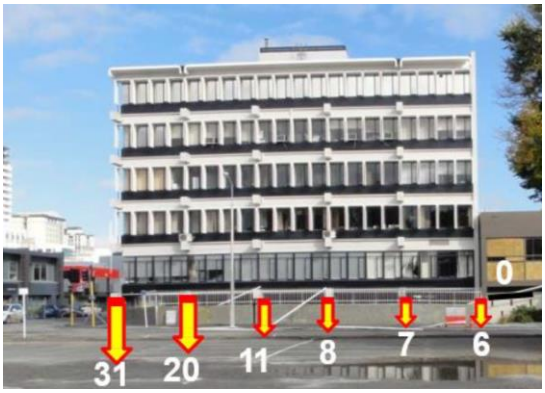

Figure 1-1 Liquefaction-induced Settlement on CTUC building in Christchurch Earthquake (2011).

While it is hard to forecast the ground motions of future earthquakes, it is more practical to estimate the intensity of ground motions associated with an earthquake, which is often represented by ground motion intensity measures (IMs). Engineering design is often based on IMs, which serve as proxies for the amplitude, frequency content and

duration of a ground motion recording. For example, peak ground motion (*PGA*) relates to the largest acceleration of the ground motion, which captures the amplitude of the earthquake; spectral accelerations (*Sa*), is a proxy for the amplitude and frequency content of a ground motion recording. There are other IMs that can actually serve as proxies for amplitude, frequency content and duration of a ground motion recording. Examples of those IMs are the cumulative absolute velocity (*CAV*), and the Arias intensity (*Ia*).

In order to quantitatively assess the possible damage an earthquake might cause to a certain structure, several analytical models have been developed, which can provide estimates of certain engineering demand parameters (EDP). Examples of EDPs in geotechnical engineering are the amount of seismically induced slope displacements, liquefaction induced building settlements (the focus of this study), among others. The existing analytical models to estimate EDPs are usually formulated in terms of IMs, site conditions, earthquake parameters (e.g. magnitude, distance) and properties of engineering systems. In practice the seismic design of engineering systems is commonly performed under concepts of performance-based earthquake engineering (PBEE), where the estimations of EDPs for different earthquake solicitations are required. Based on these estimates and performance criteria established for the system being evaluated the design is judged to be adequate or not.

Three different frameworks commonly used for the estimation of EDPs are: 1) deterministic, 2) pseudo-probabilistic and 3) performance-based probabilistic, which are illustrated in Figure 1-2 for the case of slope displacements. In a deterministic approach, only one earthquake scenario (certain magnitude, distance) is selected, in which the IMs

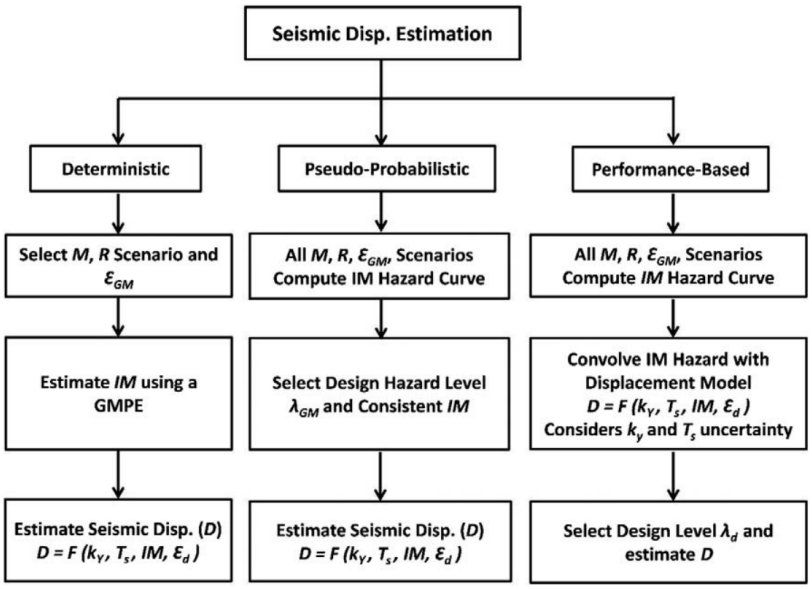

Figure 1-2 Different approaches for the estimation of EDPs.

are estimated using a GMM. Then the EDP of interest can be estimated using an analytical model. No concept of hazard is involved in this approach. In a pseudo-probabilistic approach, all earthquake scenarios are considered through a probabilistic seismic hazard analysis (PSHA), which provides a hazard curve for the IM of interest. Then, based on the hazard design level or return period a representative value of the IM consistent with the defined hazard design level is selected. Finally, the EDP of interest can be estimated using the selected IM, which is used as an input along with other parameters in an analytical model for the EPD. Although the IM is selected according to certain hazard level, the annual rate of exceedance or hazard for the estimated EDP is not the same as that of the IM. This EDP hazard remains unknown in a pseudo-probabilistic assumption, and often engineers assume that it is close to the hazard for the IM, an assumption that has not a rational basis. Finally, in a performance-based approach a hazard curve related directly the hazard with the EDP of interest is estimated. This study performs developments and implementations for the performance-based probabilistic estimation of *Ds*. In particular,

procedures to convolve the IM hazard curve with the analytical model for *Ds* developed by Bray and Macedo (2017). In this approach, the existing uncertainties in the IM and analytical model for *Ds* are explicitly considered. The final result is the annual rate of exceedance for different *Ds* levels.

Analytical models to estimate EDPs are often formulated in terms of one or more IMs. Hence, ground motion models (GMM) are needed to estimate the IMs of interest and the associated uncertainty. The issue is that, the majority of GMMs are developed for the elastic *PGA*, and *Sa*, which represent the maximum amplitude in the response of oscillators with different periods. Although *PGA* and *Sa* are useful for assessing certain engineering problems (i.e. inter-story shift), they are not the best IMs for assessing certain EDPs. This is actually the case for the EDP considered in this study, which is *Ds*. In the case of *Ds*, *CAV* has been regarded by previous researchers (e.g. Bray and Macedo, 2017) as an efficient parameter. Because of the *CAV* importance in the estimation of *Ds*, this study develops conditional ground motion models (CGMM) for *CAV* as well as scenario-based models, which can estimate the median *CAV* and its standard deviation directly from an earthquake scenario and site conditions. The CGMM and scenario-based models are developed for both shallow crustal earthquake zones and subduction (interface, instraslab) settings. In addition, *PGV* has been also regarded as a potential important parameter for estimating *Ds* (Bray and Macedo, 2017), hence a CGMM and scenario-based models for PGV are also developed.

In the context of this study, primary IMs are defined as *PGA*, and *Sa*, and secondary IMs are defined as those different from *PGA* and spectral accelerations. In practice, seismic design is typically performed relying on primary IMs defined according to a target *Sa*

design spectrum, while secondary IMs (i.e. *CAV*) are not typically considered, unless they are critical. In these cases, secondary IMs should be estimated to be consistent with the earthquake scenario and also the design response spectrum. The CGMMs derived in this study serve for this purpose as it will be elaborated in the document.

The development of *CAV* models allows the implementation of the performance-based procedure to estimate *Ds*. In practice, it is straightforward to produce hazard curves for EDPs when the analytical model for estimating EDPs includes only one IM as the predictor. For instance, the analytical models for estimating seismically induced slope displacements developed by Saygili and Rathje (2008) and by Bray and Macedo (2019) rely on only one IM. However, there are analytical models which include multiple IMs as predictors for estimating EDPs. This is the case for the *Ds* model employed in this study, which was formulated by Bray and Macedo (2017). This model used *CAV* and *Sa1* (Spectral acceleration at 1 second) as IMs. When multiple IMs are employed in the analytical models, the coefficient of correlation between the IMs is required for calculating the joint rate of exceedance for the different IMs, which is usually done through vector-hazard PSHA (e.g. Rathje et al. 2014, Macedo et al., 2020). This study provides coefficients of correlation between *CAV* and spectral accelerations for shallow crustal, and subduction (interface, intraslab) tectonic settings.

The content of this study is described as follows:

Chapter 1 presents an introduction to the study and highlights the existing gaps for the performance-based assessment of *Ds*.

Chapter2 presents the development of a CGMM and scenario-based models for *CAV* in shallow crustal tectonic settings.

Chapter 3 presents the development of a CGMM and scenario-based models for *CAV* and *PGV* in subduction tectonic settings.

Chapter 4 presents the calculation of coefficient of correlations between *CAV* and spectral accelerations. In addition, this chapter details the development of a performance-based framework for the estimation of *Ds*. This chapter also highlights the implementation of a MATLAB graphical user interface (GUI) that facilities the developments presented in this study in engineering practice.

Chapter 5 presents the conclusions of this study and recommendations for future studies.

CHAPTER 2. NEW SCENARIO-BASED CUMULATIVE ABSOLUTE VELOCITY MODELS FOR SHALLOW CRUSTAL TECTONIC SETTINGS

2.1 Introduction

The cumulative absolute velocity (*CAV*) is a scalar intensity measure parameter (IM) that is defined as:

$$CAV = \int_0^{tmax} |a(t)|dt \quad (1)$$

where $a(t)$ is the acceleration at time t in m/s^2, t_{max} is the duration of the time series (EPRI, 1988). As first introduced by Electric Power Research Institute (EPRI), CAV was used as an instrumental intensity measure to quantify earthquake damage to power plants (EPRI, 1988). CAV has been intensively studied and many of its variants were created to adapt to different earthquake engineering problems (Danciu and Tselentis, 2007, Campbell and Bozorgnia, 2010, Kostov, 2005, EPRI, 2006, Kramer and Mitchell, 2006, Fahjan et al., 2011). For instance, the EPRI (1988) panel found that, as a potential damage-related IM, CAV was the most discriminating parameter among several different IMs (Reed and Kassaware, 1990). The U.S. Nuclear Regulatory Commission (USNRC, 1997) included the standardized version of CAV (CAV_{std}) as one of the thresholds to assess earthquake damage of nuclear power plants. Fahjan et al. (2011) defined another variant of CAV, named window-based bracketed cumulative absolute velocity (BCAV-W), and used it as an indicator in online early warning systems. In the field of structural engineering,

Bozorgnia (2012) developed a relationship between CAV and different macro-seismic intensity scales and found that *CAV* might be used to rapidly assess the potential earthquake damage to a typical class of conventional structures. Muin and Mosalam (2017) explored the possibility of using CAV to identify the onset, location, and severity of local damage for structural health monitoring. In addition, Danciu and Tselentis (2007) developed fragility functions in terms of the cumulative absolute velocity above the 5 cm/sec2 acceleration threshold (CAV_5) for multiple-story RC buildings designed according to Eurocode. In the field of geotechnical engineering, Kramer and Mitchell (2006) investigated 300 candidate IMs and found CAV_5 was the most efficient IM to capture the generation in soil liquefaction. Similarly, Kwan et al. (2018) found CAV_5 as the IM for predicting liquefaction-induced displacements. CAV has been also used in soil-structure interaction problems, for instance, Bray and Macedo (2017) found that CAV and CAV_{std} are efficient IMs for the estimation of liquefaction-induced building settlements, whereas Bullock et al. (2019) found that CAV, estimated at outcrop conditions, was the most efficient parameter to the estimation of liquefaction-induced settlements, considering 3D effects.

Given the wide-range of applications for CAV, previous research efforts have developed ground motion models (GMMs) to estimate CAV (e.g. Campbell and Bozorgnia, 2010; Campbell and Bozorgnia, 2019; Du and Wang, 2012; Foulser-Piggott and Goda, 2015). Most of those models are developed as traditional GMMs that directly estimate CAV given the earthquake characteristics (e.g. Magnitude - M_w, earthquake-site distance- R_{rup}, fault type, etc.), and site conditions represented by parameters such as V_{S30} (averaged shear-wave velocity in top 30m of site profile). For example, the GMM developed by

Campbell and Bozorgnia (2010), which is also known as the CB10 model, was developed using the ground motion database from the NGA-West1 project and provides CAV estimates for the geometric mean of two horizontal ground motion components , using the earthquake characteristics and site conditions as the inputs. Then Du and Wang (2012) simplified the CB10 model by reducing the number of parameters used in the original GMM and achieved similar trends as those in the CB10 model. Later, Foulser-Piggott and Goda (2015) developed a CAV GMM using a ground motion database of Japanese ground motions. More recently, Campbell and Bozorgia (2019) updated their CB10 model by using the NGA-West2 ground motion database; the updated model will be denominated as CB19 in this study.

In this study we define as primary IMs those related with a spectral acceleration (S_a) response spectrum (i.e. PGA and spectral accelerations), whereas a secondary IM is defined as any IM that is not related with a S_a response spectrum. In practice, seismic design often relies on a S_a design spectrum, which is used for the selection of ground motions that are subsequently used in engineering analysis. Importantly, for engineering problems where a secondary IM is important (e.g. liquefaction related problems where CAV has shown to be important), the consistency between the estimated primary and secondary IMs is highly desired for subsequent selection of ground motions. This consistency is not explicitly checked in traditional GMMs that estimate secondary IMs. However, conditional ground motion models (CGMM)s, permit to explicitly address the consistency between primary and secondary IMs. In this study, a new GCMM for CAV is developed using the NGA-West2 database from the pacific earthquake engineering center (PEER) for shallow crustal earthquakes. Then, this GCMM is converted into new scenario-

based model by combining it with traditional GMMs. Specifically, this study provides five new scenario-based models for CAV that can be readily used in engineering practice. Finally, the CAV estimation of the scenario-based model is compared with traditional GMM and its application in engineering practice is portrayed.

2.2 Conditional and Non-Conditional Models

The majority of GMMs are developed for the elastic spectral accelerations. However, there are secondary intensity measures that are of major importance for evaluating structural responses and geo-hazards, such as Arias intensity (I_a), cumulative absolute velocity (CAV), peak ground velocity (PGV) and significant duration (D_{5-95}). As previously discussed, seismic design is typically performed relying on primary IMs (i.e. PGA, and spectral accelerations) defined according to a target spectral acceleration design response spectrum, while secondary IMs are not typically used, unless they are considered critical. In the following we will refer to a target spectral acceleration design response spectrum simply as a design response spectrum

Two main approaches are commonly used to estimate secondary IMs: 1) The first approach is to develop a non-conditional GMM, which directly relates the secondary IM to the source (moment magnitude M_w), path (site-source distance R), site conditions (V_{s30}) and other seismological parameters (e.g. type of fault, depth to the top of the rupture, etc.). Most GMMs for spectral accelerations have been developed in this manner (e.g. the GMM developed as part of the NGA-West1 and NGA-West2 projects). In this approach, once a design response spectrum is defined, the input parameters for estimating the secondary IM, such as M_w and R, can be obtained from the deaggregation at the specified hazard level or

from the deterministic earthquake scenario used to defined the design response spectrum . 2) In the second approach, in addition to M_w, R, site conditions, and other potential earthquake parameters; the spectral accelerations associated with the design response spectrum are also included as predictors in developing a model for a secondary IM. The models developed under this approach are denominated as conditional ground motion models (CGMMs) because the secondary IM estimate is conditioned on primary IMs.

One important advantage of CGMMs is that the estimated secondary IMs are consistent with the design response spectrum, which may not be the case if non-conditional GMMs are used in the estimation of secondary IMs. For instance, when non-conditional GMMs are employed, the secondary IM is usually computed based on the 16th-84th percentile range, whereas the design spectral accelerations may correspond to a different percentile range, for example a percentile above the 84th percentile. This may lead to inconsistencies because the design spectral acceleration and the secondary IM are, in this case, related to different epsilon (number of standard deviations above the mean) values. On the other hand, the consistency between secondary IMs and a design response spectrum is guaranteed if a CGMM is employed because this consistency is implicitly considered through the development of a CGMM. This approach is similar to the conditional mean spectrum approach proposed by Baker and Cornell (2006).

Importantly, CGMMs have smaller aleatory variability than traditional GMMs, so CGMMs can provide more reliable median estimates than traditional GMMs when a design response spectrum is provided. In addition, the smaller aleatory variability allows one single CGMM to be combined with multiple non-conditional GMMs for spectral accelerations to develop a suite of scenario-based models. For instance, Macedo et al.

(2019) derived five scenario-based models for I_a in subduction interface settings and five scenario-based models for I_a in subduction intraslab tectonic settings by combining a CGMM for I_a with GMMs for spectral accelerations in subduction settings. Similar to a non-conditional GMM model, a scenario-based model for a secondary IM provides estimates for the median and standard deviation of the secondary IM given M_w, R, site conditions and other earthquake parameters. A key advantage of the conditional approach is that the scenario-based model can inherently account for the more complex ground-motion scaling effects found in the GMMs for spectral accelerations on which it is based, such as, sediment-depth effects, soil nonlinearity effects, magnitude saturation. This is an important advantage because significant efforts were devoted to incorporating these effects in the development of non-conditional GMMs for spectral accelerations through advanced finite-fault numerical simulations to ensure physical-based extrapolations for scenarios with minimal data. For example, Abrahamson et al. (2016) combined a CGMM for I_a with the Abrahamson et al. (2014) NGA-West2 GMM for spectral accelerations, which considers hanging-wall effects and is constrained by finite-fault simulations. The resulting scenario-based models for I_a were also able to account for complex hanging-wall effects and were well constrained. Furthermore, regionalization effects can also be included in developing scenario-based models by simply using a region-specific spectral acceleration GMM for the implementation of a secondary IM scenario-based model.

2.3 Database

This study used the NGA-West2 database developed by PEER (Ancheta et al. 2014), which contains worldwide shallow crustal earthquakes that happened until 2011. The full database has 21540 recordings from 599 earthquakes. We used the following criteria to

select the subset for regression (1) recordings with missing metadata were removed (2) data with Z_{TOR} (depth to the top of the rupture) larger than 20 km was removed (3) recordings labelled as fault normal or fault parallel were removed. (4) recordings with only one horizontal component.

The selected subset has 11330 ground motion recordings (each recording has two horizontal components) from 568 earthquakes, with magnitudes from 3.0 to 7.9 and distances truncated at 100 km. The magnitude and distance distribution of the selected subset is presented in Figure 2-1.

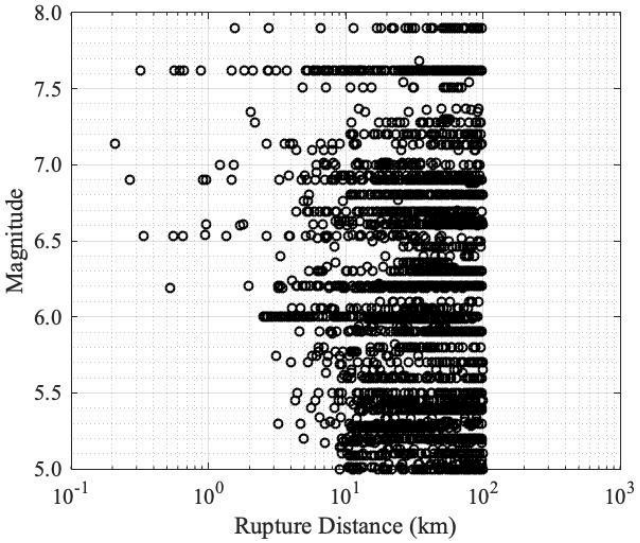

Figure 2-1 Magnitude-distance distribution of selected *CAV* subset

2.4 Conditional *CAV* Models

The following functional form is considered for the CAV CGMM, the estimate of CAV is conditioned on the PGA, the spectral acceleration at a period of 1 sec., M_w, and V_{s30}.

$$Ln[CAV(g \cdot s)] = c1 + c2LnPGA + c3M_w + c4LnV_{s30} + c5LnSa1 \qquad (2)$$

where PGA and $Sa1$ are in g, and V_{s30} is in m/s.

Because CAV is calculated by integrating absolute ground acceleration with respect to time (i.e. Eq. 1), it captures the amplitude, frequency content and duration characteristics of a ground motion recording. Hence, in terms of the parameters in Equation 2, PGA and $Sa1$ are included as proxies of amplitude, whereas $Sa1$, V_{s30}, and M_w are included as proxies for frequency content and duration.

The rupture distance (R_{rup}) is not selected because it is indirectly captured by PGA and $Sa1$. In addition, a regression including R_{rup} as an additional predictor in Equation 2 resulted in a close to zero coefficient for this term and a small t-ratio.

We calculate the coefficients in Equation 2 using random-effects regressions, which are often employed in developing ground motion models addressing the correlation in the data through the event terms (e.g., Abrahamson and Youngs 1992). The CGMM developed in this study considers random effects across different earthquakes. The resulting coefficients are listed in Table 1. The coefficient for PGA (c2 = 0.58) is larger than the coefficient for $Sa1$ (c5 = 0.11), which indicates that CAV scales more strongly with PGA than $Sa1$. This result is consistent with previous findings in Campbell and Bozorgnia (2012) Campbell and Bozorgnia (2012) found that the correlation between *CAV* and *Sa1* is close to the correlation between *Ia* and *Sa1*, but the correlation between *CAV* and *PGA* is smaller than the correlation between *Ia* and *PGA*. The conditional model for arias intensity developed by Macedo et al. (2019) took a similar functional form as this study, but the coefficient for *PGA* (1.54 for interface, 1.58 for intraslab) is almost 10 times

the coefficient for *Sa1* (0.17 for interface, 0.14 for intraslab). Consequently, it is expected to have the coefficient for *PGA* only 5 times to that of *Sa1*, which is lower than 10.

The total standard deviation for the developed CGMM is 0.28 in natural log units, which as expected is much lower than the traditional GMMs developed for CAV. For example, the recent GMM for CAV by Campbell and Bozorgnia (2019) has a standard deviation ranging from 0.45 to 0.58.

The residuals of the CGMM are shown in Figure 2-2 as a function of the predictor parameters used in Equation 2 and also other parameters of importance. The distribution of between-residuals with respect to Magnitude (M_w) and the depth to the top of rupture (ZTOR) are shown in Figure 2-2a and Figure 2-2b. Within-event residuals are plotted against PGA, $Sa1$, V_{s30}, and R_{rup}in Figure 2-2c to Figure 2-2f. No systematic trends are found in the plots for PGA, $Sa1$, M_w, indicating that the model is not biased respect to these parameters. The lack of trends in the plots against rupture distance (R_{rup}), which is not included in the functional form, shows that the distance effect is already accounted for through the selected functional form. In addition, the functional form is not biased in terms of site conditions as no trends are observed in the plot of residuals against V_{s30}.

Table 1 - Results from the Random-Effects Regression for the Conditional Ground Motion Model for *CAV* on Shallow Crustal Settings

Coefficients					Error Terms	
c1	*c2*	*c3*	*c4*	*c5*	τ	ϕ
-0.80	0.58	0.49	-0.31	0.11	0.18	0.21

Note: *c1~ c5* are the coefficients in Equation 2; τ is the between-event standard deviation, ϕ is the within-event standard deviation.

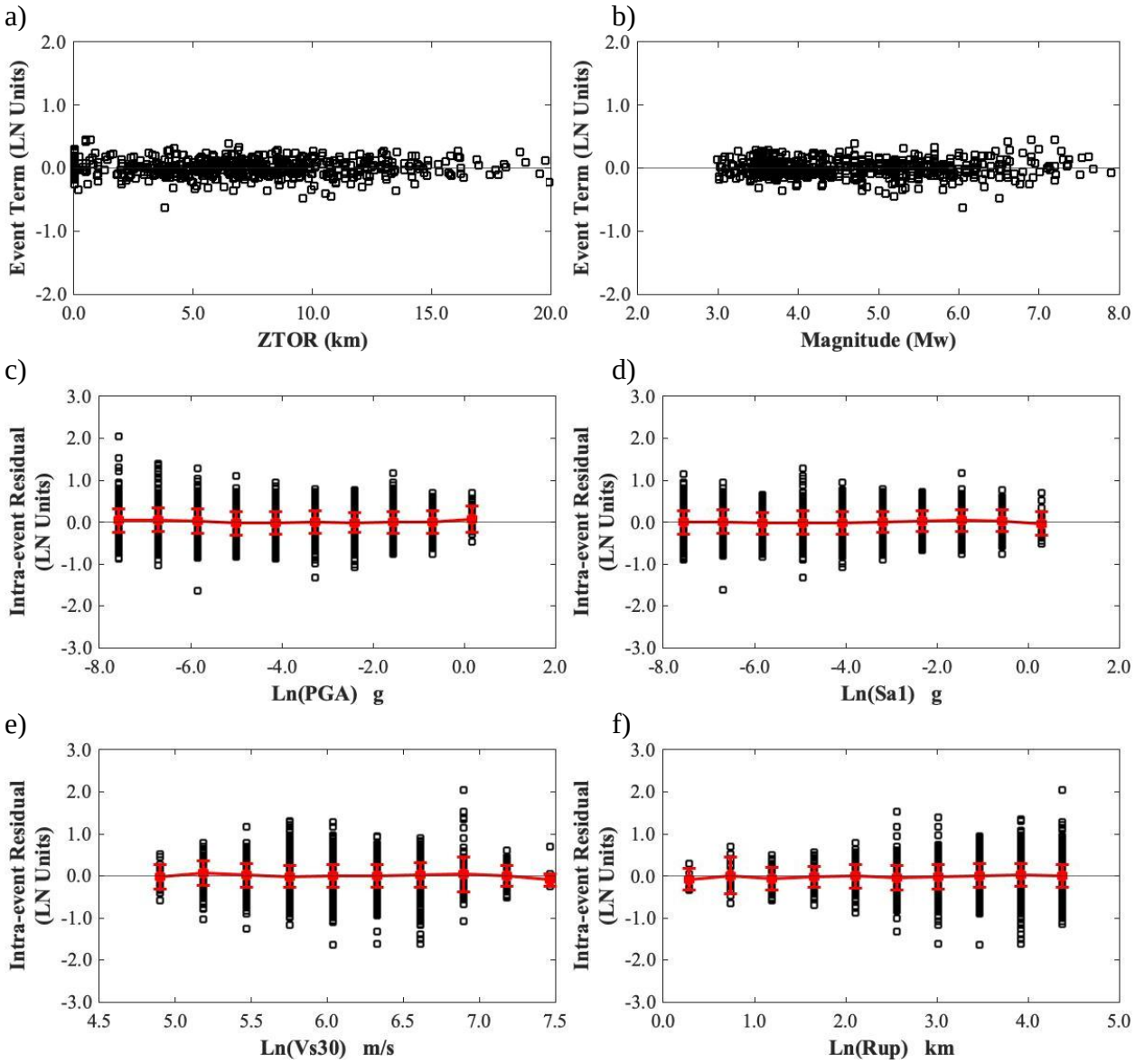

Figure 2-2 Residuals of the conditional model for *CAV*. Between residuals for a) *ZTOR*, b) Magnitude (*Mw*). Within residuals for c) *PGA*, d) *Sa1*, e) *VS30*, f) Rupture distance.

2.5 Conversion of the Conditional Models to Scenario-based Models

By combining the CGMM in the previous section with traditional non-conditional GMMs for PGA and $Sa1$, a suite of scenario-based models can be established. Five scenario-based models for CAV are developed using the GMMs for PGA and Sa1 from the NGA-West2 project. The models considered are: ASK14 (Abrahamson et al., 2014),

BSSA2014 (Boore et al., 2014), CB2014 (Campbell and Bozorgnia, 2014), CY2014 (Chiou and Youngs, 2014), and I2014 (Idriss, 2014).. The median of CAV for a given earthquake scenario can be estimated by Equation 3.

$$Ln[CAV_{med}(m/s)] = g(c1 + c2LnPGA_{med} + c3M_w + c4LnSa1_{med}) \quad (3)$$

where CAV_{med} is the median estimate in m/s, PGA_{med} and $Sa1_{med}$ are the median estimates given by the traditional GMM being considered in g.

For instance, the PGA_{med} and $Sa1_{med}$ can be estimated through Equation 4 when ASK14 (Norman A. Abrahamson, Silva, and Kamai 2014) is used:

$$\begin{aligned} Ln[Sa(g)] = {} & f_1(M, Rrup) + F_{RV} f_7(M) + F_N f_8(M) + F_{As} f_{11}(CR_{JB}) \\ & + f_5(\widehat{Sa}_{1180}, V_{s30}) + F_{HW} f_4(R_{JB} + R_{RUP} \\ & + R_x, R_{yo}, W, dip, Z_{TOR}, M) + f_6(Z_{TOR}) + f_{10}(Z_1, V_{s30}) \\ & + Regional(V_{s30}, R_{RUP}) \end{aligned} \quad (4)$$

Where M is magnitude, R_{rup} is rupture distance, dip is fault dip in degrees, W is the fault width along the dip direction , Sa stands for spectral acceleration ($PGA_{med} = Sa$ at period 0s and $Sa1_{med} = Sa$ at periods 1 s) in units of g, R_{JB} is the Joyner-Boore distance, $CR_{JB}$is the centroid R_{JB}, R_x is the horizontal distance from top of the rupture, R_{yo} is the horizontal distance off the end of the rupture measured parallel to strike, Z_{TOR} is the depth to the top of rupture, $f_1, f_4, f_5, f_6, f_7, f_8, f_{10}, f_{11}$ f_{11} and $Regional$ are functions to control the magnitude scaling, non-linear site effects, depth scaling, distance scaling, and regionalization proposed by Abrahamson et al. (2014). F_{RV} and F_N are flags for reverse and normal faulting earthquakes respectively, F_{HW} is the flag for hanging-wall sites, F_{AS} is the flag for aftershocks.

Given the standard deviation of the spectral acceleration GMMs and the correlation between PGA and Sa1, equation 5 provides the standard deviation for the scenario-based CAV models using the propagation of errors (PhR, 1969):

$$\begin{aligned}\sigma_{LnCAV}^2 = \sigma_{LnCAV|Ln(PGA),Ln(Sa1)}^2 + \sigma_{lnPGA}^2[\partial lnCAV/\partial lnPGA]^2 \\ + \sigma_{lnSa1}^2[\partial lnCAV/\partial lnSa1]^2 \\ + 2COV[lnPGA, LnSa1][\frac{\partial lnCAV}{\partial lnPGA}][\partial lnCAV/\partial lnSa1]\end{aligned} \quad (5)$$

in which

$$COV[LnPGA, LnSa] = \rho[\varepsilon_{LnPGA}, \varepsilon_{LnSa1}][\sigma_{LnPGA}, \sigma_{LnSa1}] \quad (6)$$

where ρ and ε are the coefficient of correlation and the normalized residuals from the PGA and $Sa1$ GMMs, respectively. The partial derivatives can be calculated using Equation 2 (i.e. the conditional model), which leads to $\partial lnCAV/\partial lnPGA$ = c2 and $\partial lnCAV/\partial lnSa1$ = c5. Hence, the total standard deviation of the scenario-based model can be calculated according to Equation 7:

$$\sigma_{LnCAV} = \sqrt{0.0784 + 0.3364 \times \sigma_{lnPGA}^2 + 0.0121 \times \sigma_{lnSa1}^2 + 0.1276 \times \rho[\varepsilon_{LnPGA}, \varepsilon_{LnSa1}] \times \sigma_{LnPGA}\sigma_{LnSa1}} \quad (7)$$

in which $\rho[\varepsilon_{LnPGA}, \varepsilon_{LnSa1}]$ = 0.52, σ_{LnPGA} and σ_{LnSa1} are the standard deviations given by the GMMs used for estimating the median PGA and $Sa1$, respectively.

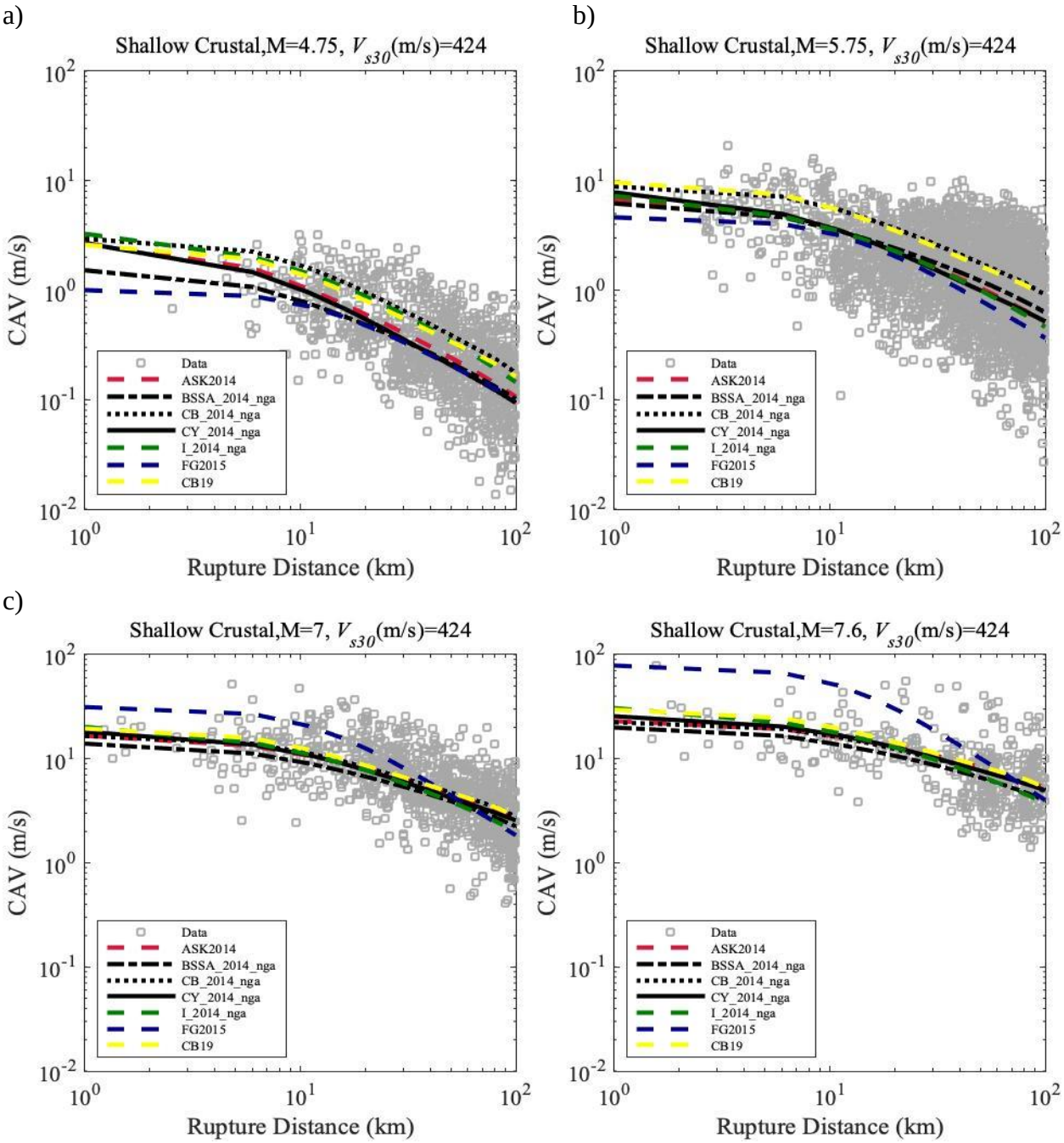

Figure 2-3 Comparisons of distance scaling of median *CAV* estimate for scenario-based *CAV* models developed in this study, and for non-conditional *CAV* GMMs. a) M_w = 4.75, V_{s30} = 424 m/s, b) M_w = 5.75, V_{s30} = 424 m/s, c) M_w = 7, V_{s30} = 424 m/s, d) M_w = 7.6, V_{s30} = 424 m/s. Spectral acceleration models: ASK14 (Abrahamson et al. 2014), BSSA2014 (Boore et al. 2014), CB2014 (Campbell and Bozorgnia 2014), CY2014 (Chiou and Youngs 2014), I2014 (Idriss 2014). Non-conditional *CAV* GMMs: FG2015 (Foulser-Piggott and Goda 2015), CB19 (Campbell and Bozorgnia 2019).

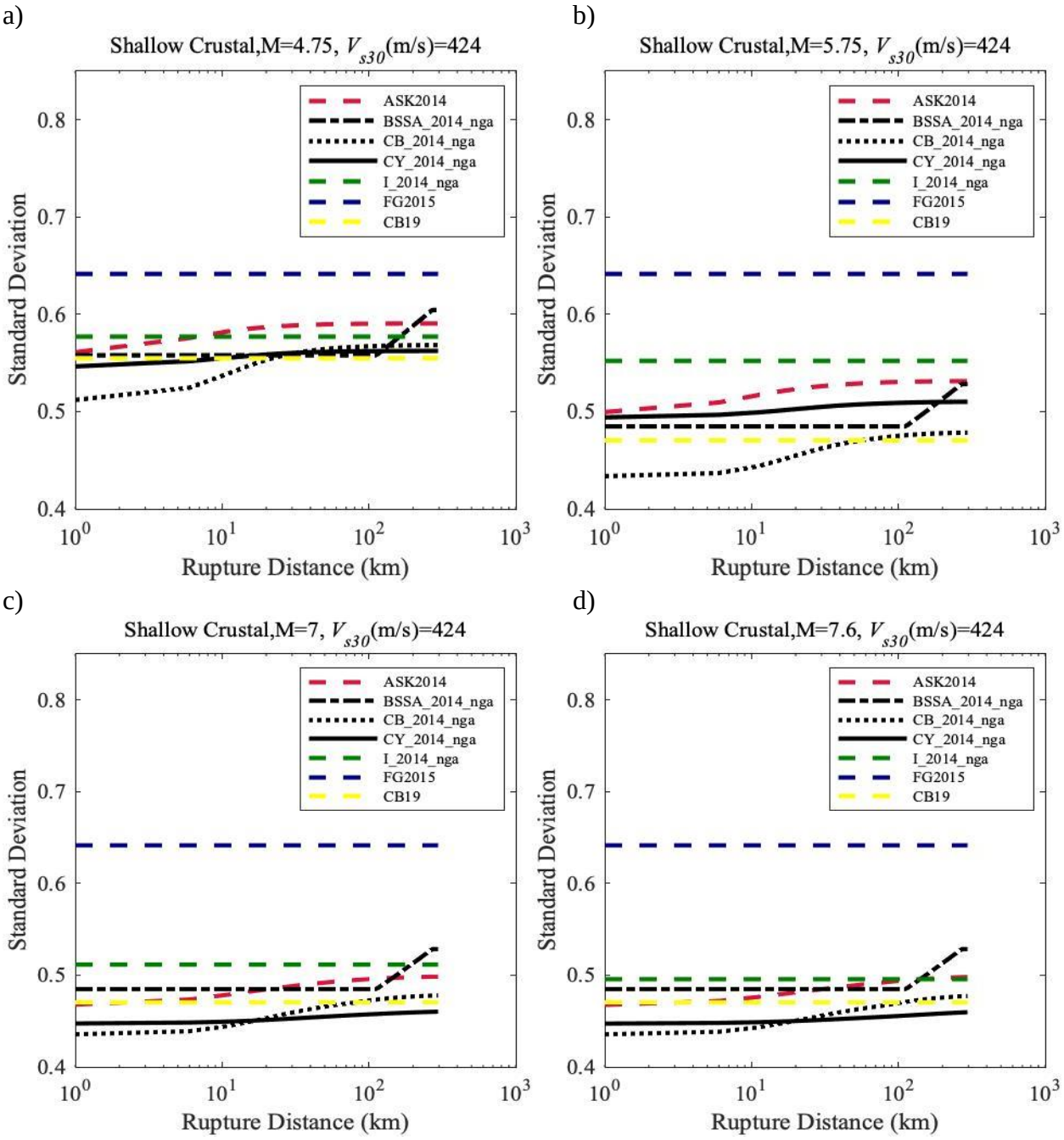

Figure 2-4 Comparisons of standard deviations against rupture distance of the five scenario-based models developed in previous section and non-conditional models for *CAV*. a) M_w = 4.75, V_{s30} = 424 m/s, b) M_w = 5.75, V_{s30} = 424 m/s, c) M_w = 7, V_{s30} = 424 m/s, d) M_w = 7.6, V_{s30} = 424 m/s. Spectral acceleration models: ASK14 (Abrahamson et al. 2014), BSSA2014 (Boore et al. 2014), CB2014 (Campbell and Bozorgnia 2014), CY2014 (Chiou and Youngs 2014), I2014 (Idriss 2014). Non-conditional *CAV* GMMs: FG2015 (Foulser-Piggott and Goda 2015), CB19 (Campbell and Bozorgnia 2019).

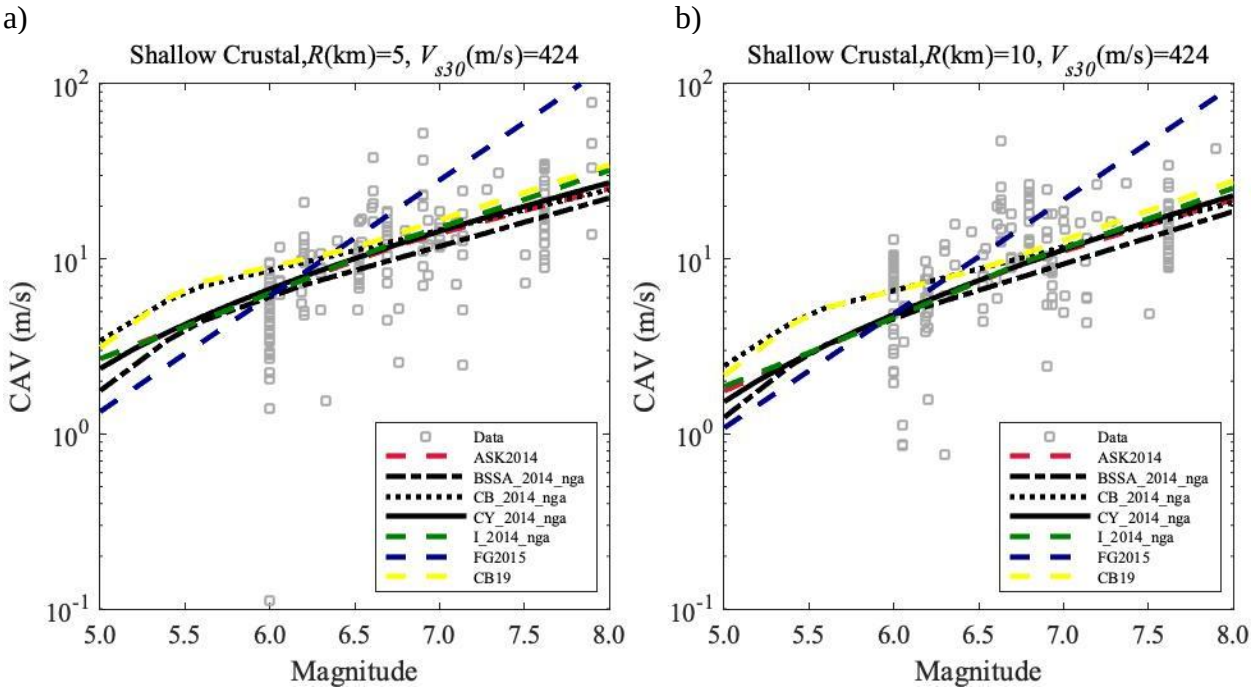

Figure 2-5 Comparisons of magnitude scaling for estimates of median *CAV* by scenario-based models and non-conditional models. (a) Rupture distance 5 km, *Vs30* 424m/s, (b) Rupture distance 10 km, *Vs30* 424m/s. Spectral acceleration models: ASK14 (Abrahamson et al. 2014), BSSA2014 (Boore et al. 2014), CB2014 (Campbell and Bozorgnia 2014), CY2014 (Chiou and Youngs 2014), I2014 (Idriss 2014). Non-conditional *CAV* GMMs: FG2015 (Foulser-Piggott and Goda 2015), CB19 (Campbell and Bozorgnia 2019).

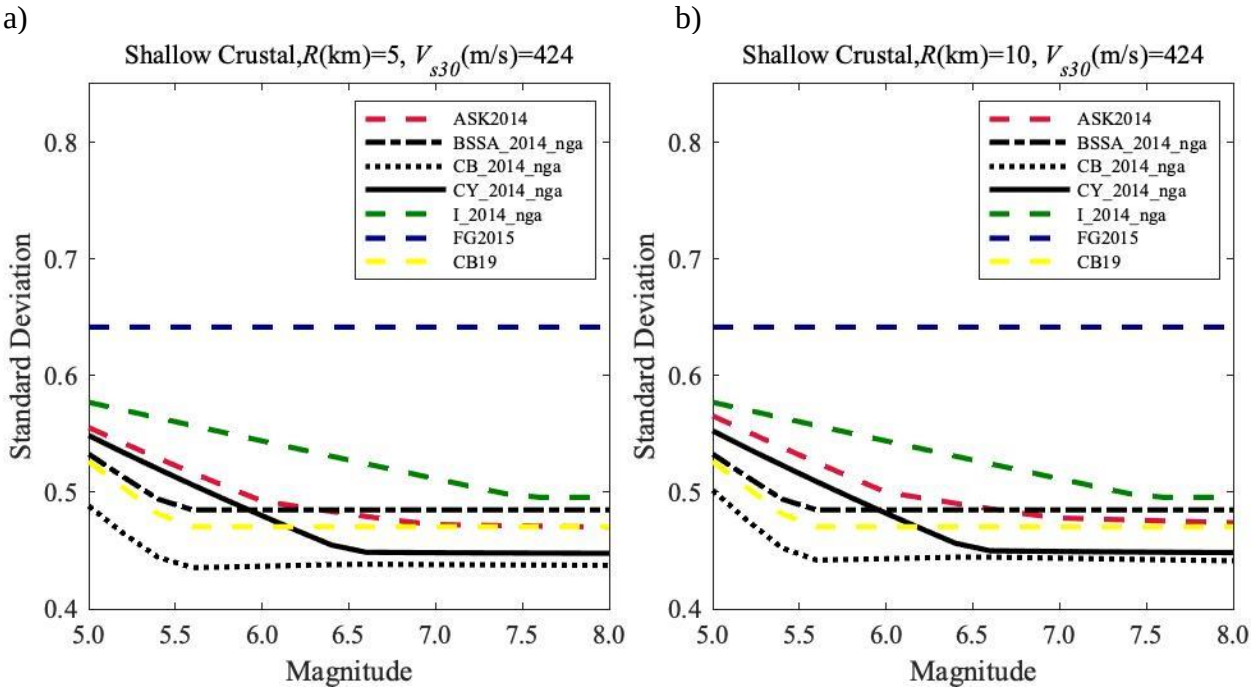

Figure 2-6 Comparisons of standard deviations against magnitude of the five scenario-based models developed in previous section and non-conditional models for *CAV*. a) Rupture distance 5 km, V_{s30} 424m/s, (b) Rupture distance 10 km, V_{s30} 424m/s. Spectral acceleration models: ASK14 (Abrahamson et al. 2014), BSSA2014 (Boore et al. 2014), CB2014 (Campbell and Bozorgnia 2014), CY2014 (Chiou and Youngs 2014), I2014 (Idriss 2014). Non-conditional *CAV* GMMs: FG2015 (Foulser-Piggott and Goda 2015), CB19 (Campbell and Bozorgnia 2019).

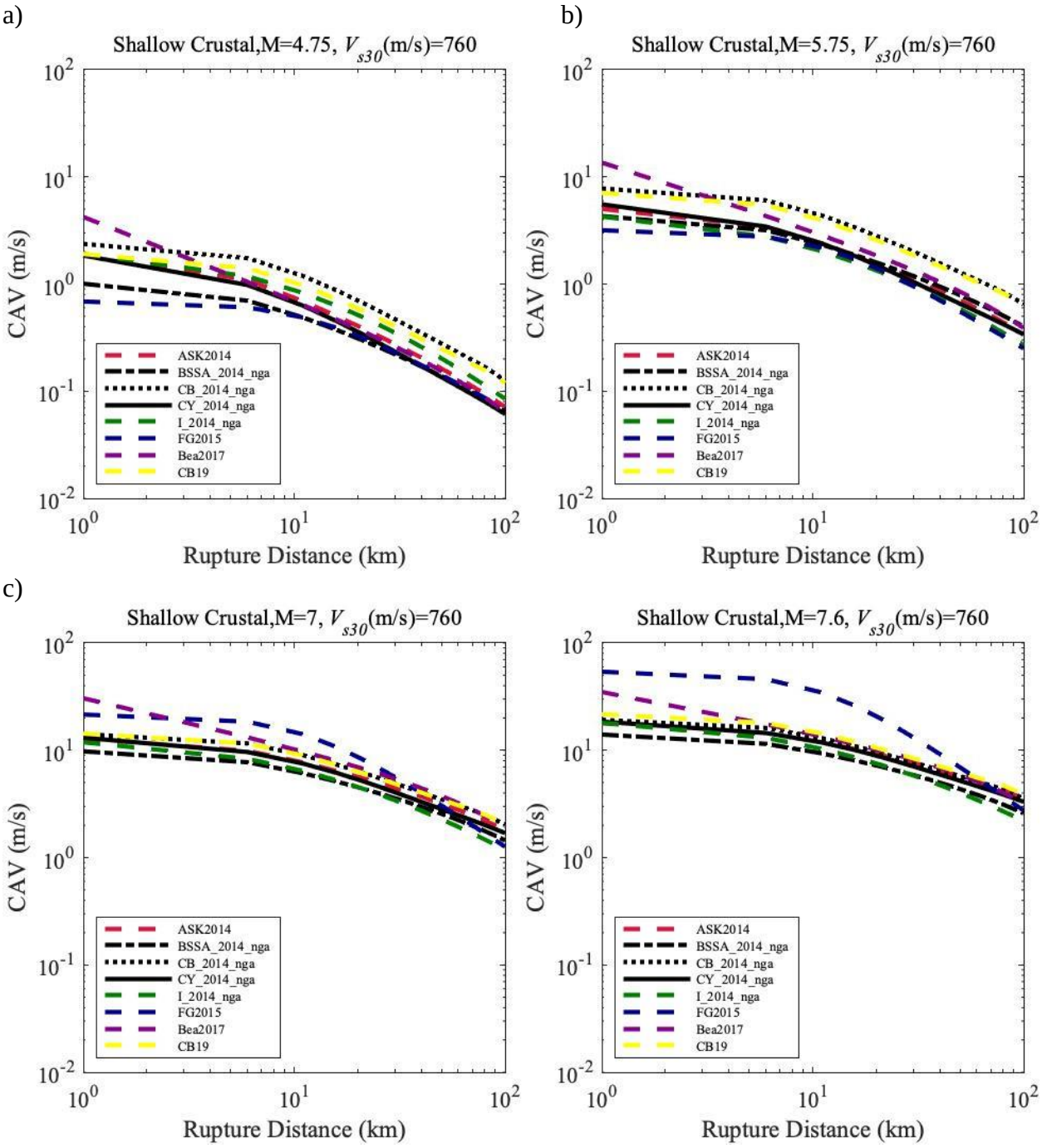

Figure 2-7 Comparisons of distance scaling of median *CAV* estimate for scenario-based *CAV* models developed in this study, and for non-conditional *CAV* GMMs. a) M_w = 4.75, V_{s30} = 424 m/s, b) M_w = 5.75, V_{s30} = 760 *m/s*, c) M_w = 7, V_{s30} = 424 m/s, d) M_w = 7.6, V_{s30} = 424 m/s. Spectral acceleration models: ASK14 (Abrahamson et al. 2014), BSSA2014 (Boore et al. 2014), CB2014 (Campbell and Bozorgnia 2014), CY2014 (Chiou and Youngs 2014), I2014 (Idriss 2014). Non-conditional *CAV* GMMs: FG2015 (Foulser-Piggott and Goda 2015), Bea2017 (Bullock et al. 2017), CB19 (Campbell and Bozorgnia 2019).

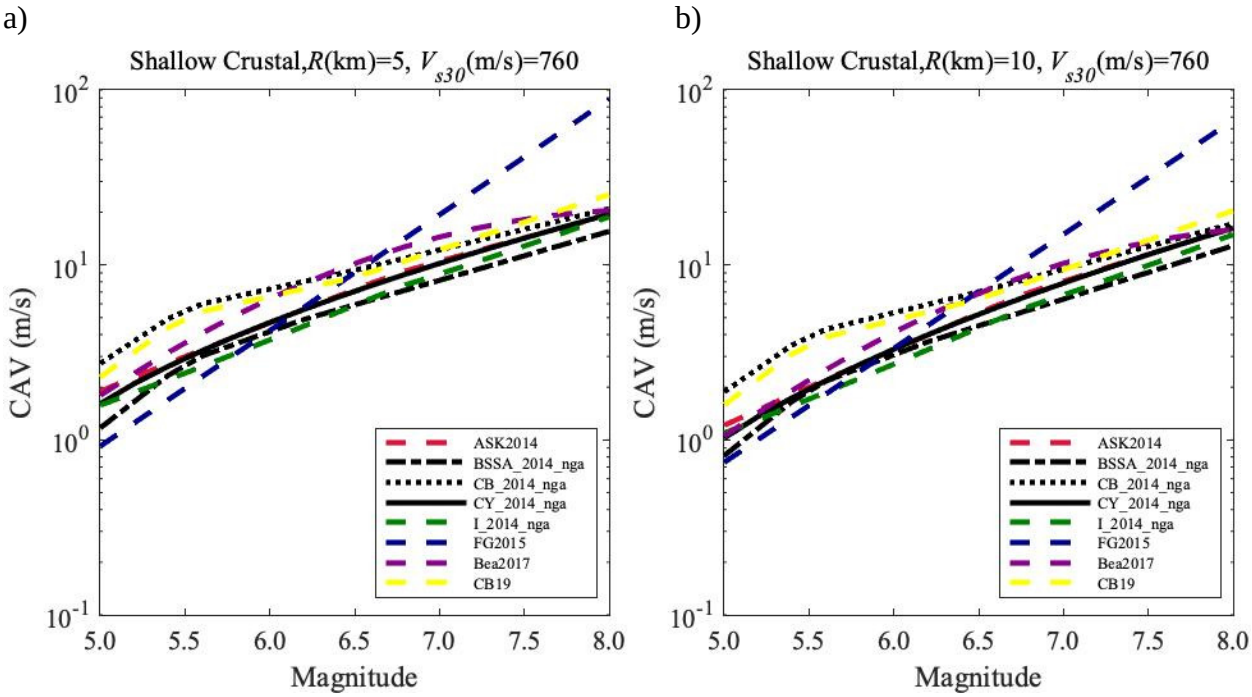

Figure 2-8 Comparisons of magnitude scaling for estimates of median *CAV* by scenario-based models and non-conditional models. (a) Rupture distance 5 *km*, V_{s30} 760 *m/s*, (b) Rupture distance 10 *km*, V_{s30} 424 *m/s*. Spectral acceleration models: ASK14 (Abrahamson et al. 2014), BSSA2014 (Boore et al. 2014), CB2014 (Campbell and Bozorgnia 2014), CY2014 (Chiou and Youngs 2014), I2014 (Idriss 2014). Non-conditional *CAV* GMMs: FG2015 (Foulser-Piggott and Goda 2015), Bea2017 (Bullock et al. 2017), CB19 (Campbell and Bozorgnia 2019).

2.6 Model Trends and Comparisons with Previous *CAV* Models

The five scenario-based models for *CAV* are compared with existing non-conditional GMMs for *CAV* to assess model trends. The considered non-conditional GMMs correspond to: FG2015 (Foulser-Piggott and Goda 2015), Bea2017 (Bullock et al. 2017), and CB19 (Campbell and Bozorgnia 2019). The scenario-based models are developed using the coefficients listed in Table 1, the mean estimates are calculated according to Equation 3, and the standard deviation according to Equation 7.

Figure 2-3 shows the distance scaling comparisons for the developed scenario-based *CAV* models, considering different earthquake scenarios (M_w values of 4.75, 5.75, 7, 7.6), site conditions (V_{s30}=424m/s), and a hypocenter depth of 20 km. Because the bea2017 model is developed for rock sites, and most of the recordings have V_{S30} smaller than 760 *m/s*, this model is not included in Figure 2-3. Instead, the scenario-based model based on Bea2017 is compared with other models in Figure 2-7.

The distance scaling of all the developed scenario-based *CAV* models is generally consistent. The *CAV* estimates in the scenario-based model derived using the CB2014 model are slightly higher than the estimates from other scenario-based models for low to moderate magnitudes (e.g. M_w=4.8, 5.8), whereas at larger magnitudes (e.g. M_w=7.0, 7.6) the estimates from all the scenario-based models are generally consistent. In terms of the non-conditional *CAV* GMM, the scaling of the CB19 model is similar to the scaling of the scenario-based models, whereas the scaling in the FG2015 model is stronger at short distances (i.e. R_{rup} <=*30* km) and large magnitudes (i.e. M_w >6.0). The *CAV* estimates from the CB19 model are generally consistent with those from the scenario-based models.

On the other hand, the estimates from the FG2015 model are generally slightly lower than those in other models (including the CB19 model) for low to moderate magnitudes (i.e. at M_w= 4.8, 5.8), and higher for large magnitudes (i.e. at M_w= 7.0, 7.6). The differences at large magnitudes may be and short distances may be associated to the treatment of the short distance saturation in the FG2015 model.

The variation of the standard deviation versus rupture distance, considering the developed scenario-based models and non-conditional GMMs are compared in Figure 2-4. The FG2015 GMM has the largest standard deviation (0.64 in Ln units) at all earthquake scenarios. The scenario-based models have similar standard deviations varying from 0.42 to 0.51 in Ln units, which are also similar to the standard deviation in CB19 model. The scenario-based model based on the CB_2014 GMM has the lowest standard deviation in most earthquake scenarios, while the scenario-based model based on the I_2014 GMM has the largest standard deviation.

The magnitude scaling for the developed scenario-based models and non-conditional GMMs are compared in Figure 2-5, considering different earthquake scenarios (R_{rup}values of 5 km and 10 km), site conditions (V_{s30} 424m/s, 760 m/s) and a hypocenter depth of 20 km. Because the bea2017 model is developed for rock sites, and most of the recordings have V_{S30} smaller than 760 m/s, this model is not included in Figure 2-5. Instead, the scenario-based model developed with Bea2017 is compared with other models in Figure 2-8. The magnitude scaling across the different scenario-based models is generally consistent, especially for large magnitudes (i.e. M_w > 6.0). In terms of the traditional non-conditional GMMs, the magnitude scaling in the CB19 and Bea2017 is consistent with the scaling in the scenario-based models, whereas the FG2015 model shows a much stronger

scaling at large magnitudes (i.e. M_w > 6.0). The estimates from all scenario-based models and non-conditional GMMs are generally consistent with exception of the FG2015 model, which provides larger estimates at large magnitudes. The consistency or discrepancy across the different scenario-based models and non-conditional models depends on the treatment of magnitude saturation.

Figure 2-6 shows the comparison of the magnitude scaling of standard deviations, where FG2015 also has the largest standard deviation of 0.65, and scenario-based models share similar standard deviations in the range of 0.5 to 0.6.

Interestingly, there is a remarkable consistency between the *CAV* scenario-based model implemented using the CB_2014_nga spectral acceleration GMM, and the non-conditional *CAV* CB19 GMM (Figure 2-3 to Figure 2-6). In this case, both the scenario-based model and the CB19 GMM have been developed with the NGA-West2 database, and the underlain CB2014-nga model for the scenario-based implementation has similar constraints as the CB19 GMM. Hence, scenario-based models can be as robust as traditional non-conditional GMM if the underlain spectral acceleration GMM used to implement a scenario-based model is also robust. As previously discussed, this is an important advantage to develop GMMs for secondary IMs, since this approach takes advantage of the efforts invested in constraining the extrapolation of spectral acceleration GMMs.

2.7 Conclusions

CAV is of vital importance for seismic hazard analysis, but few GMPEs are developed for *CAV*. In practice, using a traditional GMPE to estimate *CAV* may cause

inconsistency with the commonly used spectral accelerations in terms of hazard level. Implementing a conditional model guarantee consistency and include the more complex scaling effects of traditional GMMs for spectral accelerations.

A conditional model for *CAV* is derived using the PEER NGA-West2 shallow crustal ground motion database. The estimate of *CAV* is conditioned on the estimated *PGA*, *Sa1*, V_{s30}, and $M_w$of an earthquake scenario. It can provide a robust estimate of median values for *CAV* that has a consistent hazard with a design acceleration response spectrum.

Scenario-based models for *CAV* are derived by combining the conditional model with non-conditional models for spectral accelerations. The scenario-based model can provide estimates for *CAV* given the earthquake scenario, which is often obtained from deaggregation. Scenario-based models also include the complex scaling effects that are considered in the traditional models being used. These features enable the scenario-based models to be readily used in seismic hazard assessments and probabilistic procedures that use *CAV* as a critical intensity measure. Five scenario-based models are developed in this study for *CAV*, their scaling against magnitude and distance are shown to be consistent with established non-conditional *CAV* models in most earthquake scenarios. The scenario-based models are also capturing the trend of well-recorded ground motions, the estimate of *CAV* is always centered on the data. Due to the smaller standard deviations and better extrapolation of the data, the conditional model developed in this article should be implemented in practice for estimating *CAV*, with higher weight compared to traditional GMMs counterparts.

CHAPTER 3. CONDITIONAL MODEL FOR CUMULATIVE ABSOLUTE VELOCITY AND PEAK GROUND VELOCITY IN SUBDUCTION ZONES

3.1 Introduction

The performance-based evaluation of liquefaction-induced building settlements in subduction tectonic settings needs from suitable GMMs for this tectonic environment. In this chapter GMMs for *CAV* and *PGV* are developed. Both *CAV* and *PGV* have shown to be important IMs for the assessment of liquefaction-induced building settlements (Bray and Macedo, 2017) The NGA-Sub database is used to derive new conditional ground motion models (CGMMs) for *CAV* and *PGV* in subduction settings. The derivations follow the same procedure described in Chapter 2. The CGMMs are used to implement new scenario-based models by combining them with traditional GMMs for spectral accelerations. The magnitude and distance scaling of the median and standard deviations of the scenario-based models are compared to previous models and well recorded ground motions.

3.2 Database

This study used the NGA-SUB database developed by PEER (Kishida et al, 2018), which includes subduction earthquakes around the world that occurred between 1937 and 2016. The full database contains 71340 recordings from 1880 earthquakes in 7 regions: Alaska, Cascadia, Central America & Mexico, Japan, New Zealand, South America, Taiwan.

The subset used for this study is selected with the following criteria:(1) recordings must consist of two horizontal components; (2) recordings with *PGA* less than 5 g; (3) subduction interface earthquakes with depth to the top of the rupture (Z_{TOR}) less than 50 km, subduction intraslab earthquakes with Z_{TOR} larger than 20 km; (5) recordings with closest distance to the rupture plane (R_{rup}) less than 300 km, intraslab recordings must have R_{rup} larger than *RmaxForAnalysis* (largest rupture distance for analysis); (6) earthquakes with dip angle larger than 0 degree and rake angle larger than -250 degrees; (7) only mainshocks are selected; (8) depth to the hypocenter must be larger than zero; (10) only earthquakes with 5 or more recordings are selected. The selected recordings are show below:

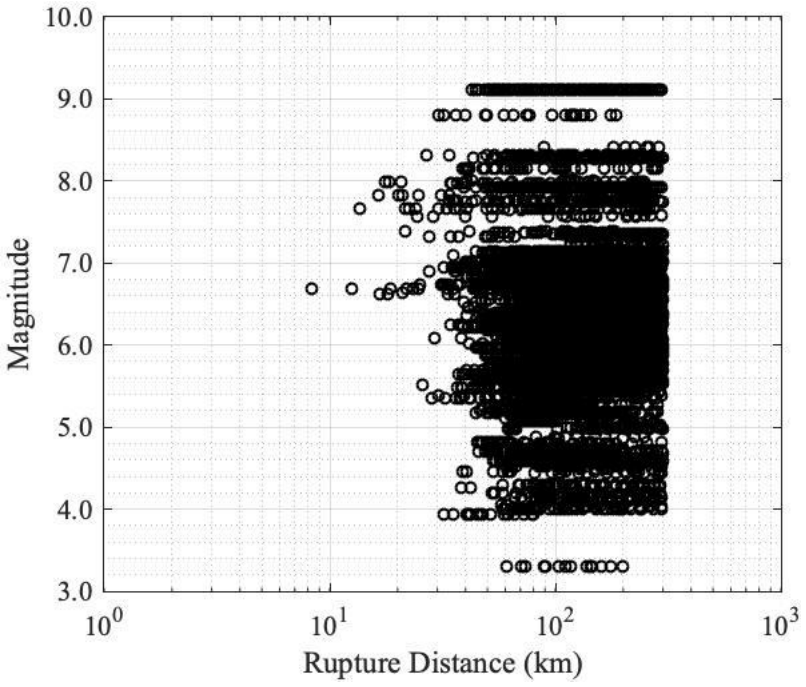

Figure 3-1 Magnitude and distance distribution of selected *CAV* dataset

The selected dataset consists of 19574 recordings in both interface and intraslab settings. The subduction interface subset has 11836 recordings with $4.8 \leq M_w \leq 9.12$ and

$0 \leq R_{rup} \leq 300\ km$; the selected subduction intraslab subset consists of 7738 recordings with $3.3 \leq M_w \leq 7.78$ and $0 \leq R_{rup} \leq 300\ km$. The magnitude and distance distribution of the subset is shown in Figure 3-1.

3.3 Conditional Ground Motion Model for *CAV*

Similar to the conditional model for *CAV* in shallow crustal settings, the same functional form and regression method are used for this model. The subset was split into interface and intraslab for regression, results are listed in Table 2.

The developed CGMM for *CAV* in subduction interface settings has a total standard deviation of 0.33 in natural log units, and the developed CGMM for *CAV* in subduction intraslab settings also has a total standard deviation of 0.33 in natural log units. These standard deviations are, as expected, much lower than the standard deviation from traditional GMMs developed for *CAV*. For example, the recent GMM for *CAV* by Campbell and Bozorgnia (2019) has a standard deviation ranging from 0.45 to 0.58.

Table 2 - Results from the Random-Effects Regression for the Conditional Ground Motion Model for *CAV* in Subduction Zones

	Coefficients					Error Terms	
	c1	*c2*	*c3*	*c4*	*c5*	τ	ϕ
Interface	1.00	0.63	0.28	-0.27	0.17	0.23	0.24
Intraslab	-1.47	0.64	0.58	-0.23	0.11	0.20	0.26

Note: *c1*~ *c5* are the coefficients in Equation 2; τ is the between-event standard deviation, ϕ is the within-event standard deviation.

The CGMM residuals are shown in Figure 3-2 and Figure 3-3 for interface and intraslab tectonic settings as a function of the predictor parameters used in Equation 3 and

also other parameters of importance. The distribution of between-residuals with respect to Magnitude (M_w) and the depth to the top of rupture (Z_{TOR}) are shown in Figure 3-2(a, b) and Figure 3-3 (a, b) Within-event residuals are plotted against *PGA*, *Sa1*, *Vs30*, in Figure 3-2 (c ~ f) and Figure 3-3 (c ~ f). No systematic trends are found in the plots for *PGA*, *Sa1*, Mw, indicating that the model is not biased respect to these parameters. The lack of trends in the plots against rupture distance (R_{rup}), which is not included in the functional form, shows that the distance effect is accounted for through *PGA* and *Sa1*. The scaling against site condition is also captured as no trends are found in the plots for *Vs30*. Similar to the results of the conditional model for *CAV* in shallow crustal settings, this functional form has properly captured the dependence of *CAV* on the source, path and site conditions.

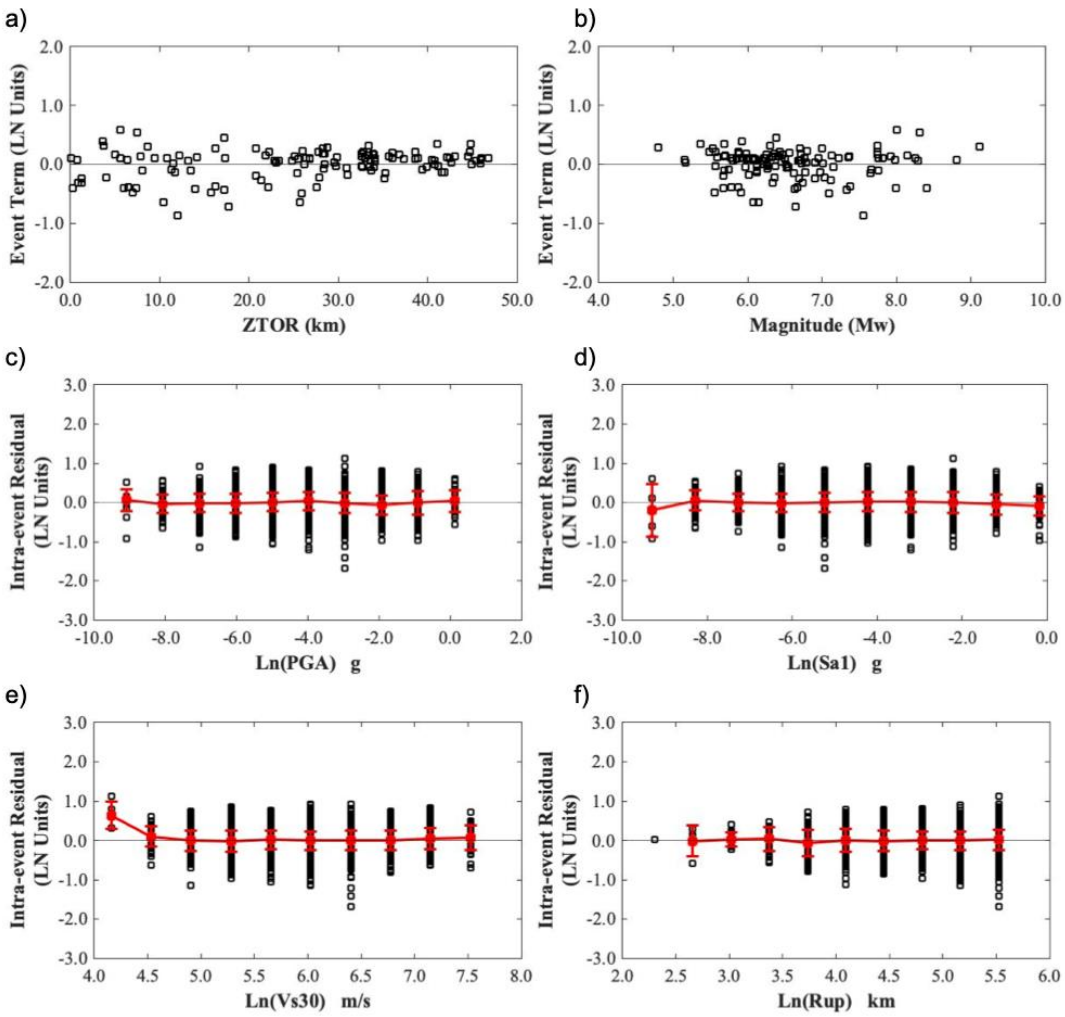

Figure 3-2 Residuals of the conditional model for *CAV* in subduction interface settings. Between residuals for a) *ZTOR*, b) Magnitude (M). Within residuals for c) *PGA*, d) *Sa1*, e) *Vs30*, f) Rupture distance.

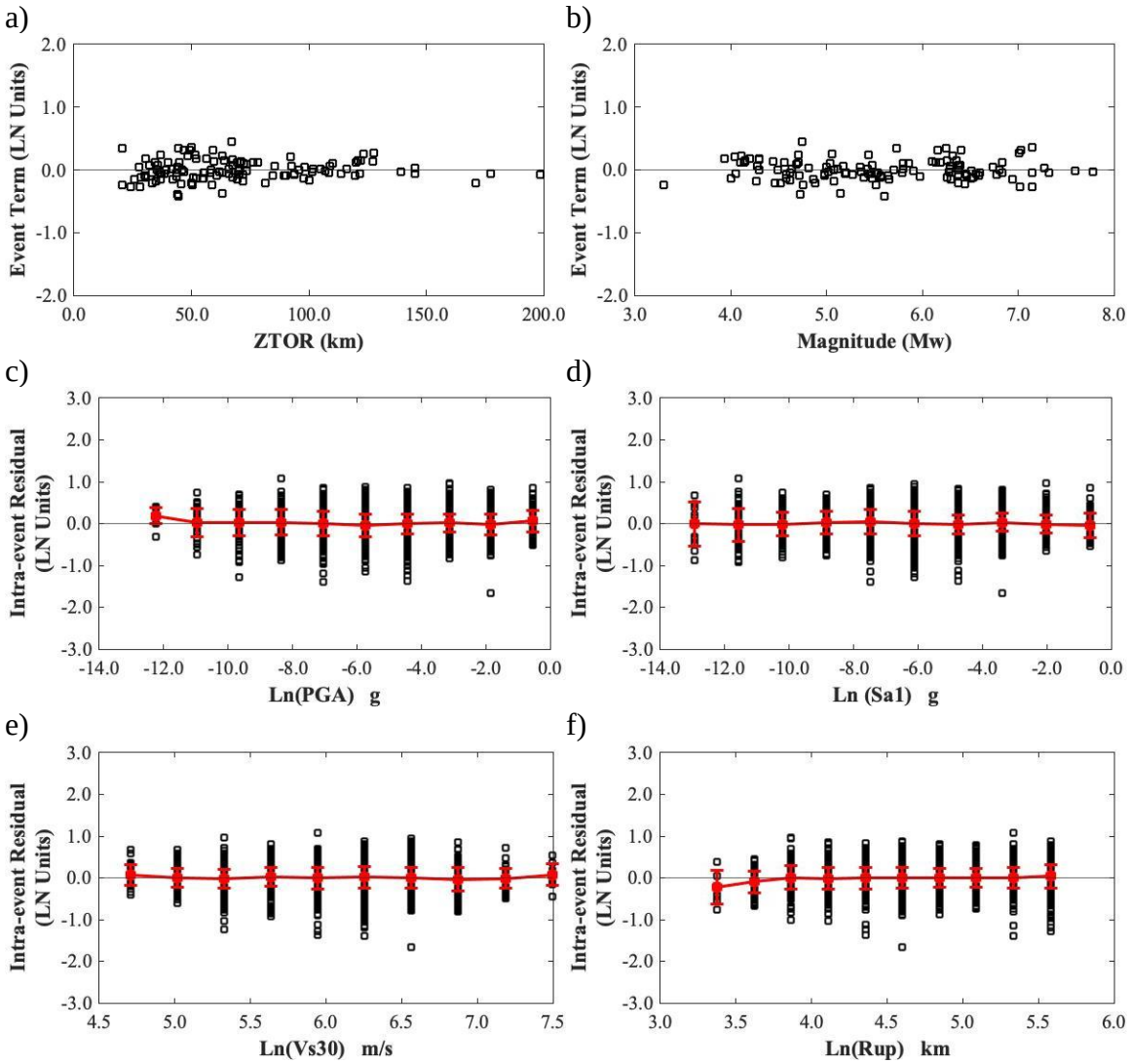

Figure 3-3 Residuals of the conditional model for *CAV* in subduction intraslab settings. Between residuals for a) *ZTOR*, b) Magnitude (*Mw*). Within residuals for c) *PGA*, d) *Sa1*, e) *Vs30*, f) Rupture distance.

3.4 Scenario-based Models for *CAV*

By combining the CGMM in the previous section with traditional GMMs for *PGA* and *Sa1*, a suite of scenario-based models can be established. Five scenario-based models for *CAV* are developed using the GMMs for *PGA* and *Sa1* from BCHydro2016 (Abrahamson et al., 2016b), BCHydro2018 (Abrahamson et al., 2018), Atkinson and Boore (2003, 2008), Zhao et al. (2006), and Montalva et al. (2017). The median and standard deviation of *CAV* for a given earthquake scenario can be estimated using Equation 3, Equation5, and Equation 6 in Chapter 2.

For example, the PGA_{med} and $Sa1_{med}$ can be estimated through Equation 8 and 9 when BCHydro2016 (Abrahamson et al., 2016b) is used:

$$\begin{aligned} Ln\left(Sa_{interface}\right) &= \theta_1 + \theta_4 \Delta C_1 \\ &+ \left(\theta_2 + \theta_3(M_w - 7.8)\right) Ln\left(R_{rup} + C_4 \exp\left(\theta_9(M_w - 6)\right)\right) \\ &+ \theta_6 R_{rup} + f_{mag}(M_w) + f_{FABA}\left(R_{rup}\right) \\ &+ f_{site}(PGA_{1100}, V_{S30}) \end{aligned} \tag{8}$$

$$\begin{aligned} Ln(Sa_{slab}) &= \theta_1 + \theta_4 \Delta C_1 \\ &+ \left(\theta_2 + \theta_{14} F_{event} + \theta_3(M_w - 7.8)\right) Ln\left(R_{hypo}\right. \\ &+ C_4 \exp\left(\theta_9(M_w - 6)\right)\Big) + \theta_6 R_{hypo} + \theta_{10} F_{event} \\ &+ f_{mag}(M_w) + f_{depth}(Z_n) + f_{FABA}\left(R_{hypo}\right) \\ &+ f_{site}(PGA_{1100, V_{S30}}) \end{aligned} \tag{9}$$

where Sa is the spectral acceleration ($PGA_{med} = Sa$ at period= 0s, $Sa1_{med} = Sa$ at period= 1.0s) in units of g; θ_1 to θ_{10}, ΔC_1, and C_4 are period-dependent coefficients of the model; R_{hypo} is the hypocenter distance; PGA_{1100} is the median *PGA* for V_{s30} 1000 m/s; and f_{mag}, f_{FABA}, f_{site}, and f_{depth} are additional functions for the magnitude scaling, forearc/backarc scaling, nonlinear site scaling, and depth scaling, respectively, proposed by Abrahamson et al. (2016b). The other parameters were defined previously.

Standard deviation for interface settings can be calculated using the following equation:

$$\sigma_{LnCAV_{interface}} = \sqrt{0.1105 + 0.3969 \times \sigma_{lnPGA}^2 + 0.0289 \times \sigma_{lnSa1}^2 + 0.2142 \times \rho[\varepsilon_{LnPGA}, \varepsilon_{LnSa1}] \times \sigma_{LnPGA}\sigma_{LnSa1}} \quad (10)$$

in which $\rho[\varepsilon_{LnPGA}, \varepsilon_{LnSa1}]$ = 0.52, σ_{LnPGA} and σ_{LnSa1} are the standard deviations given by BCHydro2016 (Abrahamson et al., 2016b).

3.5 Model Trends

3.5.1 Interface Model Trends

The five scenario-based models for *CAV* are compared with existing GMMs for *CAV* to assess model trends in terms of magnitude and distance.

Figure 3-4 shows the distance scaling comparisons for the developed scenario-based *CAV* models, considering different earthquake scenarios (M_w values of 5.7, 6.5, 7.4, 8.2), site conditions (V_{s30}=760/s), and a focal depth of 20 km. The scenario-based models are developed using the coefficients listed in Table 2. Two traditional GMMs for *CAV* such as FG2015 (Foulser-Piggott and Goda 2015), Bea2017 (Bullock et al. 2017) are included.

The distance scaling of the scenario-based *CAV* models developed with GMMs from BCHydro2016 (Abrahamson et al., 2016b), BCHydro2018 (Abrahamson et al., 2018), Atkinson and Boore (2003, 2008), Zhao et al. (2006), and Montalva et al. (2017) are close to each other in these four plots; the estimates of scenario-based models are well conformed with and centered amongst historical data; however, the traditional model Bea2017 is always underestimating *CAV,* because of its rock site dataset. The non-conditional model FG2015 shows similar behavior as that of shallow crustal settings: it exhibits larger

estimates in small distances. The lack of appropriate constraints at small distances and large magnitudes could have caused the unreasonable extrapolation of FG2015.

Figure 3-5 shows the comparison of the distance scaling of the standard deviations for the developed-based models and non-conditional models. The non-conditional model Bea2017 has the lowest standard deviation in all earthquake scenarios, this may be caused by its exclusive rock site dataset, while other models are developed using all kinds of site conditions. The scenario-based models have similar standard deviations from 0.55 to 0.7, where the scenario-based model using Z2006 has the lowest standard deviations in most earthquake scenarios, while MBR2017 has the largest standard deviation among all scenario-based models. Figure 3-7 shows the comparison of the magnitude scaling of standard deviations, where MBR2017 also has the largest standard deviation of 0.7, and bea2017 has the lowest standard deviation.

Figure 3-6 shows the magnitude scaling comparisons for the developed scenario-based *CAV* models, considering different earthquake scenarios (R_{rup}values of 80 km and 250 km), site conditions (V_{s30} 760m/s) and a focal depth of 20 km. FG2015 shows a linear scaling against magnitude which is different from all other models, magnitude saturation may not be considered in its model development; remaining scenario-based models and non-conditional models have highly consistent scaling among all magnitudes with historic data.

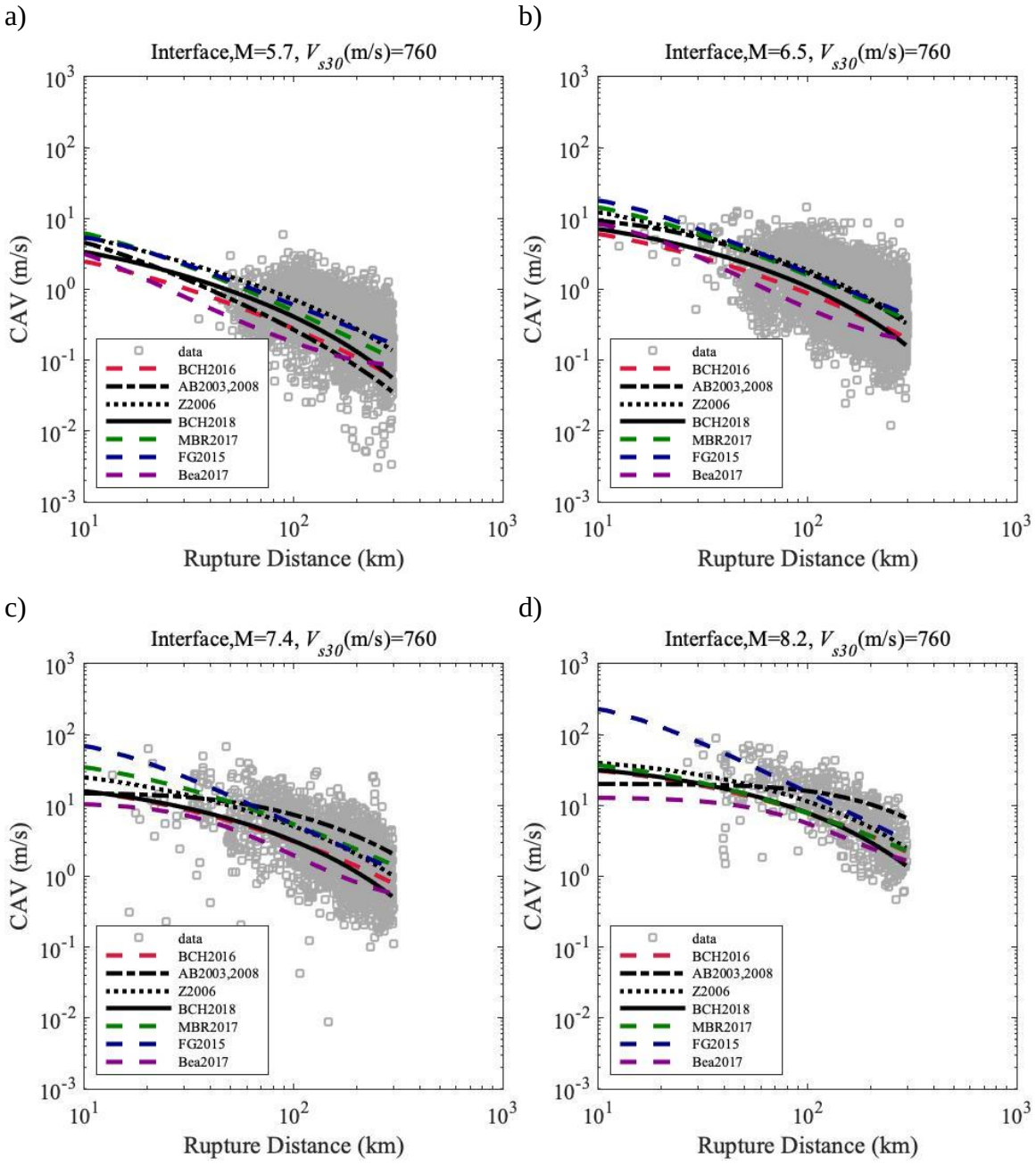

Figure 3-4 Comparisons of distance scaling of median *CAV* estimate for scenario-based *CAV* models developed in this study, and for non-conditional *CAV* GMMs. a) M_w = 5.7, V_{s30} = 760 m/s, b) M_w = 6.5, V_{s30} = 760 m/s, c) Mw = 7.4, V_{s30} = 760 m/s, d) M_w = 8.2, V_{s30} = 760 m/s. Spectral acceleration models: BCHydro2016 (Abrahamson et al., 2016b), BCHydro2018 (Abrahamson et al., 2018), Atkinson and Boore (2003, 2008), Zhao et al. (2006), and Montalva et al. (2017). Non-conditional *CAV* GMMs: FG2015 (Foulser-Piggott and Goda 2015), Bea2017 (Bullock et al. 2017).

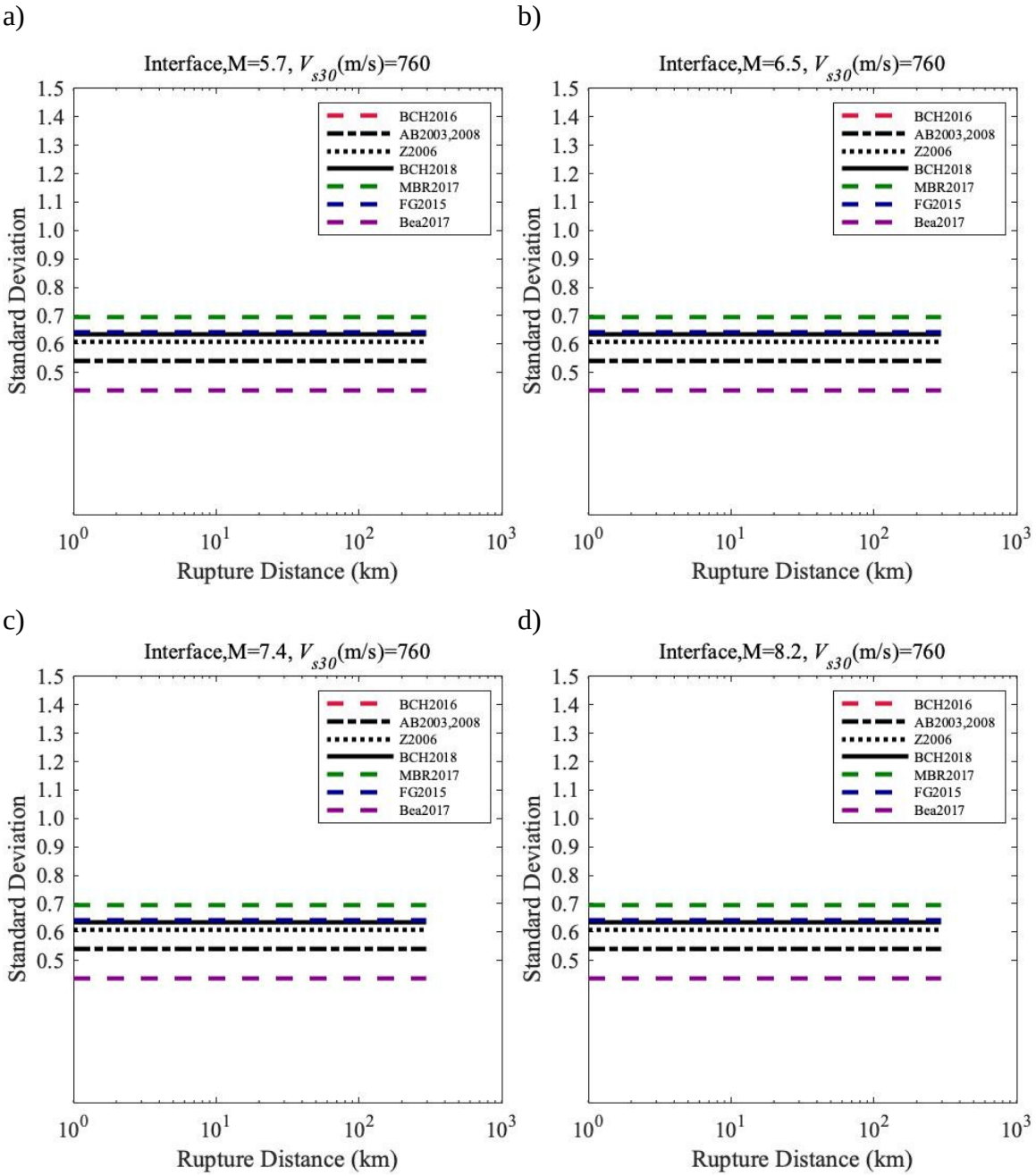

Figure 3-5 Comparisons of standard deviations against rupture distance of the five scenario-based models developed in previous section and non-conditional models for *CAV*. a) M_w = 5.7, V_{s30} = 760 m/s, b) M_w = 6.5, V_{s30} = 760 m/s, c) M_w = 7.4, V_{s30} = 760 m/s, d) M_w = 8.2, V_{s30} = 760 m/s. Spectral acceleration models: BCHydro2016 (Abrahamson et al., 2016b), BCHydro2018 (Abrahamson et al., 2018), Atkinson and Boore (2003, 2008), Zhao et al. (2006), and Montalva et al. (2017). Non-conditional *CAV* GMMs: FG2015 (Foulser-Piggott and Goda 2015), Bea2017 (Bullock et al. 2017).

a) b)

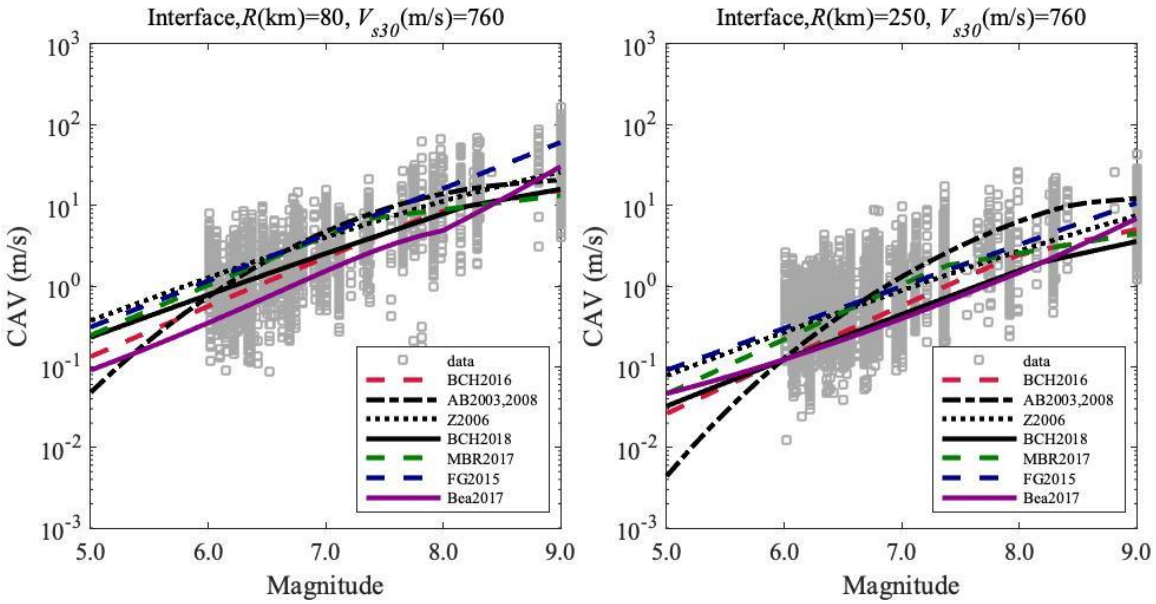

Figure 3-6 Comparisons of magnitude scaling for estimates of median *CAV* by scenario-based models and non-conditional models. (a) Rupture distance 80 km, V_{s30} 760 m/s, (b) Rupture distance 250 km, V_{s30} 760 m/s. Spectral acceleration models: BCHydro2016 (Abrahamson et al., 2016b), BCHydro2018 (Abrahamson et al., 2018), Atkinson and Boore (2003, 2008), Zhao et al. (2006), and Montalva et al. (2017). Non-conditional *CAV* GMMs: FG2015 (Foulser-Piggott and Goda 2015), Bea2017 (Bullock et al. 2017).

a) b)

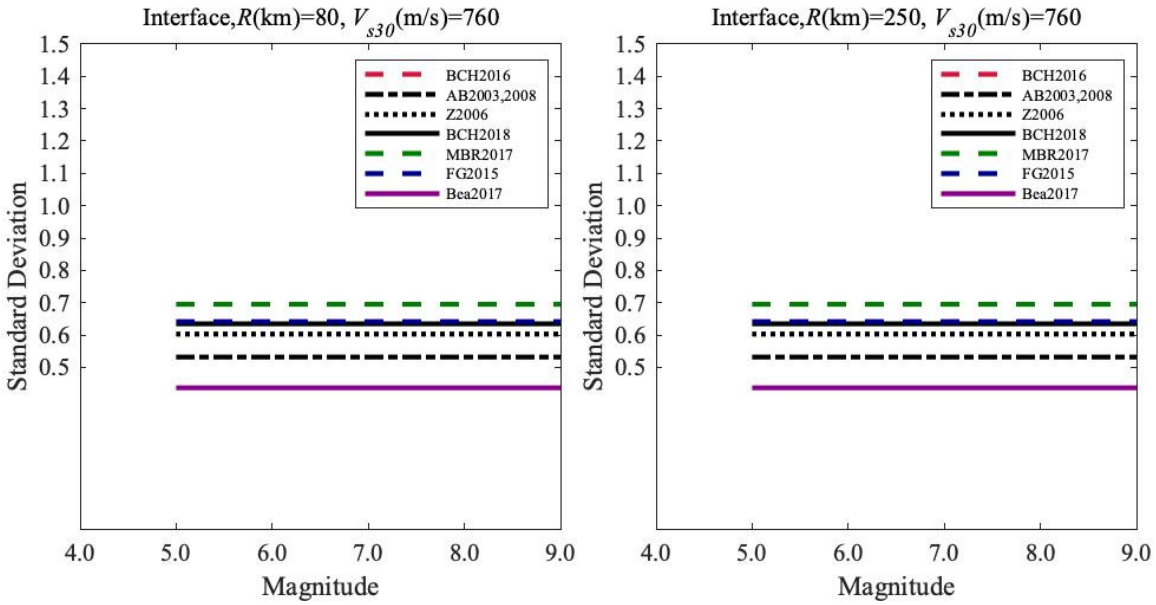

Figure 3-7 Comparisons of standard deviations against magnitude of the five scenario-based models developed in previous section and non-conditional models for *CAV*. (a) Rupture distance 80 km, *Vs30* 760 m/s, (b) Rupture distance 250 km, *Vs30* 760 m/s. Spectral acceleration models: BCHydro2016 (Abrahamson et al., 2016b), BCHydro2018 (Abrahamson et al., 2018), Atkinson and Boore (2003, 2008), Zhao et al. (2006), and Montalva et al. (2017). Non-conditional *CAV* GMMs: FG2015 (Foulser-Piggott and Goda 2015), Bea2017 (Bullock et al. 2017).

3.5.2 ***Intraslab Model Trends***

The five scenario-based models for *CAV* are compared with existing GMMs for *CAV* to assess model trends in terms of magnitude and distance.

Figure 3-8 shows the distance scaling comparisons for the developed scenario-based *CAV* models, considering different earthquake scenarios ($M_w$values of 4.5, 5, 6, 7), site conditions (V_{s30}=760/s), and a focal depth of 20 km. The scenario-based models are developed using the coefficients listed in Table 2. Two traditional GMMs for *CAV* such as FG2015 (Foulser-Piggott and Goda 2015), Bea2017 (Bullock et al. 2017) are included. The distance scaling of the scenario-based *CAV* models developed with GMMs from BCHydro2016 (Abrahamson et al., 2016b), BCHydro2018 (Abrahamson et al., 2018), Atkinson and Boore (2003, 2008), Zhao et al. (2006), and Montalva et al. (2017) are close to each other in these four plots; the estimates of scenario-based models are well conformed with and centered amongst historical data; however, the traditional model Bea2017 is always underestimating *CAV*, because of its rock site dataset.

Figure 3-9 shows the comparison of the distance scaling of the standard deviations for the developed-based models and non-conditional models. The non-conditional model Bea2017 has the lowest standard deviation in all earthquake scenarios, this may be caused by its exclusive rock site dataset, while other models are developed using all kinds of site conditions. The scenario-based models have similar standard deviations from 0.55 to 0.68, where the scenario-based model using AB2003,2008 has the lowest standard deviations in most earthquake scenarios, while MBR2017 has the largest standard deviation among all scenario-based models. Figure 3-11 shows the comparison of the magnitude scaling of

standard deviations, where MBR2017 also has the largest standard deviation of 0.7, and bea2017 has the lowest standard deviation.

Figure 3-10 shows the magnitude scaling comparisons for the developed scenario-based *CAV* models, considering different earthquake scenarios (R_{rup}values of 80 km and 250 km), site conditions (V_{s30} 760m/s) and a focal depth of 20 km. Bea2017 again underestimates the *CAV* value and its trend is lower than all models; scenario-based models are centered among historical data, which means the magnitude scaling is well captured by the model.

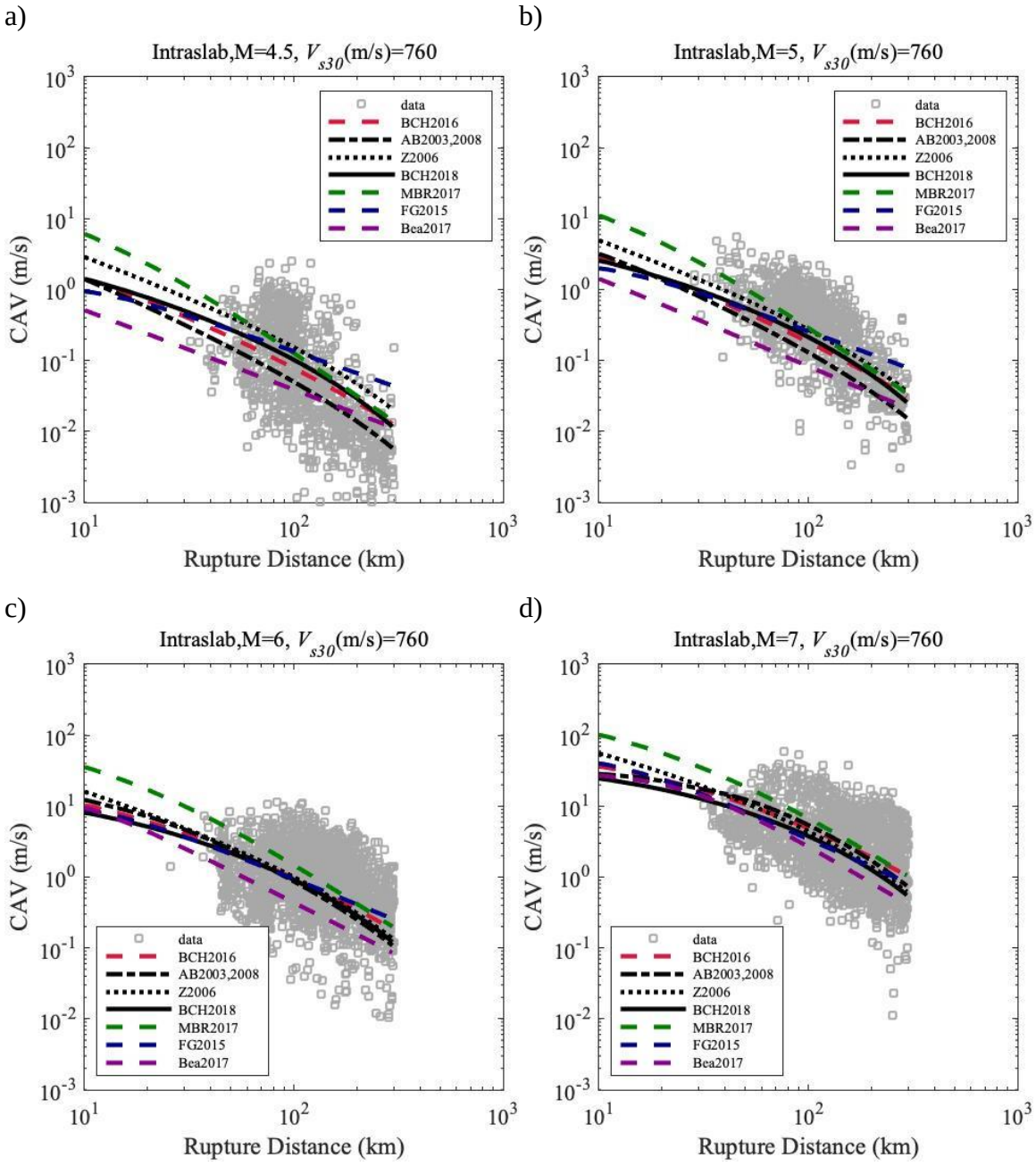

Figure 3-8 Comparisons of distance scaling of median *CAV* estimate for scenario-based CAV models developed in this study, and for non-conditional *CAV* GMMs. a) M_w = 4.5, V_{s30} = 760 m/s, b) M_w = 5, V_{s30} = 760 m/s, c) M_w = 6, V_{s30} = 760 m/s, d) M_w = 7, V_{s30} = 760 m/s. Spectral acceleration models: BCHydro2016 (Abrahamson et al., 2016b), BCHydro2018 (Abrahamson et al., 2018), Atkinson and Boore (2003, 2008), Zhao et al. (2006), and Montalva et al. (2017). Non-conditional *CAV* GMMs: FG2015 (Foulser-Piggott and Goda 2015), Bea2017 (Bullock et al. 2017).

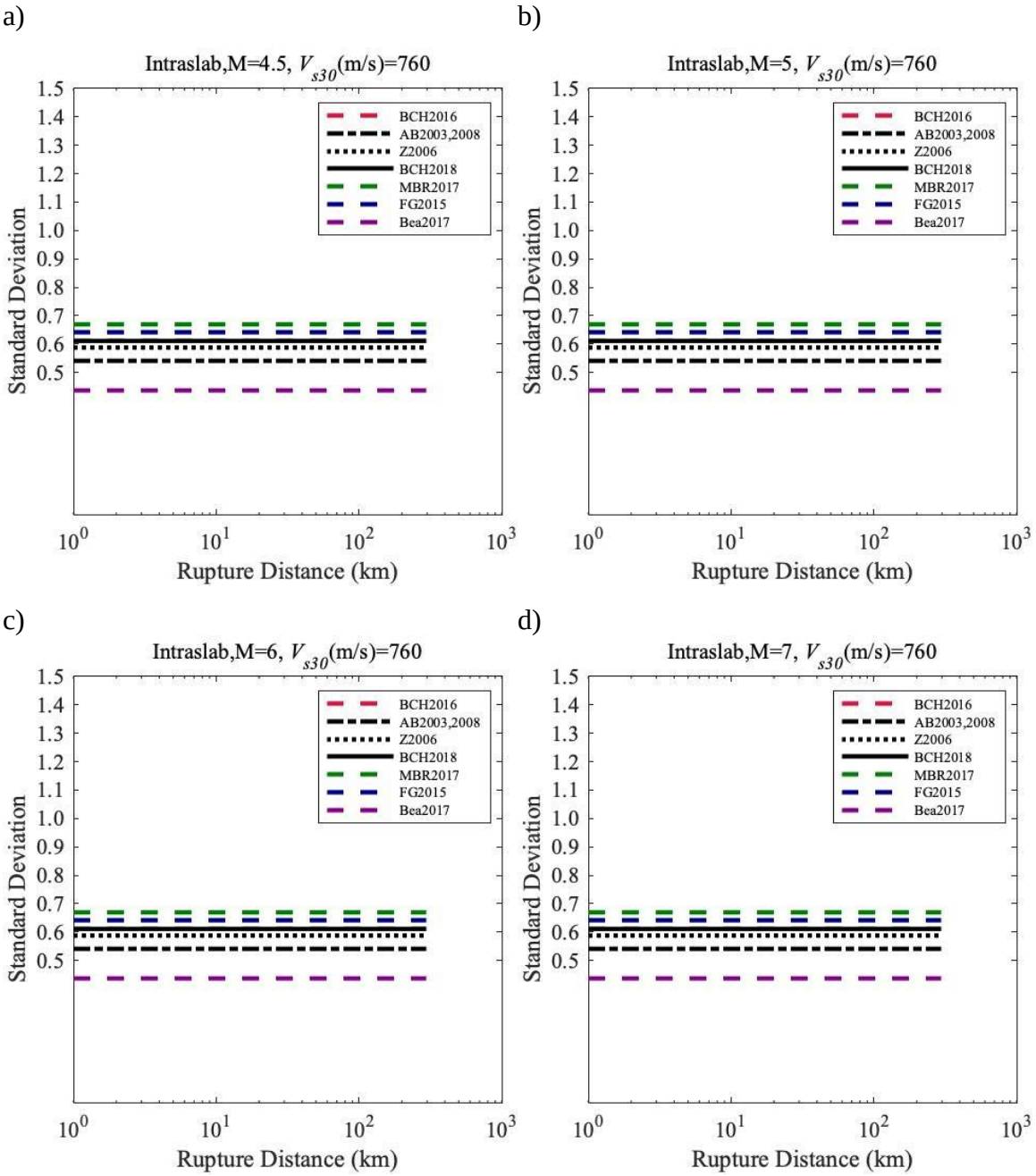

Figure 3-9 Comparisons of standard deviations against rupture distance of the five scenario-based models developed in previous section and non-conditional models for *CAV*. a) *Mw* = 4.5, V_{s30} = 760 m/s, b) M_w = 5, V_{s30} = 760 m/s, c) M_w = 6, V_{s30} = 760 m/s, d) M_w = 7, V_{s30} = 760 m/s. Spectral acceleration models: BCHydro2016 (Abrahamson et al., 2016b), BCHydro2018 (Abrahamson et al., 2018), Atkinson and Boore (2003, 2008), Zhao et al. (2006), and Montalva et al. (2017). Non-conditional *CAV* GMMs: FG2015 (Foulser-Piggott and Goda 2015), Bea2017 (Bullock et al. 2017).

a) b)

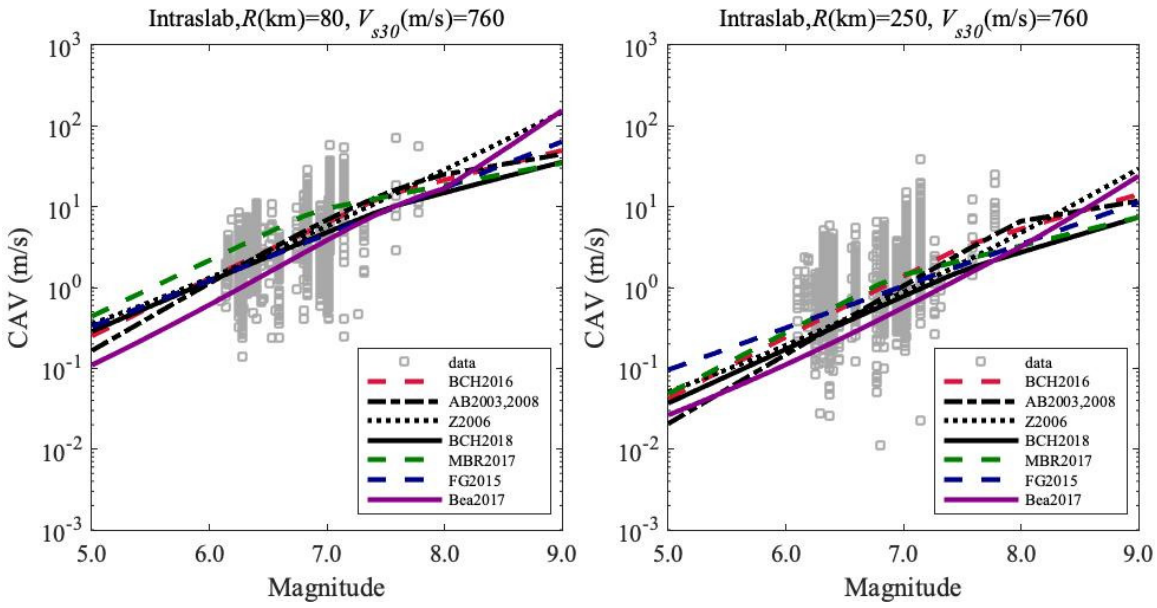

Figure 3-10 Comparisons of magnitude scaling for estimates of median *CAV* by scenario-based models and non-conditional models. (a) Rupture distance 80 km, V_{s30} 760 m/s, (b) Rupture distance 250 km, V_{s30} 760 m/s. Spectral acceleration models: BCHydro2016 (Abrahamson et al., 2016b), BCHydro2018 (Abrahamson et al., 2018), Atkinson and Boore (2003, 2008), Zhao et al. (2006), and Montalva et al. (2017). Non-conditional *CAV* GMMs: FG2015 (Foulser-Piggott and Goda 2015), Bea2017 (Bullock et al. 2017).

a) b)

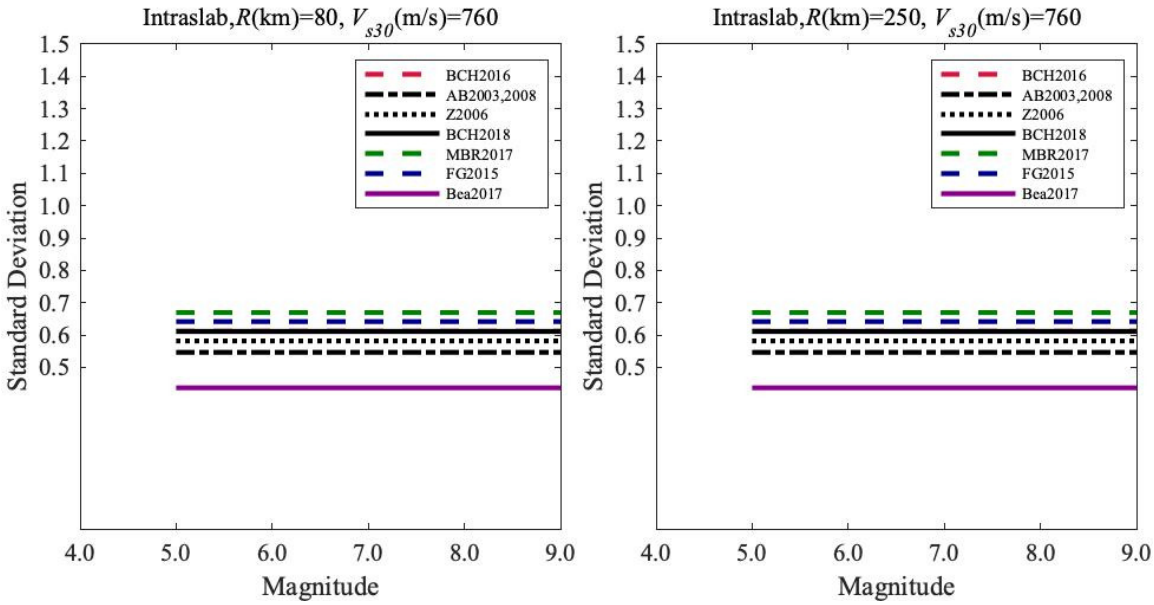

Figure 3-11 Comparisons of standard deviations against magnitude of the five scenario-based models developed in previous section and non-conditional models for *CAV*. (a) Rupture distance 80 km, V_{s30} 760 m/s, (b) Rupture distance 250 km, V_{s30} 760 m/s.

3.6 Conditional Ground Motion Model for *PGV* in Subduction Zones

The functional form of the conditional model is given by Equation 11. R_{rup} is included as the proxy for distance, T_{PGV} and *PSA* are included as proxies for amplitude, duration and frequency content.

$$\ln(PGV) = a_1 + a_2(M-6) + a_6(M_1 - M)^2 + f_1(M)\ln\left(PSA(T_{PGV})\right) + a_4\ln\left(R_{rup} + 5e^{(0.4(M-6))}\right) + a_7 R_{rup} \tag{11}$$

where M is the magnitude, R_{rup} is the rupture distance, and *PSA* is the 5%damped spectral acceleration in g, T_{PGV} is the spectral period at which the strongest correlation between *PSA* and *PGV* occurs, $a_1 \sim a_7$ are coefficients. With preliminary regressions, a_7 is found to be statistically insignificant, thus it was fixed to zero. $f_1(M)$ is a magnitude dependent term that accounts for the magnitude dependence of the difference in aleatory standard deviations between ln (PGV) and ln $(PSA(T_{PGV}))$. The functional form considered for $f_1(M)$ is shown below:

$$f_1(M) = \begin{cases} a_3, & for\ M < 5 \\ a_3 + (a_5 - a_3)/2.5 \times (M-5), & , \quad for\ 5 \le M \le 7.5 \\ a_5, & for\ M > 7.5 \end{cases} \tag{12}$$

The M_1 term is set to 10 according to the functional form which Abrahamson (2016b) used for subduction earthquakes. According to Abrahamson and Bashin (2019), the finite-fault term is fixed as $5e^{(0.4(M-6))}$ using horizontal component data in shallow crustal zones.

The function form for T_{PGV} was considered magnitude dependent according to the following equation:

$$T_{PGV} = \mathrm{b}_1 + b_2\mathrm{M} \quad (13)$$

In order to determine the *b1* and *b2*, the data set was divided into 6 equally spaced magnitude bins to find the spectral period that results in the strongest correlation between *PSA* and *PGV*. *PSA* at different periods was regressed against *PGV* within each magnitude bins; then the regression with the smallest standard deviation was identified. The identified spectral period for the considered magnitude bin is T_{PGV}. Using the estimated T_{PGV} values for all magnitude bins, T_{PGV} was regressed against magnitude to determine *b1* and *b2*. The procedure mentioned above was performed separately for subduction interface and intrastate settings, the results are shown in Table 3, Table 4 and Figure 3-12.

Table 3 – Coefficients for T_{PGV}-Magnitude Relationship

	b1	*b2*
Interface	-2.243	0.273
Intraslab	-2.188	0.222

Table 4 – Coefficients for Conditional PGV Model

	a1	*a2*	*a3*	*a4*	*a5*	*a6*	*a7*
Interface	5.962	0.012	0.764	-0.406	0.627	-0.072	0.000
Intraslab	4.572	0.750	0.819	-0.470	0.668	0.026	0.000

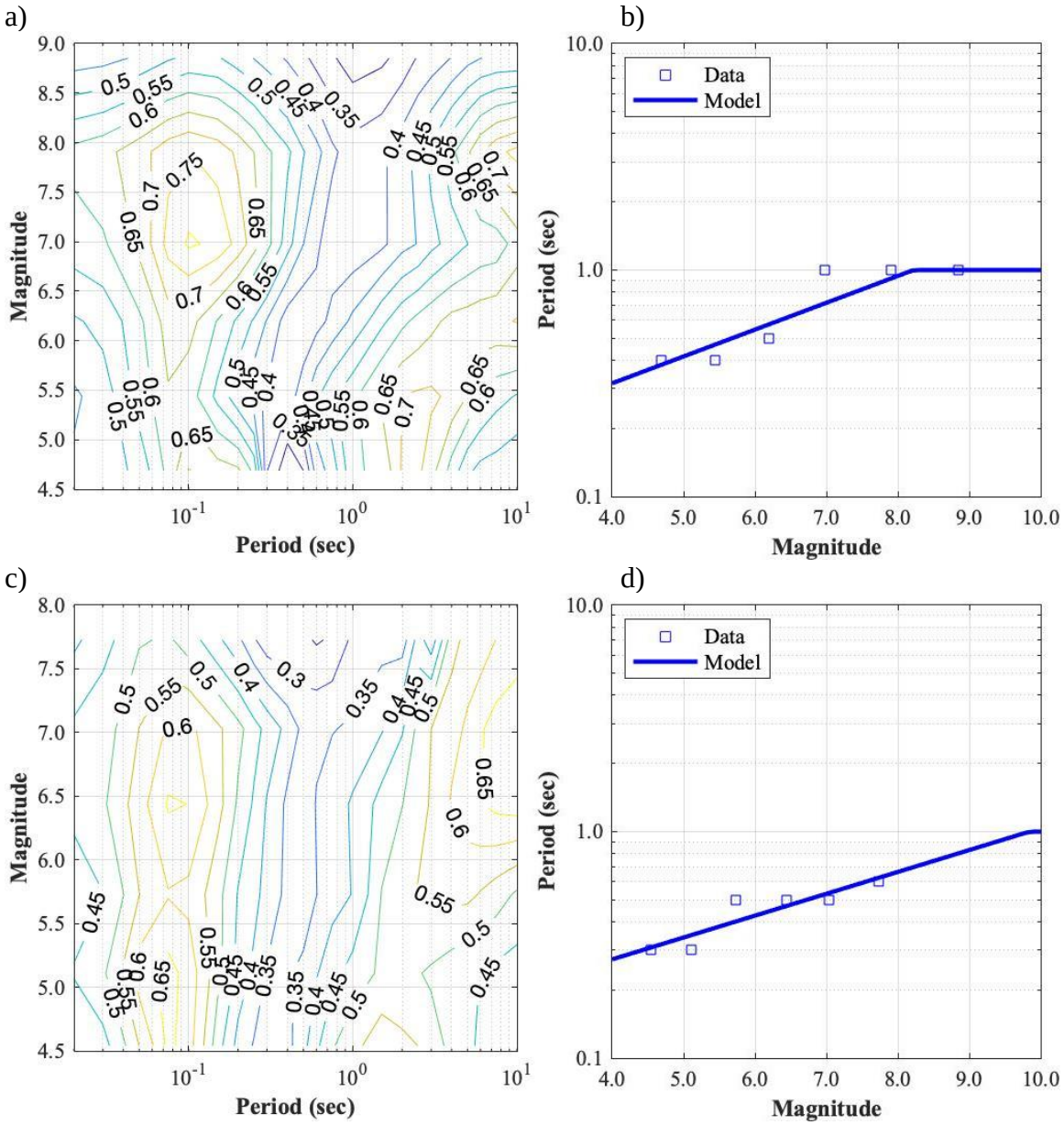

Figure 3-12 Standard deviation contours and magnitude scaling of T_{PGV}. a) (interface) standard deviation contours of regressions; b) (interface) magnitude dependence of T_{PGV} ; c) (intraslab) standard deviation contours of regressions; d) (intraslab) magnitude dependence of T_{PGV}.

In Table 3, *b2* is positive both in interface and intraslab settings, indicating that T_{PGV} has a positive dependence on magnitude. According to Table 4, the magnitude dependence is well captured by the functional form, but the $(M-6)$ term is statistically insignificant for interface settings; $a_7 R_{rup}$ is not statistically significant, since distance scaling is already captured by $\ln\left(R_{rup}+5e^{(0.4(M-6))}\right)$.

The CGMM residuals are shown in Figure 3-13 and Figure 3-14 as a function of the predictor parameters used in Equation 11 and also other parameters of importance. The distribution of between-residuals with respect to Magnitude (M_w) and the depth to the top of rupture (Z_{TOR}) are relatively small, indicating that the random effects for earthquakes are well captured; the between-residuals for intraslab earthquake are smaller than that of interface earthquakes. Within-event residuals are plotted against $R_{rup}$and $PSA(T_{PGV})$**.** No systematic trends are found in these plots, indicating that the model is not biased respect to these parameters, and this functional form has properly captured the dependence of *CAV* on the source, path and site conditions.

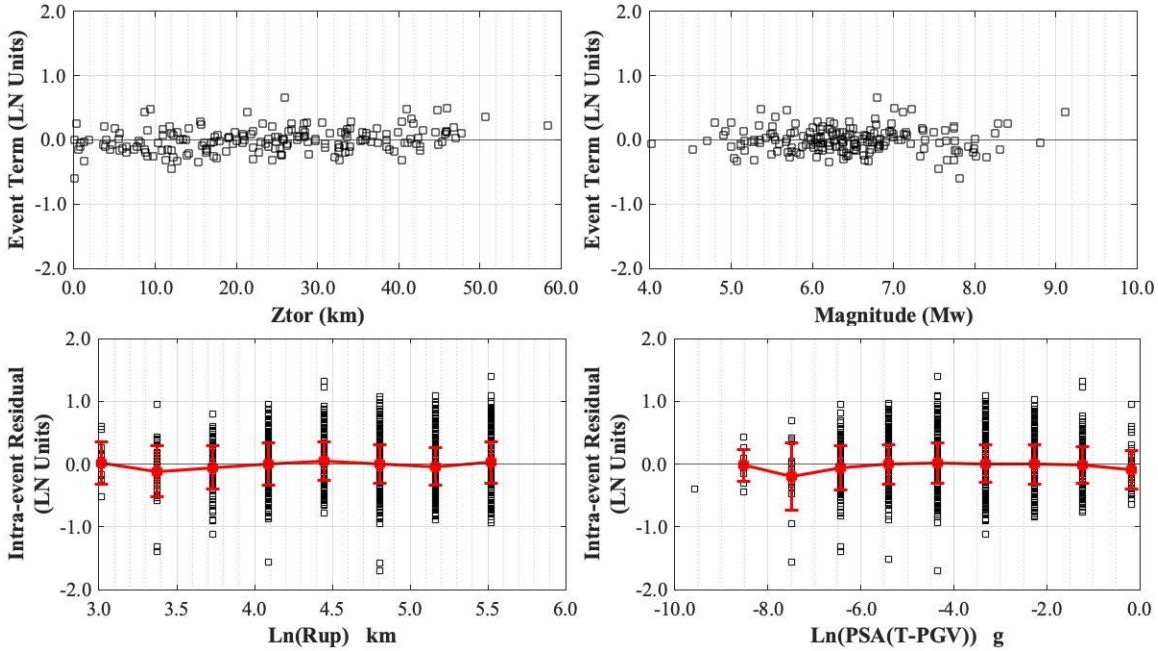

Figure 3-13 Residuals of the conditional model for *PGV* in subduction interface settings. Between residuals for a) ZTOR, b) Magnitude (M). Within residuals for c) Rup, d) $PSA(T_{PGV})$.

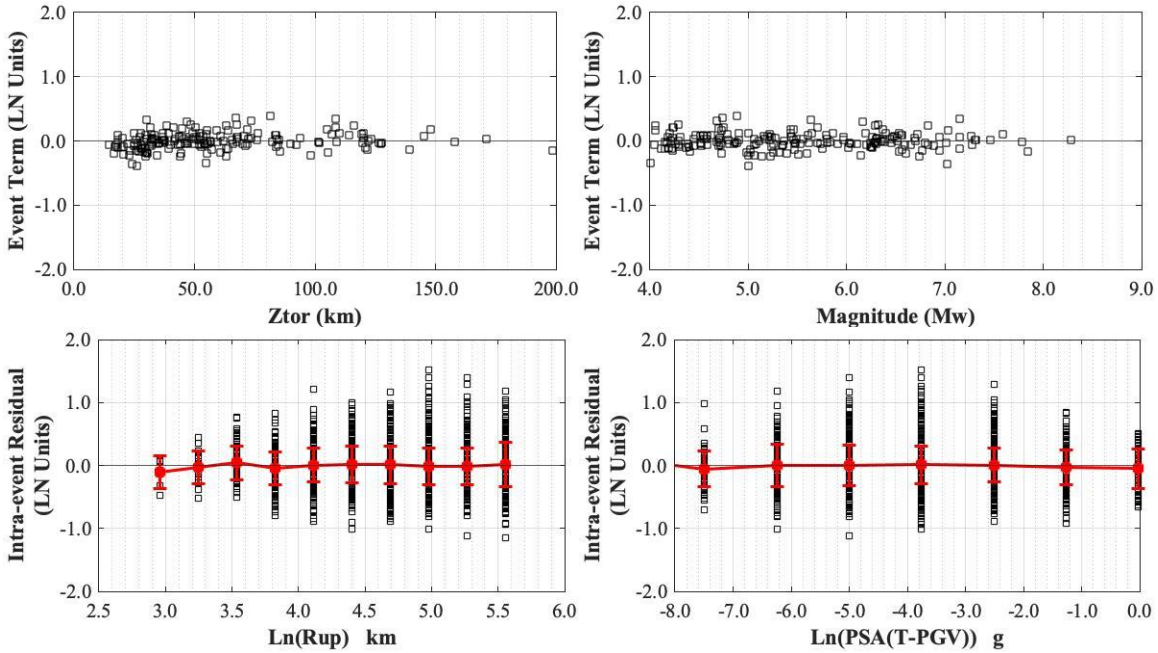

Figure 3-14 Residuals of the conditional model for *PGV* in subduction intraslab settings. Between residuals for a) ZTOR, b) Magnitude (M). Within residuals for c) Rup, d) $PSA(T_{PGV})$.

3.7 Converting to Scenario-based Model

By combining the CGMM in the previous section with traditional GMMs for *PSA*, a suite of scenario-based models can be established. Five scenario-based models for *PGV* are developed using the GMMs for *PGA* and *Sa1* from BCHydro2016 (Abrahamson et al., 2016b), BCHydro2018 (Abrahamson et al., 2018), Atkinson and Boore (2003, 2008), Zhao et al. (2006), and Montalva et al. (2017). The median and standard deviation of CAV for a given earthquake scenario can be estimated using Equation 3, Equation5, and Equation 6 in Chapter 2. An illustrative example is presented in section 3.4 using BCHydro16, other scenario-based models can be derived through the same approach.

3.8 Model Trends

3.8.1 Interface Model Trends

The five scenario-based models for *PGV* are compared plotted against in terms of magnitude and distance to examine the model trends.

Figure 3-15 shows the distance scaling comparisons for the developed scenario based *PGV* models, considering different earthquake scenarios ($M_w$values of 5.3, 6, 7, 8), site conditions (V_{s30}=760/s), and a hypocenter depth of 30 km. The scenario-based models are developed using the coefficients listed in Table 3 and Table 4.

The distance scaling of the scenario-based *PGV* models developed with GMMs from BCHydro2016 (Abrahamson et al., 2016b), BCHydro2018 (Abrahamson et al., 2018), Atkinson and Boore (2003, 2008), Zhao et al. (2006), and Montalva et al. (2017) are close to each other except for the plot of Magnitude 5.3, where AB2003,2008 diverges towards

underestimation; overall, the estimates of scenario-based models are well centered amongst historical data.

Figure 3-16 shows the comparison of the distance scaling of the standard deviations for the developed-based models. All scenario-based models have very close standard deviations except MBR2017, which has slightly higher standard deviations than others. All models have constant standard deviation with differing distances; however, standard deviations of all models slightly decrease as magnitude increases in the magnitude scaling plot (Figure 3-18). This is due to the $f_1(M)$ term in the functional form of the CGMM, where coefficients are magnitude dependent.

Figure 3-17 shows the magnitude scaling comparisons for the developed scenario based *PGV* models, considering different earthquake scenarios (R_{rup}values of 80 km and 250 km), site conditions (V_{s30} 760m/s) and a focal depth of 30 km. All scenario-based models have similar trends against magnitude, with the models centered among historical data. The scenario-based models are closer to each other at lower distance (80km) but disperse slightly at larger distances (250km), this might be caused by lack of data with large magnitudes and large distances in the NGA-SUB database.

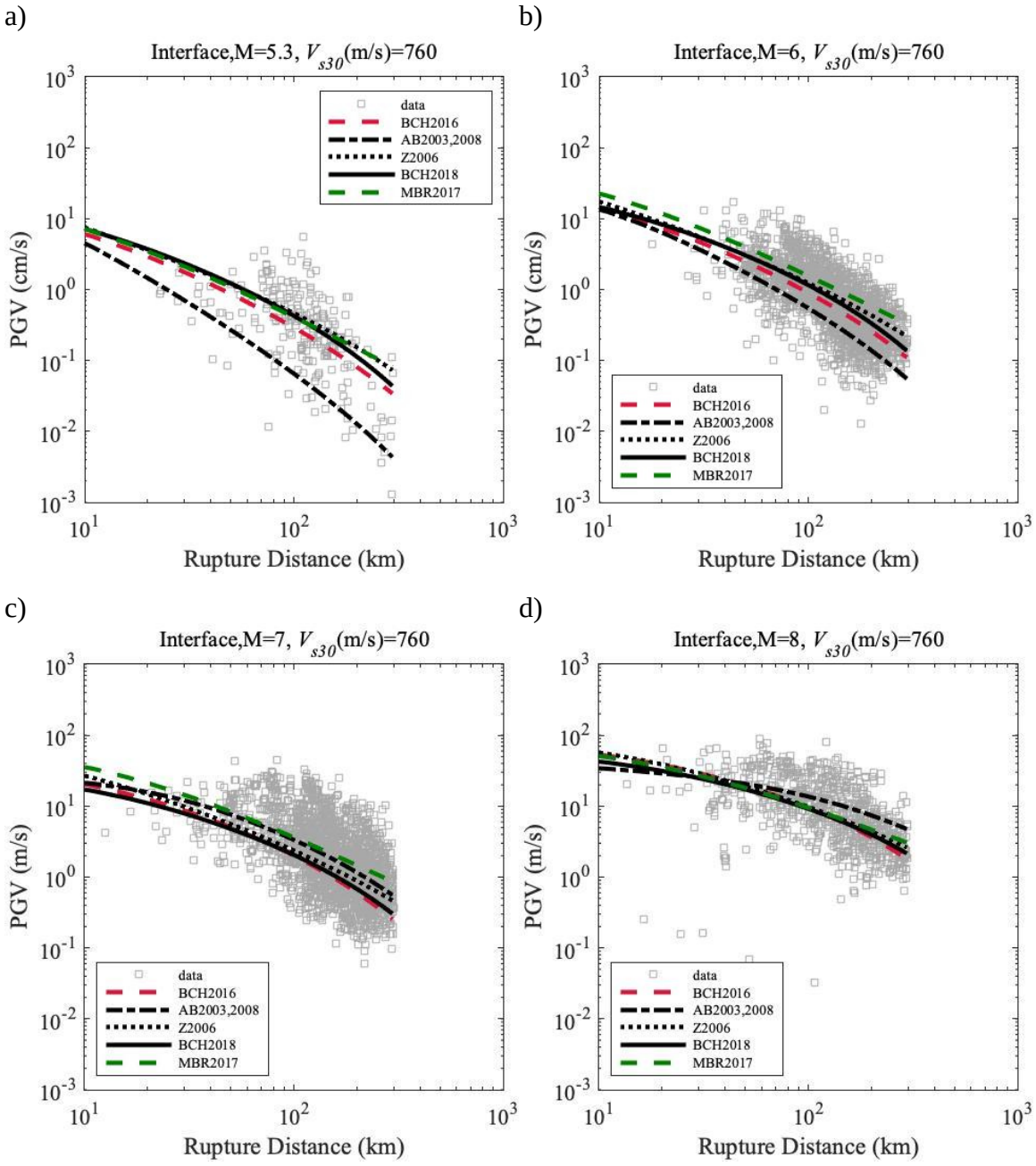

Figure 3-15 Comparisons of distance scaling of median estimate for scenario-based *PGV* models developed in this study. a) M_w = 5.3, V_{s30} = 760 m/s, b) M_w = 6, V_{s30} = 760 m/s, c) M_w = 7, V_{s30} = 760 m/s, d) M_w = 8, V_{s30} = 760 m/s. Spectral acceleration models: BCHydro2016 (Abrahamson et al., 2016b), BCHydro2018 (Abrahamson et al., 2018), Atkinson and Boore (2003, 2008), Zhao et al. (2006), and Montalva et al. (2017).

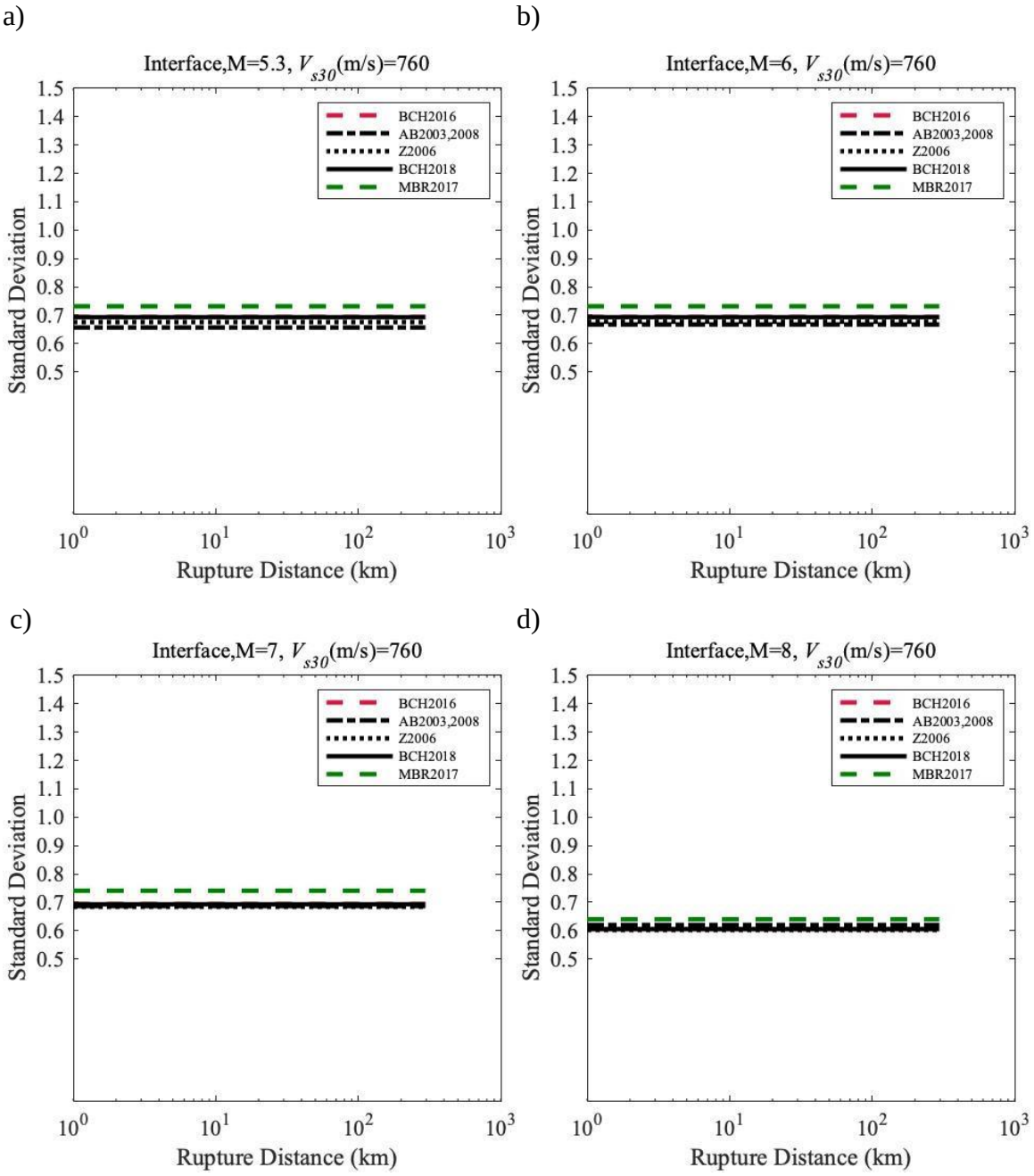

Figure 3-16 Comparisons of standard deviations against rupture distance of the five scenario-based models for *PGV* developed in previous section. a) M_w = 5.3, V_{s30} = 760 m/s, b) M_w = 6, V_{s30} = 760 m/s, c) Mw = 7, V_{s30} = 760 m/s, d) M_w = 8, V_{s30} = 760 m/s. Spectral acceleration models: BCHydro2016 (Abrahamson et al., 2016b), BCHydro2018 (Abrahamson et al., 2018), Atkinson and Boore (2003, 2008), Zhao et al. (2006), and Montalva et al. (2017).

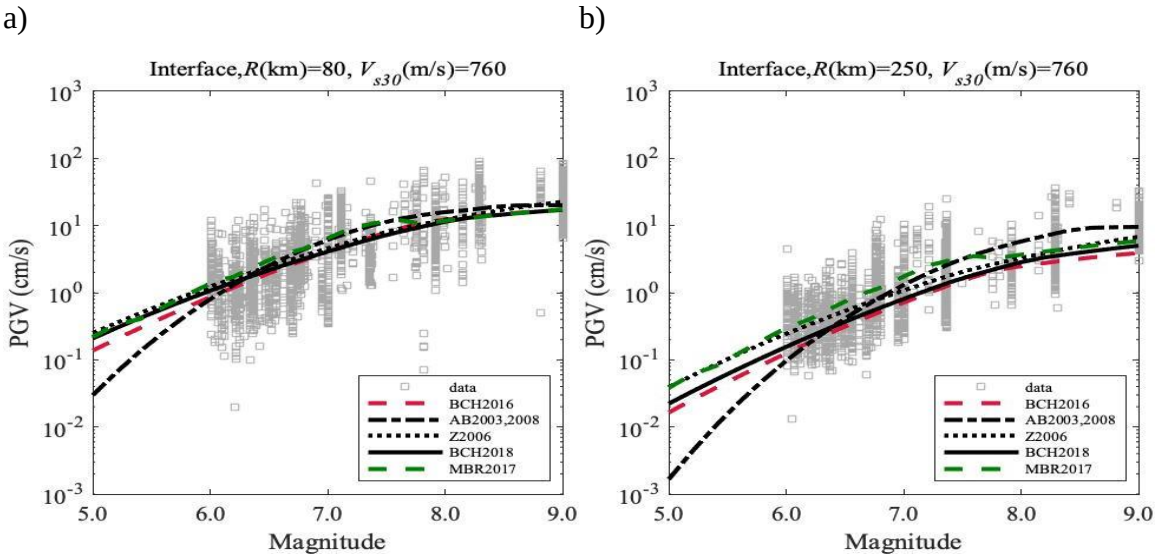

Figure 3-17 Comparisons of magnitude scaling for estimates of median *PGV* by scenario-based models and non-conditional models. (a) Rupture distance 80 km, V_{s30} 760 m/s, (b) Rupture distance 250 km, V_{s30} 760 m/s. Spectral acceleration models: BCHydro2016 (Abrahamson et al., 2016b), BCHydro2018 (Abrahamson et al., 2018), Atkinson and Boore (2003, 2008), Zhao et al. (2006), and Montalva et al. (2017).

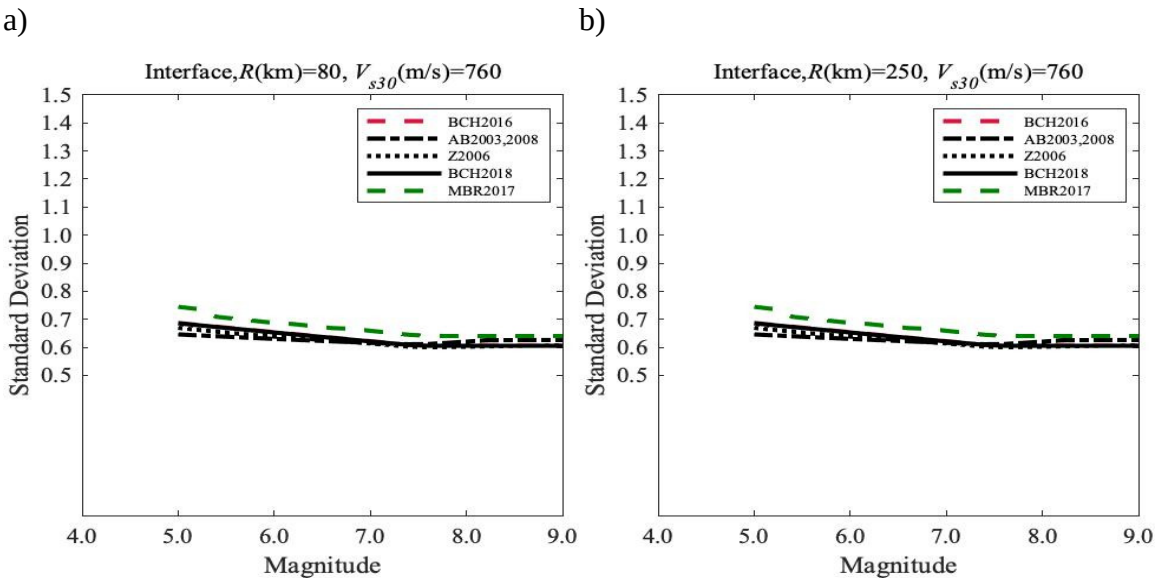

Figure 3-18 Comparisons of standard deviations against magnitude of the five scenario-based models developed in previous section and non-conditional models for *PGV*. (a) Rupture distance 80 km, V_{s30} 760 m/s, (b) Rupture distance 250 km, V_{s30} 760 m/s. Spectral acceleration models: BCHydro2016 (Abrahamson et al., 2016b), BCHydro2018 (Abrahamson et al., 2018), Atkinson and Boore (2003, 2008), Zhao et al. (2006), and Montalva et al. (2017).

3.8.2 Intraslab Model Trends

The five scenario-based models for *PGV* in intraslab settings are compared in terms of magnitude and distance to examine the model trends.

Figure 3-19 shows the distance scaling comparisons for the developed scenario based *PGV* models, considering different earthquake scenarios ($M_w$values of 5.3, 6.2, 7, 8), site conditions (V_{s30}=760/s), and a hypocenter depth of 60 km. The scenario-based models are developed using the coefficients listed in Table 3 and Table 4.

The distance scaling of the scenario-based *PGV* models developed with GMMs from BCHydro2016 (Abrahamson et al., 2016b), BCHydro2018 (Abrahamson et al., 2018), Atkinson and Boore (2003, 2008), Zhao et al. (2006), and Montalva et al. (2017) are close to each other except for the plot of Magnitude 5.3, where AB2003,2008 underestimates the *PGV* value; overall, the estimates of scenario-based models are well centered amongst historical data.

Figure 3-20 shows the comparison of the distance scaling of the standard deviations for the developed-based models. All scenario-based models have very close standard deviations except MBR2017, which has slightly higher standard deviations than others. All models have constant standard deviation with differing distances; however, standard deviations of all models slightly decrease as magnitude increases in the magnitude scaling plot (Figure 3-22). This is due to the $f_1(M)$ term in the functional form of the CGMM, where coefficients are magnitude dependent.

Figure 3-21 shows the magnitude scaling comparisons for the developed scenario based *PGV* models, considering different earthquake scenarios (R_{rup}values of 80 km and 250 km), site conditions (V_{s30} 760m/s) and a focal depth of 60 km. All scenario-based models have similar trends against magnitude, with the models centered among historical data. The scenario-based models underestimate *PGV* for magnitudes from 7.0~8.0 with distance of 250 km, which is due to the lack of data in this range.

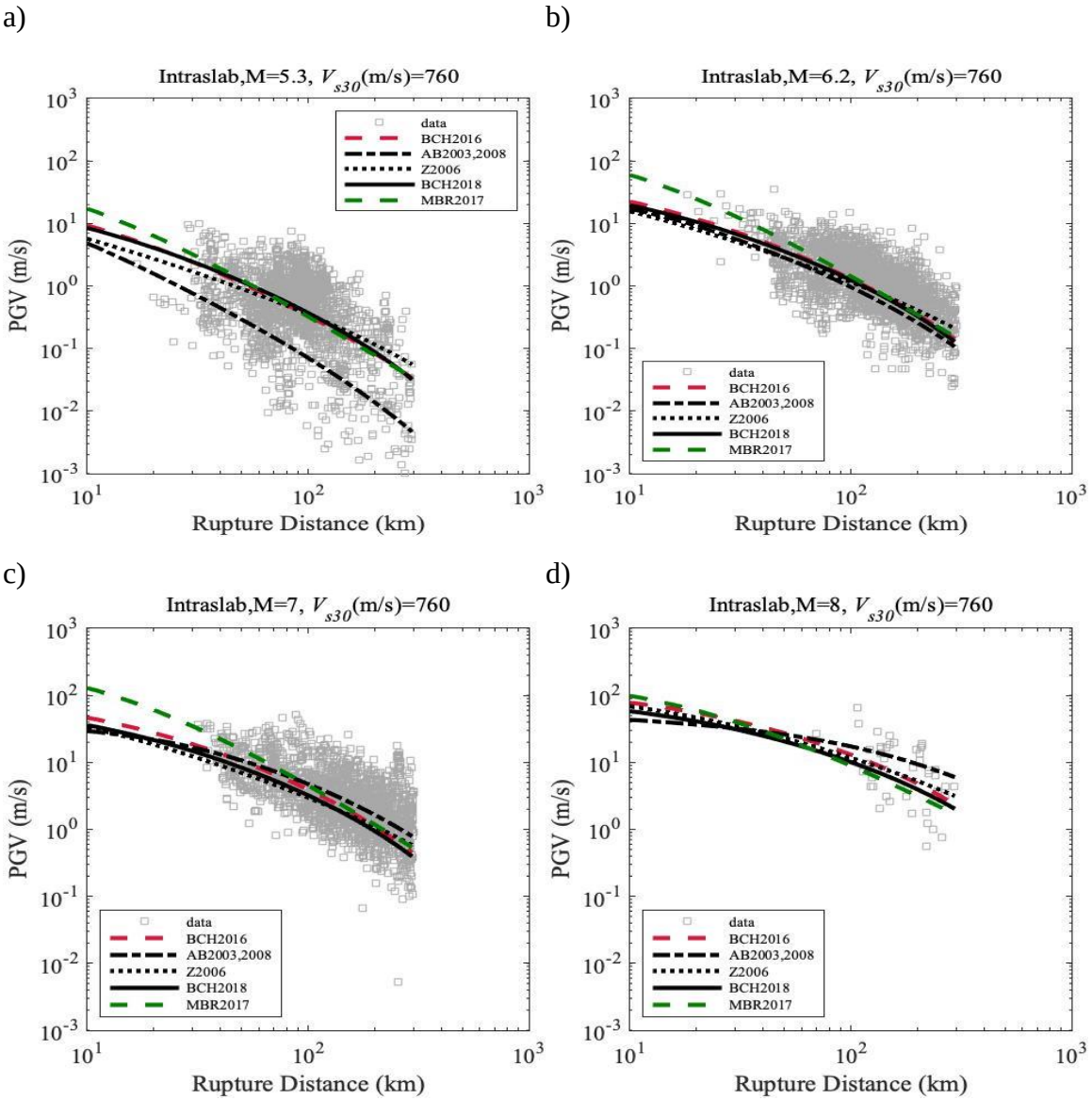

Figure 3-19 Comparisons of distance scaling of median *PGV* estimate for scenario-based *PGV* models developed in this study. a) M_w = 5.3, V_{s30} = 760 m/s, b) M_w = 6.2, V_{s30} = 760 m/s, c) M_w = 7, V_{s30} = 760 m/s, d) M_w = 8, V_{s30} = 760 m/s. Spectral acceleration models: BCHydro2016 (Abrahamson et al., 2016b), BCHydro2018 (Abrahamson et al., 2018), Atkinson and Boore (2003, 2008), Zhao et al. (2006), and Montalva et al. (2017).

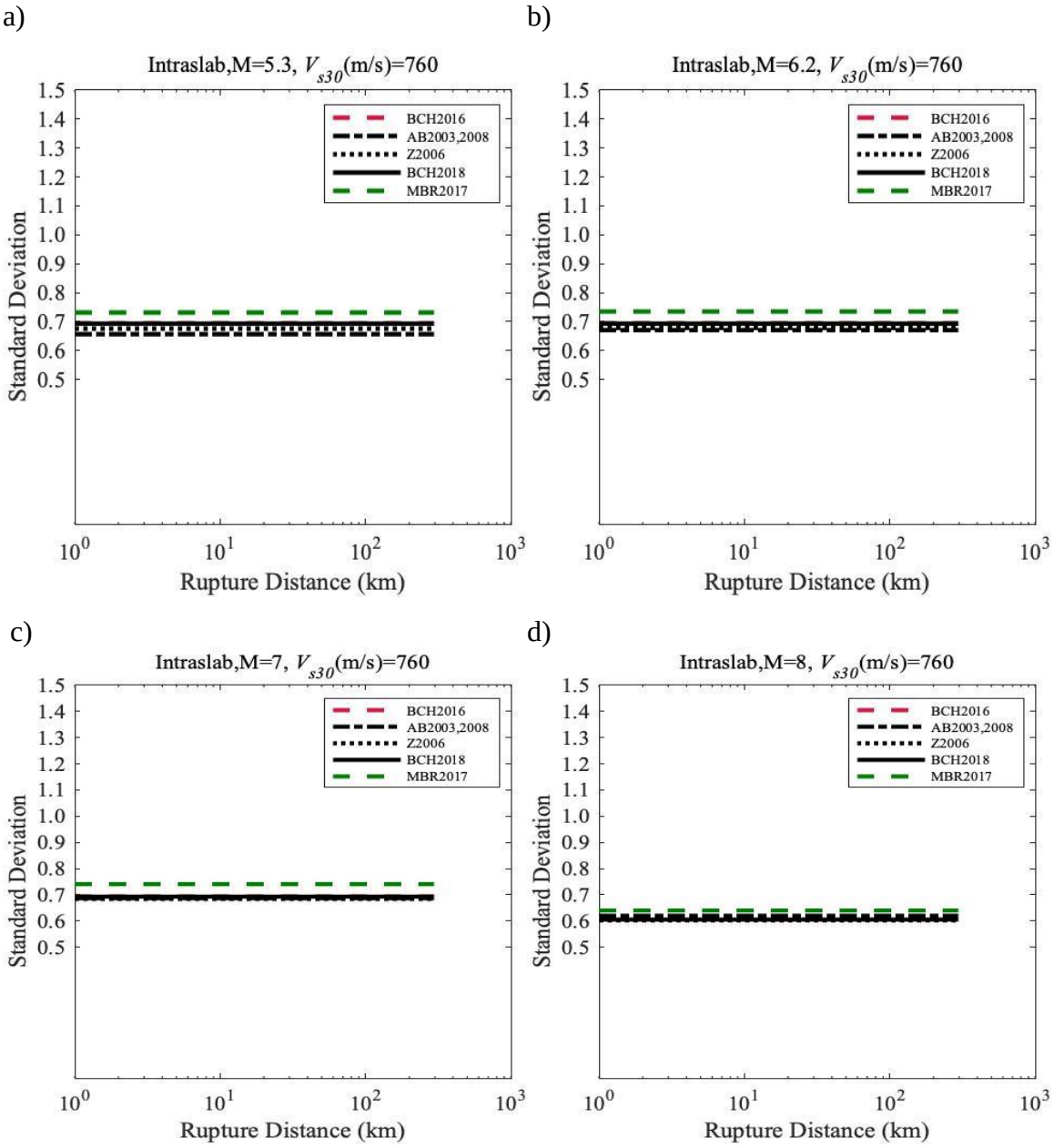

Figure 3-20 Comparisons of standard deviations against rupture distance of the five scenario-based models for *PGV* developed in previous section. a) M_w = 5.3, V_{s30} = 760 m/s, b) M_w = 6, V_{s30} = 760 m/s, c) M_w = 7, V_{s30} = 760 m/s, d) M_w = 8, V_{s30} = 760 m/s. Spectral acceleration models: BCHydro2016 (Abrahamson et al., 2016b), BCHydro2018 (Abrahamson et al., 2018), Atkinson and Boore (2003, 2008), Zhao et al. (2006), and Montalva et al. (2017).

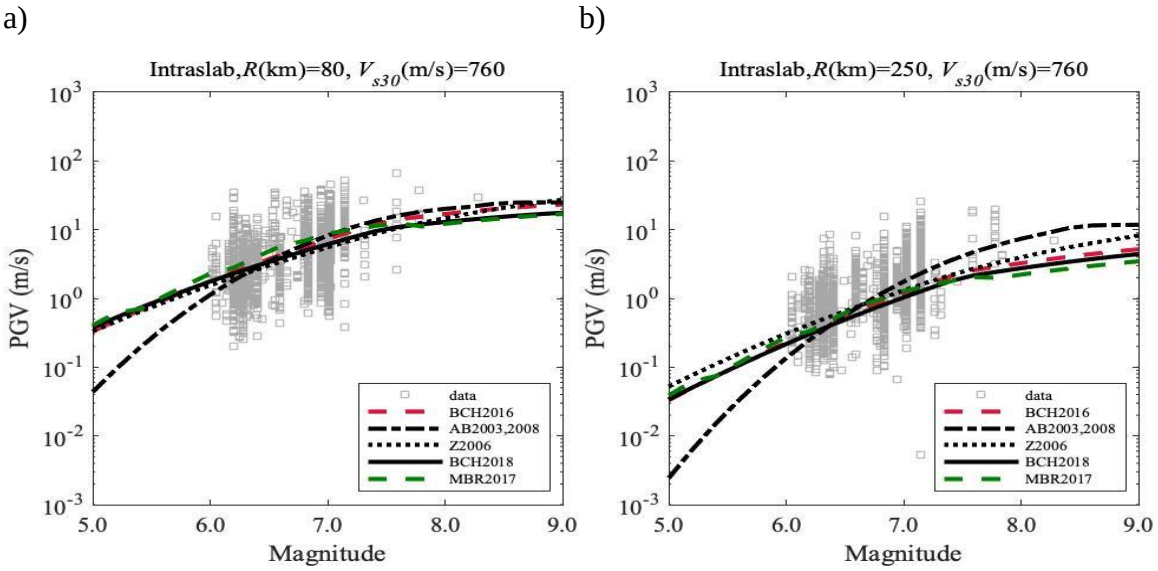

Figure 3-21 Comparisons of magnitude scaling for estimates of median *PGV* by scenario-based models and non-conditional models. (a) Rupture distance 80 km, V_{s30} 760 m/s, (b) Rupture distance 250 km, V_{s30} 760 m/s. Spectral acceleration models: BCHydro2016 (Abrahamson et al., 2016b), BCHydro2018 (Abrahamson et al., 2018), Atkinson and Boore (2003, 2008), Zhao et al. (2006), and Montalva et al. (2017).

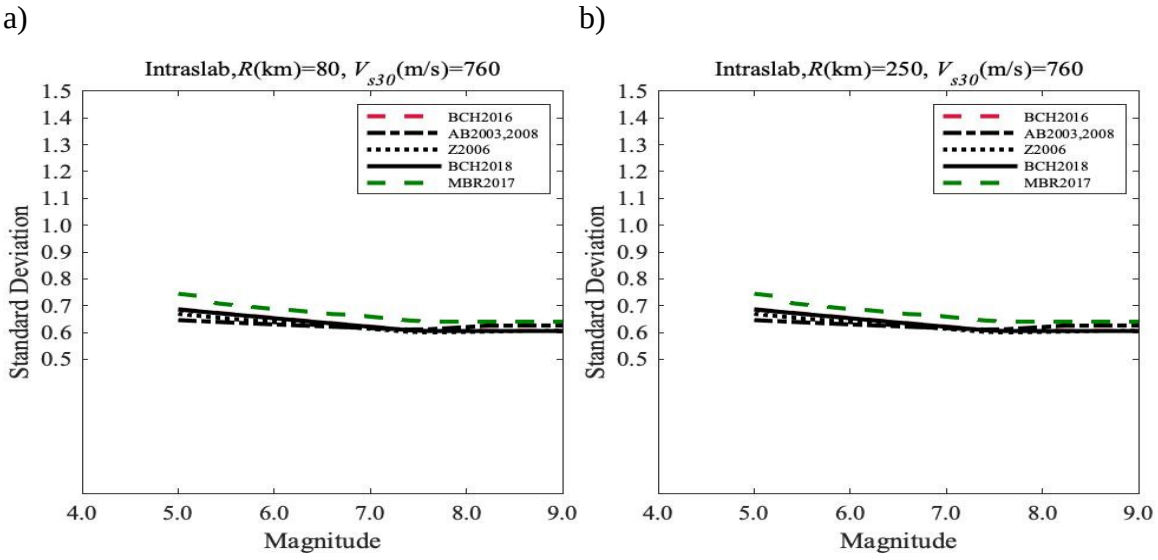

Figure 3-22 Comparisons of standard deviations against magnitude of the five scenario-based models developed in previous section and non-conditional models for *PGV*. (a) Rupture distance 80 km, V_{s30} 760 m/s, (b) Rupture distance 250 km, V_{s30} 760 m/s. Spectral acceleration models: BCHydro2016 (Abrahamson et al., 2016b), BCHydro2018 (Abrahamson et al., 2018), Atkinson and Boore (2003, 2008), Zhao et al. (2006), and Montalva et al. (2017).

CHAPTER 4. PERFORMANCE-BASED PROBABILISTIC ASSESSMENT ON LIQUEFACTION-INDUCED BUILDING SETTLEMENT

4.1 Introduction

To perform the seismic design of a geotechnical system (e.g. slopes, buildings over liquefiable soils), engineers often rely on analytical procedures, which are used to evaluate the seismic performance of the system being designed. The available procedures often include an analytical model which provides estimate for engineering demand parameters (EDPs) based on IMs, site conditions and other earthquake parameters. To estimate liquefaction induced building settlements (*Ds*), extensive previous studies have been carried out to develop simplified procedures. Ishihara and Yoshimine (1992) developed an empirical procedure for estimating post-liquefaction one-dimensional (1-D) consolidation settlement for free-field conditions. Bray and Dashti (2014) suggest that shear-induced ground deformation and shear-induced ground deformation should be considered in addition to volumetric-induced ground deformation. Numerical simulation has been used to simulate the condition in measured experiments or case histories. For example, Bray and Macedo (2017) performed nonlinear dynamic soil-structure-interaction (SSI) effective stress analyses for shallow-founded buildings on liquefiable soils to estimate shear-induced building settlement. Based on the key trends found in the analyses, an equation has been proposed for estimating shear-induced building settlement, which requires 2 IMs (CAV_{dp}, Sa1), building parameters and site conditions as inputs.

The estimation of the IM is usually performed as an independent step where a single IM value is selected given a desired hazard level. The EDP is then estimated using the analytical model based on the selected IM value. However, the hazard level of the estimated EDP is not necessarily consistent with the hazard level of the IM. Since the hazard of the EDP is not explicitly calculated, this approach is often referred as pseudo-probabilistic. For example, Bray and Macedo (2017) and Bullock et al. (2018) developed simplified procedures that separate the estimation of IMs from the estimation of EDPs, and only single values of IMs are considered.

In order to explicitly evaluate the hazard associated with an EDP, an engineer needs to evaluate a hazard curve for the EDP of interest. The approach where an EDP hazard curve is estimated is referred as a performance-based approach and it is the focus of this chapter. Few performance-based procedures for different geotechnical systems have been proposed in previous efforts. For example, Rathje et al (2014) developed a performance-based procedure for estimating seismically induced slope displacements, using two different analytical models (one of which uses only 1 IM, the other uses 2 IMs). The model with 2 IMs adds complexity to the calculation of hazard, thus vector hazard analysis was employed to address this issue. Macedo et al (2018) used the Bray and Travasarou (2007), and the Bray et al. (2018) models to estimate seismically induced slope displacement hazard curves

In this study, a performance-based framework for assessing liquefaction-induced building settlement (*Ds*) is presented, the analytical model developed by Bray and Macedo (2017) for estimating seismic-induced building settlement (referred to as BM17) is used for that purpose. Since more than one IM are included in the analytical model, vector

hazard analysis is used to address the probability of joint occurrence of two IMs. The final result is a *Ds* hazard curve which gives the annual rate of exceedance for different levels of *Ds*.

4.2 Performance-based Implementations

This section implements a performance-based approach to calculate the annual rate of exceedance for different levels of seismic-induced settlement (*Ds*). The functional form of the analytical model developed by Bray and Macedo (2017) is shown in Equation 15:

$$\begin{aligned} Ln(Ds) = {} & c1 + 4.59 * Ln(Q) - 0.42 * Ln(Q)^2 + c2 * LBS + 0.58 \\ & * Ln\left(Tanh\left(\frac{HL}{6}\right)\right) - 0.02 * B + 0.84Ln(CAVdp) + 0.41 \\ & * Ln(Sa1) + \varepsilon \end{aligned} \quad (14)$$

Where Ds is the shear-induced building settlement in the units of mm; *c1* = -7.48 and *c2* = 0.014 for *LBS* > 16 and *c1* = -8.35 and *c2* = 0.072 for *LBS* ≤ 16; *LBS* is the liquefaction-induced building settlement index, which can be calculate using Equation 16:

$$LBS = \int W * \frac{\varepsilon_{shear}}{z} dz \quad (15)$$

HL is the sum of the thickness of liquefiable layers in the units of *m*; *Q* is the foundation contact pressure in *kPa*; *B* is the foundation width in *m*; CAV_{dp} is a variation of *CAV* in the units of g-s, *CAV* is used in this study for convenience. ε is a normal distributed random variable with a mean of 0 and standard deviation of 0.50.

BM17 uses two IMs（*CAV* and *Sa1*） as predictors for estimating *Ds*, thus VPSHA is required to calculate the probability of the joint occurrence of *CAV* and *Sa1*, which is later used as input for the performance-based calculations. The final result from the

performance-based assessment is the annual rate of exceedance (λ_{Ds}) for different levels of building settlement in the units of mm. For simplicity, *Q*, *HL*, and *B* are treated as deterministic in this study, a logic tree is introduced to account for the epistemic uncertainty of LBS. The hazard calculation for λ_{Ds} is expressed in Equation 17:

$$\begin{aligned}\lambda_{Ds}(d) &= MRE_{Ds}(d) \\ &= \iint P[Ds > d|Sa1 = z, CAV \\ &= y] \cdot MRD_{Sa1,CAV(z,y)} \cdot dz \cdot dy\end{aligned} \tag{16}$$

where $P[Ds > d|Sa1 = z, CAV = y]$ is the probability that the building settlement exceeds d mm, given the $Sa1 = z, CAV = y$; $MRD_{Sa1,CAV(z,y)}$ is the joint mean rate density of $Sa1$ and CAV, which equals to the joint probability of occurrence of $Sa1 = z\ and\ CAV = y$. Since $Sa1$ and CAV are estimated from GMMs based on all possible earthquake scenarios (different magnitude *m*, and distance *r*), $MRD_{Sa1,CAV(z,y)}$ can be expressed as (Bazzurro and Cornell, 2002):

$$\begin{aligned}&MRD_{Sa1,CAV(z,y)} \\ &= \lambda_0 \cdot \int_m \int_r f_{Sa1,CAV}(z, y|m, r) \cdot f_M(m) \cdot f_R(r) \cdot dm \cdot dr\end{aligned} \tag{17}$$

where λ_0 is activity rate, which equals to the annual rate of earthquakes greater than the minimum magnitude; $f_{Sa1,CAV}(z, y|m, r)$ is the joint probability density function for *Sa1* and *CAV* given *m* and *r*; $f_M(m), f_R(r)$ are probability density functions for *m* and *r*, which can be obtained from the deaggregation of the primary IM *Sa1*. According to Bazzurro and Cornell (2002), $f_{Sa1,CAV}(z, y|m, r)$ can be written in a conditional form (i.e. the probability density function for *CAV* is conditioned on the probability density function for *Sa1*):

$$f_{Sa1,CAV}(z, y|m, r) = f_{Sa1}(z|m, r) \cdot f_{CAV|Sa1}(y|z, m, r) \tag{18}$$

where $f_{Sa1}(z|m,r)$ is the probability density function for *Sa1*, which is assumed to be lognormally-distributed. As a result, $f_{Sa1}(z|m,r)$ can be calculated using the standard lognormal probability density function:

$$f_{Sa1}(z|m,r) = \frac{1}{z \cdot \sigma_{lnSa1|m,r} \cdot \sqrt{2\pi}} \cdot \exp\left(\frac{-(lnz - \mu_{\ln Sa1|m,r})^2}{2 \cdot \sigma_{lnSa1|m,r}{}^2}\right) \quad (19)$$

where $\sigma_{lnSa1|m,r}$ and $\mu_{\ln Sa1|m,r}$ are the standard deviation and mean estimates for *Sa1* provided by the GMM given the earthquake scenario *m* and *r*.

The $f_{CAV|Sa1}(y|z,m,r)$ conditional probability density function for *CAV* is also assumed to be lognormal and can be calculated using Equation 19, but the mean and standard deviation of *CAV* should be modified using Equation 20 and 21.

$$\mu_{\ln CAV|z,m,r} = \mu_{\ln CAV|m,r} + \rho \frac{\sigma_{lnCAV|m,r}}{\sigma_{lnSa1|m,r}} \cdot (\ln z - \mu_{\ln Sa1|m,r}) \quad (20)$$

$$\sigma_{\ln CAV|z,m,r} = \sigma_{\ln CAV|m,r} \cdot \sqrt{1 - \rho^2} \quad (21)$$

where $\mu_{\ln CAV|m,r}$ and $\sigma_{lnCAV|m,r}$ are the mean and standard deviation given by the GMM for *CAV*; ρ is the coefficient of correlation between *CAV* and *Sa1*. The calculation of this coefficient of correlation is shown in the next section.

4.3 Estimation of Coefficients of Correlation Between *CAV* and *Sa*

New coefficient of correlation between *CAV* and *Sa* on subduction interface, subduction intraslab and shallow crustal tectonic settings are derived. The coefficients of correlation in subduction settings are derived using the updated NGA-SUB database

developed by Pacific Earthquake Engineering Research (PEER) Center, whereas the coefficient of correlation for shallow crustal tectonic settings are based on the NGA-West2 database. These datasets have been discussed in previous chapters. Coefficients of correlation are of vital importance in different applications of performance-based earthquake engineering (PBEE). In particular, in this study the coefficients of correlation between *CAV* and *Sa1* are needed for the performance-based estimation of liquefaction induced building settlements.

4.4 Previous Studies on Coefficients of Correlation Between Different IMs

As discussed in the introduction section, most of effort of previous research on coefficients of correlation were focused on shallow crustal settings. For example, coefficients of correlation between spectral velocities from 0.1s to 4s was derived by Inoue and Cornell (1990) using 64 ground motion recordings from 12 shallow crustal earthquakes and Joyner and Boore (1982) GMM. Cordova et al (2001) calculated coefficients of correlation for spectral acceleration at 2 different vibration periods for assessing building collapse. Baker and Cornell (2006b) calculated coefficients of correlation for spectral accelerations in the period range of 0.05s to 5s and developed an analytical model for estimating coefficients of correlation using 469 ground motion recordings from 31 shallow crustal earthquakes and the Abrahamson and Silva (1997) GMM for estimating spectral accelerations. This study was later updated by Baker and Jayaram (2008) to a wider range of vibration periods of 0.01s to 10s using the NGA-West1 dataset (Chiou et al 2008). This study also used different GMMs from the NGA-West1 project to calculate the coefficients of correlation and found that the coefficients of correlation are stable across different GMMs; conclusion were draw that correlations are controlled by the variability of spectral

ordinates from record to record, instead of the variability of the GMMs being used. Furthermore, the coefficients of correlation were found to be stable for different definitions of spectral accelerations. For example, geo mean of orthogonal components of recordings, and the orientation independent GMRotI. With the advent of NGA-West2 project by Ancheta et al. (2014), this study was updated by Baker and Bradley (2017) adding the coefficient of correlation for *PGV* and significant duration with respect to spectral accelerations at different periods. The coefficients of correlation were found to be consistent with previous studies using the NGA-West1 database, as well as those developed for other tectonic settings. This study proposes that correlation is largely independent of the GMMs used and recording parameters such as magnitude, rupture distance, and *Vs30*, which represent the source, path and site conditions. In contrast, Azarbakht et al. (2014) did similar work using 1151 ground motions from the NGA-West1 dataset and found that coefficients of correlation were dependent on magnitude, and distance. Baker and Abrahamson (2017) raised suspicion that this finding might be a false effect caused by small-sample variability and the lack the mixed-effects in the process of computing correlations using a smaller dataset.

4.5 Estimation of Coefficients of Correlation

The estimation of IMs can be provided by GMMs, given the earthquake magnitude *M*, source to site distance *R*, and the site conditions (θ), which can be expressed in the following equation:

$$\mathrm{IM}_{i,j} = \mu_{IM}\left(R_{i,j}, \mathrm{M}_i, \theta_j\right) + \delta B_i + \delta W_{i,j} \tag{22}$$

where IM is the mean value of the intensity measure in natural log units, $\mu_{IM}(R_{i,j}, \mathrm{M}_i, \theta_j)$ is the estimate provided by the GMM, the subscript i stands for the i^{th}earthquake, the subscript j stands for the j^{th} site. δB_i is the average difference between the observed value of IMs from a given earthquake and the median IMs estimate from a GMM. The within-residual $\delta W_{i,j}$ equals to the observed value of the IM at a given site for a given earthquake minus the estimate from the GMM and the between residual (Al Atik et al., 2010), the total residual is then defined as the sum of δB_i and $\delta W_{i,j}$. The between and within standard deviation are typically provided by the GMM, and the total standard deviation can be estimated by:

$$\sigma = \sqrt{\tau^2 + \varphi^2} \tag{23}$$

where τ is the standard deviation of δB_i, and φ is the standard deviation of $\delta W_{i,j}$.

The mixed-effects regression approach by Jayaram and Baker (2010) is used in this study to estimate the δB_i and $\delta W_{i,j}$ for each ground motion recording in the selected dataset. The Jayaram and Baker (2010) approach calculates residuals from GMMs and then performs the partition of the between and within components. In terms of spectral acceleration, the BCHydro GMM (Abrahamson, et al. 2018) is used in subduction settings, and the GMM by Abrahamson, Silva and Kamai (2014) is used in shallow crustal settings. In terms of *CAV*, the conditional GMM developed in this study for shallow crustal settings and subduction zones are employed.

Once the δB_i and $\delta W_{i,j}$ residual components have been calculated, the coefficient of correlation between the IMs can be calculated through Equation 24:

$$\rho_{total}(CAV, \mathrm{Sa}) = \frac{\tau_1 \tau_2}{\sigma_1 \sigma_2} \rho_B(CAV, \mathrm{Sa}) + \frac{\varphi_1 \varphi_2}{\sigma_1 \sigma_2} \rho_W(CAV, \mathrm{Sa}) \quad (24)$$

where σ, τ and φ are total, between and within standard deviations from GMMs, the subscript 1, 2 stands for the corresponding GMM. $\rho_B(IM_1, IM_2)$ is the between coefficient of correlation between IM_1 and IM_2, $\rho_W(IM_1, IM_2)$ is the within coefficient of correlation between IM_1 and IM_2, $\rho_{total}(IM_1, IM_2)$ is the total coefficient of correlation between IM_1 and IM_2.

4.6 Results for Shallow Crustal, Subduction Interface and Subduction Intraslab Tectonic Settings

Figure 4-1 shows the coefficients of correlation between *CAV* and *Sa* at different vibration periods in three different tectonic settings (i.e. shallow crustal, subduction interface and subduction intraslab) according to the procedure in the previous section. The four figures are showing the coefficients of correlation between *CAV* and *Sa* at periods from 0s to 10s respectively.

In Figure 4-1a, coefficients of correlation for *CAV* and *Sa* calculated in this study are compared with previous studies by Campbell & Bozorgnia (2012), and Bradley (2015). The results of this study are in good agreement with previous studies.

Coefficients of correlation for *CAV* and *Sa* in subduction interface and subduction intraslab settings are shown in Figure 4-1b, Figure 4-1c, respectively. The coefficients of correlation for *CAV* and *Sa* plateau between periods between. 0.01s and 0.4s but decrease significantly as the vibration period increases beyond 0.4s.

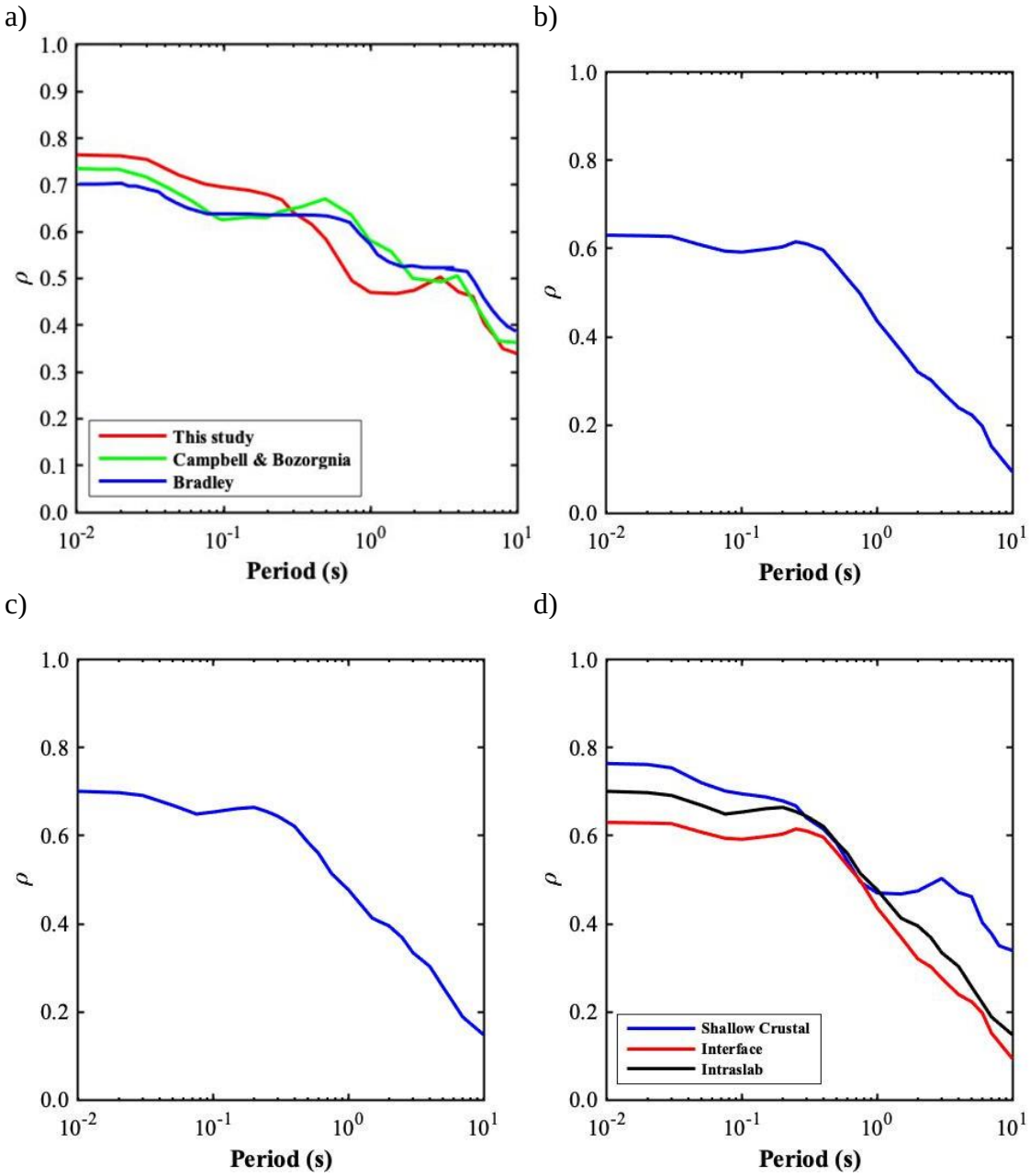

Figure 4-1 Coefficients of correlation for *CAV* and *Sa*. a) Comparison of coefficient of correlation calculation for *CAV* and Sa in shallow crustal settings between this study, Campbell & Bozorgnia (2012), and Bradley (2015). b) Coefficient of correlation for *CAV* and *Sa* in Subduction interface settings. c) Coefficient of correlation for *CAV* and *Sa* in Subduction intraslab settings. d) Comparison of coefficient of correlation for *CAV* and Sa in 3 tectonic settings.

Results for three tectonic settings are compared in Figure 4-1d. Coefficients of correlation in shallow crustal settings are larger than those of subduction settings in all vibration periods. The results for subduction interface and intraslab settings are similar, but

coefficients of correlation in subduction intraslab settings are slightly larger than the results in subduction interface settings. The evaluation of the physics behind these trends is outside of the scope of this thesis but should be explored in further studies.

4.7 Implementation

The performance-based estimation of liquefaction induced building settlements (i.e. Equation 14 to 21) has been implemented in a MATLAB graphical user interface (GUI), to facilitate its use in engineering practice (see Appendix A for the GUI details). An example of the GUI is shown below:

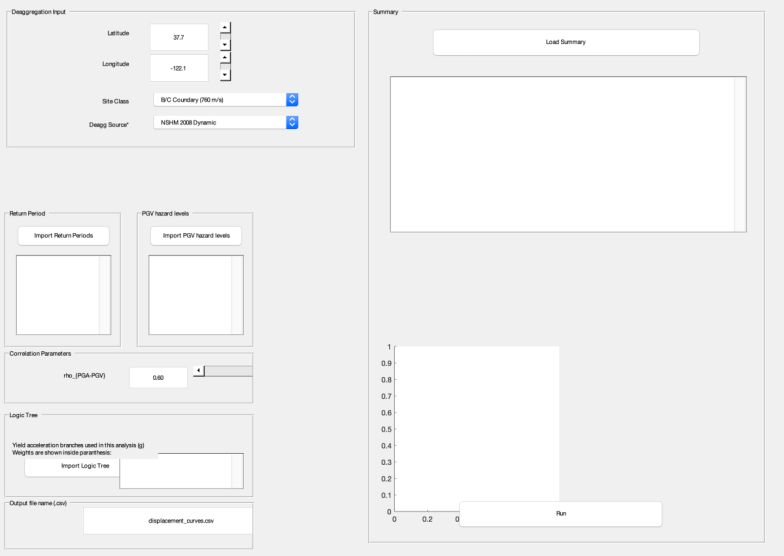

Figure 4-2 Example of the GUI developed for the implementation of the performance-based procedure

The following steps are recommended to perform a performance-based evaluation of liquefaction-induced building settlements in engineering practice (in the case of the U.S. all the steps are already incorporated in the implemented GUI):

(1) Derive the hazard curve for *Sa1* by performing a probabilistic seismic hazard analysis (PSHA), the input includes the site location, site condition (i.e. *Vs30*), and earthquake scenarios.

(2) Perform deaggregation for different levels of *Sa1* values, to estimate the contribution from different *m* and *r* combinations to the *Sa1* hazard. The deagregation is used in Equations 17 and 18 for the estimation of *Ds* hazard curves.

(3) Use the *m* and *r* from deaggregation as the input for a GMM for *CAV* to estimate the mean and standard deviation of *CAV* using the developed models in Chapter 2 and 3, then modify the results using Equation 20 and 21.

(4) Use Equation 19 to calculate the conditional probability density function for *CAV* and the probability density function for *Sa1*, then $MRD_{Sa1,CAV(z,y)}$ can be calculated using Equation 18 and 19 and the coefficients of correlation between *CAV* and *Sa1*.

(5) Assuming the estimate of *Ds* is lognormally distributed, $P[Ds > x|Sa1 = z, CAV = y]$ is calculated using the standard lognormal probability density function.

(6) Calculate the annual rate of exceedance (λ_{Ds}) for *Ds* using Equation 16 through integration

(7) Iterate step 1~6 for different levels of *Ds* (i.e. z values) to calculate the corresponding λ_{Ds}.

(8) Plot z values against λ_{Ds} to produce the hazard curve for *Ds*.

For applications in the United States all the steps are automated within the implemented GUI. In particular, the GUI connects with the USGS website and retrieves the hazard

and deagregation for any site in the United States. For applications outside the United States the information for (1) and (2) can be obtained from a site specific PSHA study.

4.8 Illustrative Examples

As mentioned before, the pseudo-probabilistic approach only considers the hazard of IMs but without regards of hazard in the estimation of EDPs (i.e. *Ds*), thus the estimated EDP is related to only one IM value. However, the performance-based approach can provide the hazard curve for the EDP (*Ds*) of interest. In this section we show the application of the performance-based approach for 3 different sites in the United States. All the performance-based calculations are performed with the implemented GUI.

The performance-based estimations consider 3 different sites in the United States, which are listed below.

(1) Yerba Buena Island (YB), California (N37.81 W122.36);

(2) Salt Lake City (SL), Utah (N40.75 W111.88);

(3) Seattle (S), Washington (N47.42 W123.56).

The site YB and SL is mostly influenced by crustal earthquakes, while the S site is influenced by subduction seismic sources and shallow crustal seismic sources. The analysis is performed following the 8 steps described in the previous section.

4.8.1 Pseudo-probabilistic Approach

The first step is to select IMs at a target return period. According to Equation 15, the IMs used in the BM17 model are *Sa1* and *CAV*. While *Sa1* hazard curves can be obtained from the USGS Unified Tool. However; hazard curves for *CAV* are not available. In this study, *CAV* values for each site are estimated using the conditional model developed in Chapter 2. The target return period selected for the estimation of primary IMs is 1000 years.

Hazard curves for *Sa1* is obtained from the USGS Unified Tool based on the location of the sites (latitude and longitude), which are shown in Figure 4-3. For each site, a single *Sa1* value is selected according to 1000-year return period, the selected *Sa1* values for YB, SL and S are 0.487, 0.220, and 0.370 in the units of *g*.

CAV values are estimated using Equation 2, which requires *PGA*, *Sa1*, *M* and *Vs30* as inputs. *PGA* values can be selected using the same approach as *Sa1*, the selected *PGA* values are 0.561, 0.409, 0.481 in the units of g; the *Sa1* values selected in the previous paragraph are used as inputs for Equation 2; *Vs30* is fixed to 760 m/s for all sites; *Mw* is the magnitude of the controlling earthquake which can be obtained from the deaggregation of *Sa1*, the resulting *Mw* for YB, SL and S are 7.1, 6.5, 8.5 respectively. The resulting estimate of *CAV* are listed in Table 5:

Table 5 Result of Pseudo-probabilistic Approach

Site	***Mw***	***PGA (g)***	***Sa1 (g)***	***Vs30 (m/s)***	***CAV (g*s)***	***Ds (mm)***
YB	7.1	0.561	0.487	760	1.219	158
SL	6.5	0.409	0.220	760	0.693	71
S	8.5	0.481	0.370	760	2.149	227

The second step is estimating *Ds*. The selected *Sa1* and *CAV* values are used as inputs for Equation 15. For simplicity, *Q* is fixed as 100 kPa, *HL* equals to 3.46 m, *B* equals to 29 m, *LBS* is 100. The resulting estimate of *Ds* are listed in Table 5.

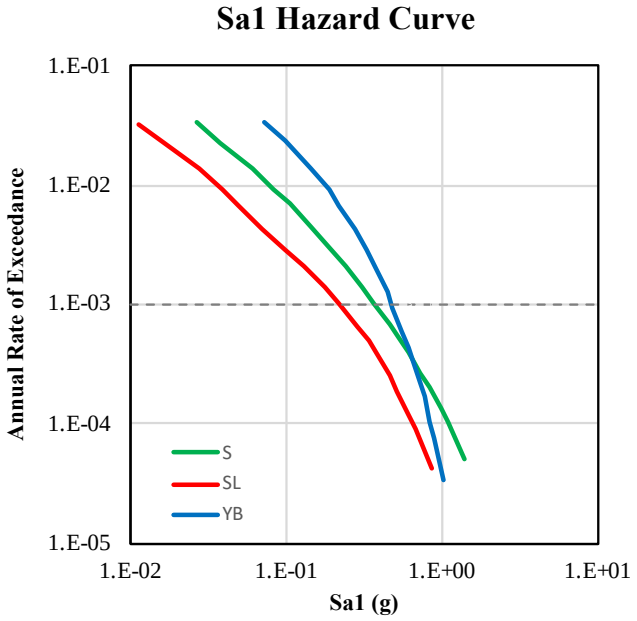

Figure 4-3 *Sa1* Hazard Curve for Three Sites in the US: YB, SL and S.

4.8.2 Performance-based Approach

The first step is identical to the pseudo-probabilistic approach, where latitude and longitude of the three sites are used as inputs for the USGS Unified Hazard Tool to obtain hazard curves for *Sa1*, which are shown in Figure 4-3.

Following the Implementation Guidelines, hazard curves for *Ds* are derived, which are shown in Figure 4-5. The input for BM17 are identical to the pseudo-probabilistic

procedure, where *Q* is fixed as 100 kPa, *HL* equals to 3.46 m, *B* equals to 29 m. The only difference is that the epistemic uncertainty of *LBS* is considered in a logic tree, where different values of *LBS* are assigned with different weighting factors. The logic tree is shown in Figure 4-4:

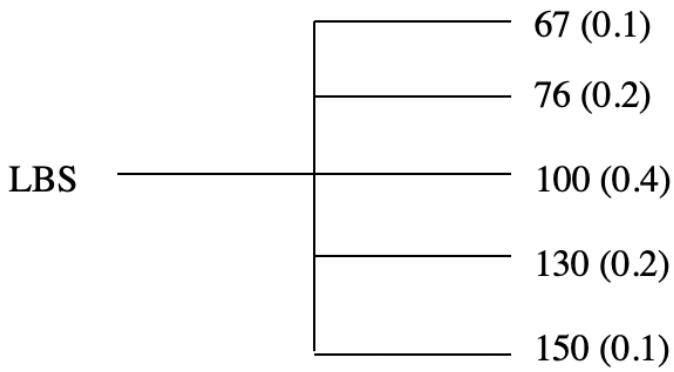

Figure 4-4 Logic Tree for *LBS*. Numbers before the brackets are LBS values, numbers in the brackets are weighting factors.

In Figure 4-5, The five black lines are results from the *LBS* logic tree, the red line is the mean hazard curve for *Ds*, which locates in the middle of five black lines.

Using the same return period as the pseudo-probabilistic procedure (1000 year), *Ds* values can be obtained from the hazard curves. For comparison, the estimated *Ds* values are listed together with the results from the pseudo-probabilistic approach in Table 6.

Table 6 Comparison of *Ds* Estimates Between Performance Based Procedure and Pseudo-probabilistic Procedure for Three Sites in the US: YB, SL and S.

Site	***Pseudo-probabilistic Ds (mm)***	***Performance-based Ds (mm)***
YB	158	247
SL	71	98
S	227	86

For the two sites in shallow crustal settings (i.e. YB, SL), the *Ds* estimates using the developed performance-based procedures are higher than the estimates from pseudo-probabilistic procedures. The performance-based estimation of *Ds* in the YB case is significantly higher than the pseudo-probabilistic estimation, however, the performance-based estimation of *Ds* in SL is comparable to the pseudo-probabilistic estimation. These results are caused by the higher recurrence of earthquakes in California compared to the recurrence of earthquakes in Utah, which result in steeper *Sa* hazard curves for YB than that of SL.

In the case of the S site (subduction interface) the Ds estimate from the developed performance-based procedure is lower than the estimate using a pseudo-probabilistic procedure. This is because the pseudo-probabilistic procedure is considering only one magnitude which is large (*Mw*=8.5) and is inflating the *Ds* estimates. On the other hand, the performance-based procedure considers all the possible combinations of magnitudes and distances providing a more robust estimate. In general, the developed performance-based procedure does not necessarily provide higher or lower estimations compared to pseudo-probabilistic procedures, it depends on the seismic activity, the tectonic setting and hazard level.

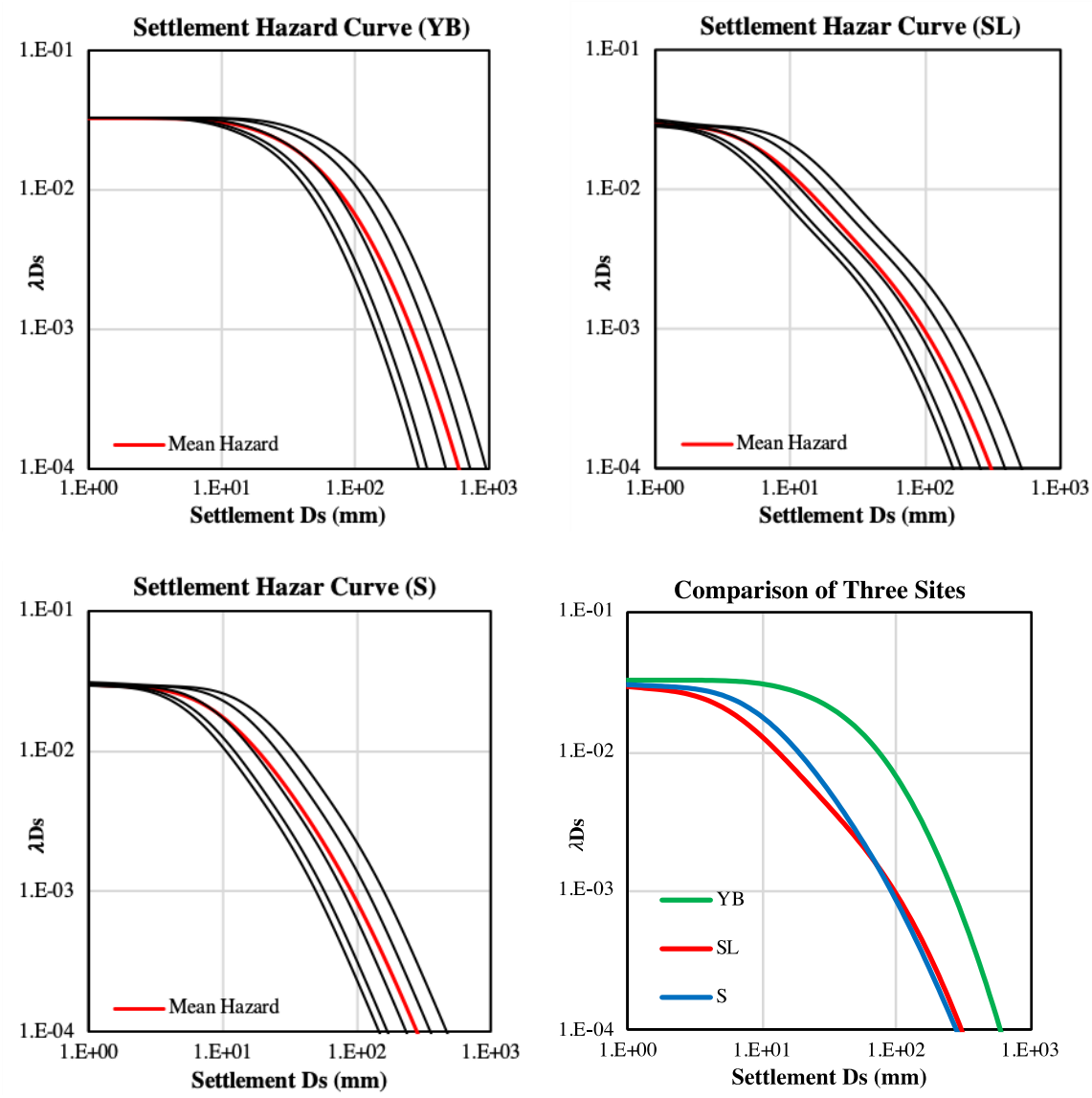

Figure 4-5 Settlement Hazard Curves for the three selected sites: YB, SL and S.

CHAPTER 5. CONCLUSIONS

The implementation of a performance-based, hazard-consistent framework for the estimation of liquefaction-induced building settlements (*Ds*), in cases where the shearing component of settlement is dominant has been presented.

As part of the proposed framework for the performance-based estimation of *Ds*, this thesis has proposed new conditional ground motion models (CGMM) and scenario-based models for *CAV* and *PGV*. Implementing conditional ground motion models guarantees the consistency of secondary intensity measures with a given spectral acceleration design response spectrum. In addition, a CGMM allows to include the more complex scaling effects of traditional GMMs for spectral accelerations in ground motion models for secondary intensity measures. New CGMMs for *CAV* in shallow crustal settings have been developed based on the NGA-West2 database by PEER (Ancheta et al, 2014); new CGMMs for *CAV* and *PGV* in subduction tectonic settings have been derived based on the NGA-Sub database by PEER (Kishida et al, 2018). The CGMMs show a smaller aleatory variability than traditional models and have then be used to develop a suite of scenario-based models by combining the developed CGMMs with traditional GMMs.

Scenario-based models are derived by combining the CGMMs with non-conditional models for spectral accelerations. The scenario-based model can provide estimates for IMs (*CAV* and *PGV*) given an earthquake scenario and site conditions similar to traditional ground motion models. Scenario-based models also include the complex scaling effects that are considered in underlying ground motion models for spectral accelerations being used. These features enable the scenario-based models to be readily

used in seismic hazard assessments and probabilistic procedures that use *CAV* or *PGV* as a critical intensity measure. In terms of the suite of scenario-based models developed in this study for *CAV* and *PGV*, their scaling against magnitude and distance are shown to be consistent with established non-conditional models in most earthquake scenarios. The scenario-based models are also capturing the trend of well-recorded ground motions; the estimate of *CAV* is always centered on the data. Due to the smaller standard deviations and better extrapolation of the data in cases where differences are observed against traditional models, the scenario-based models developed in this thesis should be considered as part of the epistemic uncertainty in GMMs and implemented in practice for estimating *CAV* or *PGV* with higher weight compared to traditional GMMs counterparts.

Coefficient of correlation for spectral accelerations for *CAV* and *Sa* are estimated for shallow crustal, subduction interface and subduction intraslab earthquakes. The results for shallow crustal settings are in good agreement with previous estimations. The results for subduction intraslab settings are generally larger than the results for subduction interface settings. The coefficients of correlation for *CAV* and *Sa1* are later used in the implementation of performance-based procedures.

Using the developed CGMMs, scenario-based models and coefficients of correlation, this study has implemented a performance-based procedure for the assessment of liquefaction induced building settlements. Due to its complexity, performance-based procedures are not widely understood by engineers. Compared to commonly used procedures (i.e. pseudo-probabilistic, deterministic procedures), performance-based procedures allow a robust treatment of uncertainties in earthquake ground motions, building parameters and site conditions, hence they should be used. Additionally,

performance-based procedures can provide estimations that are consistent design hazard levels, while pseudo-probabilistic and deterministic procedures do not provide hazard consistent estimates. To enable easy implementation of the developed performance-based procedures in engineering practice, a graphic user interface (GUI) has been developed. The GUI can be accessed through this website:

https://www.dropbox.com/sh/pc8y88p80x956va/AAC2OAa2KXZTnon3LqIXurZSa?dl=0

In terms of the implemented performance-based procedure for estimating liquefaction-induced building settlements, the deterministic model proposed by Bray and Macedo (2017) has been used. Illustrative examples are presented, where the estimation of *Ds* at three sites in the US are performed. The results are compared with the estimation from pseudo-probabilistic procedures. Performance-based procedures do not necessarily give higher or lower estimations compared to pseudo-probabilistic procedures. Depending on the hazard level or tectonic settings, the relatives of their estimations may vary. The performance-based procedure is recommended because it better considers uncertainties and provides estimations of EDPs directly related to design hazard levels.

Finally, for future work we recommend including other mechanistic-based components that may affect the amount of liquefaction-induced building settlements, which include volumetric mechanisms and ejecta. Currently, there are not robust probabilistic models that allow the inclusion of these components in performance-based procedures. Future research should provide such models to enable a fully performance-based estimation of liquefaction-induced building settlements.

APPENDIX A.

The graphic user interface (GUI) for easy implementation of performance-based assessment of *Ds* is developed, the user interface is shown below:

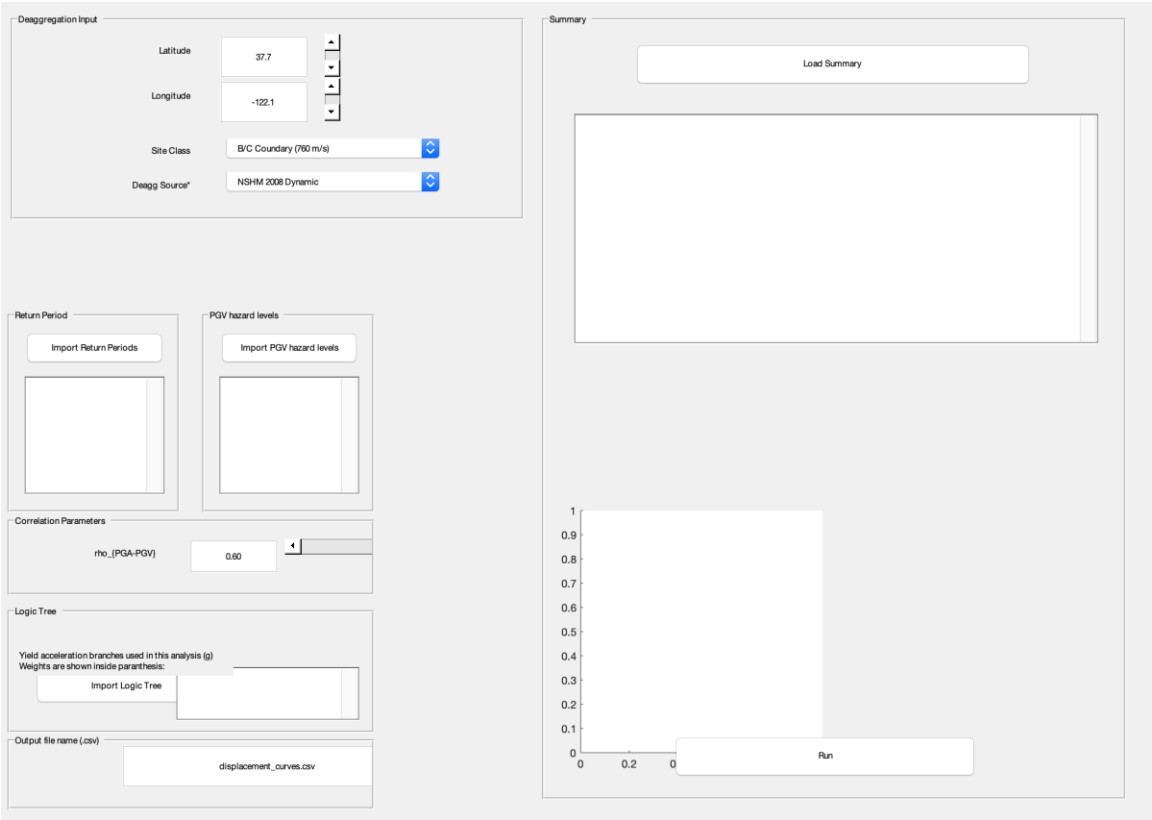

Figure A-1 Example of GUI for the Implementation of Performance-based Assessment of *Ds*

To run analysis, the user needs to follow the steps shown below:

1. Input manually the longitude, latitude of the considered site, then select the site class and deaggregation source from the drop-down menu.
2. Store the return periods and hazard levels in csv files and provide the file path to the GUI.
3. Manually input the coefficient of correlation for *CAV* and *Sa*.
4. Choose a name for output file for the *Ds* hazard curve.

5. Click run, the results will show on the right-hand side.

A.1 Implementation Example

Take the illustrative example for Yerba Buena Island (YB) in section 4.7 as an example:

- Manually input the location of the site: N37.81 W122.36 in the upper left boxes.
- Select site class as B/C boundary (760m/s).
- Select NSHM 2008 Dynamic as the deagg source.
- Choose a csv files as input for return periods, which are simply an array of numbers from as small as 30 to 20000. The numbers can be customized manually in the csv file.
- Choose a csv file for CAV hazard levels, which are simply an array of *CAV* values from as small as 0.01 g.s to 9 g.s. The numbers can be customized manually in the csv file, as long as the range is reasonable for *CAV*.
- Input the coefficient of correlation between *CAV* and *Sa1*, which can be found in section 4.6. In this case, the coefficient of correlation is 0.50.
- Then import the logic tree from a .csv file, which contains a matrix of different LBS values and corresponding weighting factors:

LBS	Weighting Factor
67	0.1
77	0.2
100	0.4
130	0.2
150	0.1

- Choose a name for saving the Ds displacement curves, in this case "*Ds_curves.csv*" is used.
- Click Run and the Sa hazard curve and Ds hazard curve will be displayed on the right-hand side.

REFERENCES

Abrahamson, Charlotte, Hao-Jun Michael Shi, and Brian Yang. (2016a). "Ground-Motion Prediction Equations for Arias Intensity Consistent with the NGA-West2 Ground-Motion Models." *PEER Report*.

Abrahamson, N.A., N. Gregor and K. Addo (2016b). "BC Hydro ground motion prediction equations for subduction earthquakes0." *Earthquake Spectra*, 32: 23–44.

Abrahamson, N.A., N. Kuehn, Z. Gulerce, N. Gregor, Y. Bozorgnia, G. Parker, J. Stewart, B. Chiou, I.M. Idriss, K. Campbell and R. Youngs (2018). "Update of the BC hydro subduction ground-motion model using the NGA- subduction dataset." *PEER 2018/02 Report*.

Abrahamson, N.A., and R. R. Youngs. (1992). "A stable algorithm for regression analyses using the random effects model." *Bulletin of the Seismological Society of America* 82 (1): 505–10. https://doi.org/10.1007/BF00203353.

Abrahamson, Norman A., Walter J. Silva, and Ronnie Kamai. (2014). "Summary of the ASK14 Ground Motion Relation for Active Crustal Regions." *Earthquake Spectra* 30 (3): 1025–55. https://doi.org/10.1193/070913EQS198M.

Ancheta, T. D., Darragh, R. B., Stewart, J. P., Seyhan, E., Silva, W. J., Chiou, B. S. -J., Wooddell, K. E., Graves, R. W., Kottke, A. R., Boore, D. M., Kishida, T., and Donahue, J. L., (2014). NGA-West2 database, *Earthquake Spectra* 30, 989–1005.

Abrahamson, N. A., and Silva W. J. (1997). "Empirical response spectral attenuation relations for shallow crustal earthquakes", *Seism. Res. Lett*., **68**(1), 94–127. https://doi.org/10.1785/gssrl.68.1.94

Al Atik, L., N. Abrahamson, J. Bommer, F. Scherbaum, F. Cotton, and N. Kuehn (2010). "The variability of ground-motion prediction models and its components", *Seismol. Res. Lett.* 81, no. 5, 794–801.

Arteta, C., and Abrahamson, N. (2018). "Conditional Scenario Spectra (CSS) For Hazard-Consistent Analysis of Engineering Systems." *Earthquake Spectra* In-Press.

Atkinson, G. M. and D.M. Boore (2003). "Empirical ground-motion relations for

subduction-zone earthquakes and their application to Cascadia and other regions." *Bulletin of the Seismological Society of America,* 93, no. 4, 1703–1729.

Atkinson, G. M. and D.M. Boore (2008). Erratum: Empirical ground-motion relations for subduction zone earthquakes and their application to Cascadia and other regions. *Bulletin of the Seismological Society of America*, 98, 2567-2569.

Azarbakht, A., Mousavi, M., Nourizadeh, M. and Shahri, M., (2014). Dependence of correlations between spectral accelerations at multiple periods on magnitude and distance. *Earthquake Engineering & Structural Dynamics*, 43(8), 1193-1204.

Baker, J. W., and Bradley, B. A. (2017). "Intensity measure correlations observed in the NGA-West2 database, and dependence of correlations on rupture and site parameters." *Earthquake Spectra*, 33(1), 145–156

Baker, Jack W., and C. Allin Cornell. (2006a). "Spectral Shape, Epsilon and Record Selection." *Earthquake Engineering and Structural Dynamics* 35 (9): 1077–95. https://doi.org/10.1002/eqe.571.

Baker, J. W., and Cornell, C. A. (2006b). "Correlation of response spectral values for multi-component ground motions." *Bull. Seismol. Soc. Am.*, **96**(1), 215-227.

Baker, J. W., and Lee, C. (2018). "An Improved Algorithm for Selecting Ground Motions to Match a Conditional Spectrum." *Journal of Earthquake Engineering*, 22(4), 708–723.

Baker, Jack W., and Nirmal Jayaram. (2008). "Correlation of Spectral Acceleration Values from NGA Ground Motion Models." *Earthquake Spectra* 24 (1): 299–317. https://doi.org/10.1193/1.2857544.

Bazzurro, P., and Cornell, C. A.（2002）. "Vector-valued probabilistic seis- mic hazard analysis（VPSHA）." Proc., *7th U.S. National Conf. on Earthquake Engineering*, Vol. II, EERI, Oakland, Calif., 1313–1322.

Bevington, P. R., and D. K. Robinson (1969). "Data Reduction and Error Analysis for the Physical Sciences", Vol. 336, McGraw-Hill, New York, New York.

Boore, David M., Jonathan P. Stewart, Emel Seyhan, and Gail M. Atkinson. (2014). "NGA-West2 Equations for Predicting PGA, PGV, and 5% Damped PSA for Shallow

Crustal Earthquakes." *Earthquake Spectra* 30 (3): 1057–85. https://doi.org/10.1193/070113EQS184M.

Bray, Jonathan, et al. "Liquefaction effects on buildings in the central business district of Christchurch." *Earthquake Spectra* 30.1 (2014): 85-109.

Bray J.D, & Macedo J. (2017). "6th Ishihara lecture: simplified procedure for estimating liquefaction-induced building settlement." *Soil Dyn Earthq Eng* 2017;102:215–31

Bray, J.D., Macedo, J., and Travasarou, T. (2018) "Simplified Procedure for Estimating Seismic Slope Displacements for Subduction Zone Earthquakes," *Journal of Geotechnical and Geoenvironmental Engineering,* ASCE, V. 144(3): 04017124, DOI:10.1061/(ASCE)GT.1943-5606.0001833.

Bullock, Zach, Shideh Dashti, Abbie Liel, Keith Porter, Zana Karimi, and Brendon Bradley. (2017). "Ground-Motion Prediction Equations for Arias Intensity, Cumulative Absolute Velocity, and Peak Incremental Ground Velocity for Rock Sites in Different Tectonic Environments." *Bulletin of the Seismological Society of America* 107 (5): 2293–2309. https://doi.org/10.1785/0120160388.

Bullock, Z., Dashti, S., Liel, A. B., Porter, K. A., & Karimi, Z. (2019). "Assessment Supporting the Use of Outcropping Rock, Evolutionary Intensity Measures for Prediction of Liquefaction Consequences." *Earthquake Spectra*. doi: 10.1193/041618eqs094m

Campbell, K. W., & Bozorgnia, Y. (2010). "A Ground Motion Prediction Equation for the Horizontal Component of Cumulative Absolute Velocity (CAV) Based on the PEER-NGA Strong Motion Database." *Earthquake Spectra*, 26(3), 635–650. https://doi:10.1193/1.3457158

Campbell, K. W., & Bozorgnia, Y. (2011). "Prediction equations for the standardized version of cumulative absolute velocity as adapted for use in the shutdown of U.S. nuclear power plants." *Nuclear Engineering and Design*, 241(7), 2558–2569. https://doi: 10.1016/j.nucengdes.2011.04.020

Campbell, Kenneth W., and Yousef Bozorgnia. (2012). "A Comparison of Ground Motion Prediction Equations for Arias Intensity and Cumulative Absolute Velocity Developed Using a Consistent Database and Functional Form." *Earthquake Spectra* 28 (3): 931–41. https://doi.org/10.1193/1.4000067.

Campbell, K. W., & Bozorgnia, Y. (2012). “Cumulative Absolute Velocity (CAV) and Seismic Intensity Based on the PEER-NGA Database.” *Earthquake Spectra*, 28(2), 457–485. doi: 10.1193/1.4000012

Campbell, K. W., & Bozorgnia, Y. (2014). “NGA-West2 Ground Motion Model for the Average Horizontal Components of PGA, PGV, and 5% Damped Linear Acceleration Response Spectra.” *Earthquake Spectra* 30 (3): 1087–1114. https://doi.org/10.1193/062913EQS175M.

Campbell, K. W., & Bozorgnia, Y. (2019). “Ground Motion Models for the Horizontal Components of Arias Intensity (AI) and Cumulative Absolute Velocity (CAV) Using the NGA-West2 Database.” *Earthquake Spectra*, 35(3), 1289–1310. doi: 10.1193/090818eqs212m

Carlton, B., and Abrahamson, N. (2014). “Issues and Approaches for Implementing Conditional Mean Spectra in Practice.” *Bulletin of the Seismological Society of America* 104 (1): 503–12. https://doi.org/10.1785/0120130129.

Chiou, B. S.-J., and Youngs, R. R., (2008). “An NGA model for the average horizontal component of peak ground motion and response spectra”, *Earthquake Spectra* 24, 173–216

Chiou, Brian S J, and Robert R. Youngs. (2014). “Update of the Chiou and Youngs NGA Model for the Average Horizontal Component of Peak Ground Motion and Response Spectra.” *Earthquake Spectra* https://doi.org/10.1193/072813EQS219M.

Cimellaro, G. P., 2013. “Correlation in spectral accelerations for earthquakes in Europe”, *Earthq Eng Struct Dyn* 42, 623–633.

Cordova, P. P., G. G. Deierlein, S. S. F. Mehanny, and C. A. Cornell (2001). “Development of a two-parameter seismic intensity measure and probabilistic assessment procedure”, in The Second U.S.-Japan Workshop on Performance-Based Earthquake Engineering Methodology for Re-inforced Concrete Building Structures, Sapporo, Hokkaido, 11–13 September 2000, 187–206.

Danciu, L., and Tselentis, G., (2007). “Engineering ground-motion parameters attenuation relation- ships for Greece”, *Bull. Seismol. Soc. Am.* 97, 162–183.

Du, W., & Wang, G. (2012). “A simple ground-motion prediction model for cumulative absolute velocity and model validation.” *Earthquake Engineering & Structural*

Dynamics, 42(8), 1189–1202. doi: 10.1002/eqe.2266

Electrical Power Research Institute (EPRI), (1988). "A Criterion for Determining Exceedance of the Operating Basis Earthquake", *EPRI NP-5930*, Palo Alto, CA.

Electrical Power Research Institute (EPRI), (2006). "Program on Technology Innovation: Use of Cumulative Absolute Velocity (CAV) in Determining Effects of Small Magnitude Earthquakes on Seismic Hazard Analyses", *EPRI 1014099*, Palo Alto, CA.

Fahjan, Y. M., Alcik, H., & Sari, A. (2011). "Applications of cumulative absolute velocity to urban earthquake early warning systems." *Journal of Seismology*, 15(2), 355–373. doi: 10.1007/s10950-011-9229-8

Foulser-Piggott, Roxane, and Katsuichiro Goda. (2015). "Ground-Motion Prediction Models for Arias Intensity and Cumulative Absolute Velocity for Japanese Earthquakes Considering Single- Station Sigma and within-Event Spatial Correlation." *Bulletin of the Seismological Society of America* 105 (4): 1903–18. https://doi.org/10.1785/0120140316.

Goda, K. and Atkinson, G. M., (2009). "Probabilistic characterization of spatially correlated response spectra for earthquakes in Japan." *Bulletin of the Seismological Society of America*, 99(5), 3003-3020.

Idrissa, I. M. (2014). "An NGA-West2 Empirical Model for Estimating the Horizontal Spectral Values Generated by Shallow Crustal Earthquakes." *Earthquake Spectra* 30 (3): 1155–77. https://doi.org/10.1193/070613EQS195M.

Inoue, T., and C. A. Cornell (1990). "Seismic hazard analysis of multi-degree-of-freedom structures, reliability of marine structures", RMS-8, Stanford, California, 70 pp.

Joyner W.B and Boore, D.M. (1982). *"*Estimation of response-spectral values as functions of magnitude, distance, and site conditions*." USGS Open File Report,* 82-881.

Kishida T., Contreras V., Bozorgnia Y., Abrahamson N.A., Ahdi S.K., Ancheta T.D., Boore D.M., Campbell K.W., Chiou B., Darragh R., Gregor N., Kuehn N., Kwak D.Y., Kwok A.O., Lin P., Magistrale H., Mazzoni S., Muin, S., Midorikawa S., Si H., Silva W.J., Stewart J.P., Wooddell K.E., Youngs R.R. (2018). "NGA-Sub ground-motion database", Proceedings, *11NCEE,* Los Angeles, CA.

Kostov, M., (2005). "Site-specific estimation of cumulative absolute velocity", in Proc.,

18th *Inter- national Conference on Structural Mechanics in Reactor Technology (SMiRT 18)*, Beijing, 3041–3050.

Kramer, S. L., and Mitchell, R. A., (2006). "Ground motion intensity measures for liquefaction hazard evaluation", *Earthquake Spectra* 22, 413–438.

Kwan, W., Sideras, S. & Mohtar, C. (2018). "Liquefaction Triggering, Consequences, and Mitigation", presented at Geotechnical Earthquake Engineering and Soil Dynamics V (pp. 450-462), Tx: ASCE. https://doi.org/10.1061/9780784481455.043.

Macedo, J., Abrahamson, N., & Bray, J. D. (2019). "Arias Intensity Conditional Scaling Ground-Motion Models for Subduction Zones." *Bulletin of the Seismological Society of America.*

Montalva, G., N. Bastias and A. Rodriguez-Marek (2017). "Ground motion prediction equation for the Chilean subduction zone." *Bulletin of the Seismological Society of America,* 107, no. 2, doi: 10.1785/0120160221.

Muin, S., & Mosalam, K. M. (2017). "Cumulative Absolute Velocity as a Local Damage Indicator of Instrumented Structures." *Earthquake Spectra*, 33(2), 641–664. doi: 10.1193/090416eqs142m

Newmark, N. M. and Hall, W. J. (1982). Earthquake spectra and design, Earthquake Engineering Research Institute, El Cerrito, California.

Reed, J. W., and Kassawara, R. P., (1990). "A criterion for determining exceedance of the Operating Basis Earthquake", *Nucl. Eng*. Des. 123, 387–396.

Rathje, E.M., Wang, Y., Stafford, P., Antonakos, G., and Saygili, G. (2014). "Probabilistic Assessment of the Seismic Performance of Slopes," *Bulletin of Earthquake Engineering*, 12(3), 1071-1090, doi:10.1007/s10518-013-9485-9.

Saygili and Rathje (2008). "Empirical predictive models for earthquake-induced sliding displacements of slopes." *Journal of Geotechnical and Geoenvironmental Engineering*, ASCE, 134 (6) (2008), pp. 790-803

U.S. Nuclear Regulatory Commission (USNRC), (1997). "Pre-earthquake Planning and Immediate Nuclear Power Plant Operator Postearthquake Actions", Regulatory Guide 1.166, Washington, D.C.

Zhao, J.X., J. Zhang, A. Asano, Y. Ohno, T. Oouchi, T. Takahashi, H. Ogawa, K. Irikura,

H.K. Thio, P.G. Somerville, Y. Fukushima and Y. Fukushima (2006). “Attenuation relations of strong ground motion in Japan using site classification based on predominant period.” *Bulletin of the Seismological Society of America*, 96(3): 898–913.